Future indirect detection using dwarf spheroidal galaxies

Koji Ichikawa (코지 이치카와)

In collaboration with
Kohei Hayashi , Masahiro Ibe, Miho N. Ishigaki,
Shigeki Matsumoto and Hajime Sugai.

KAVLI IPMU

CosKASI, June 9-11, 2015

Dark Matter Search

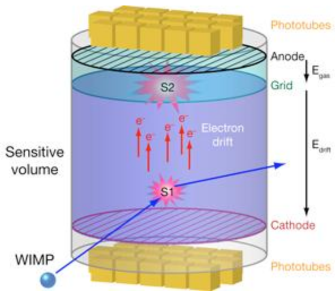

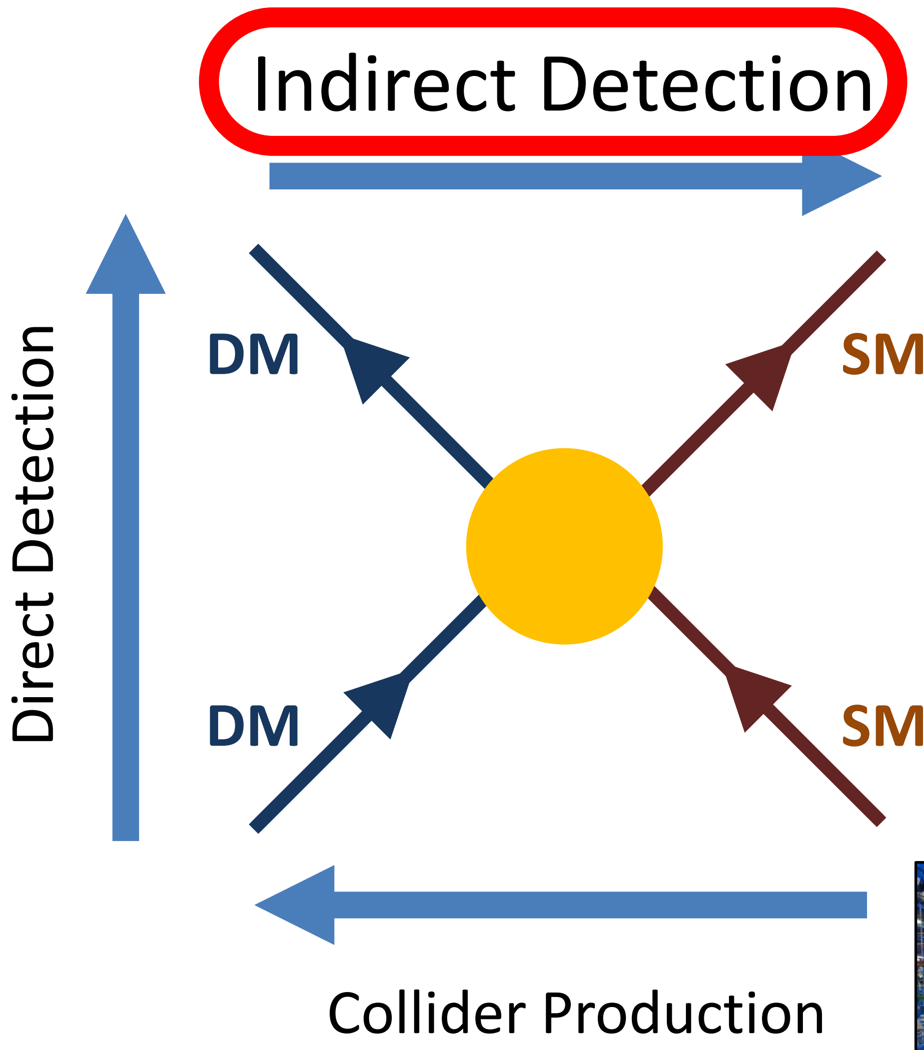

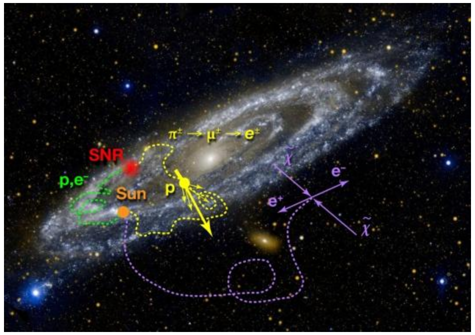

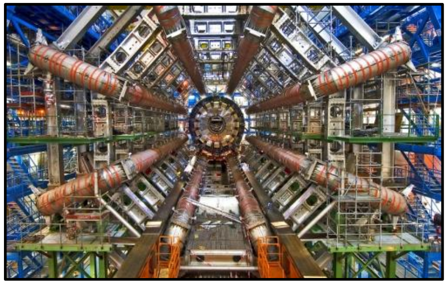

Signal Target

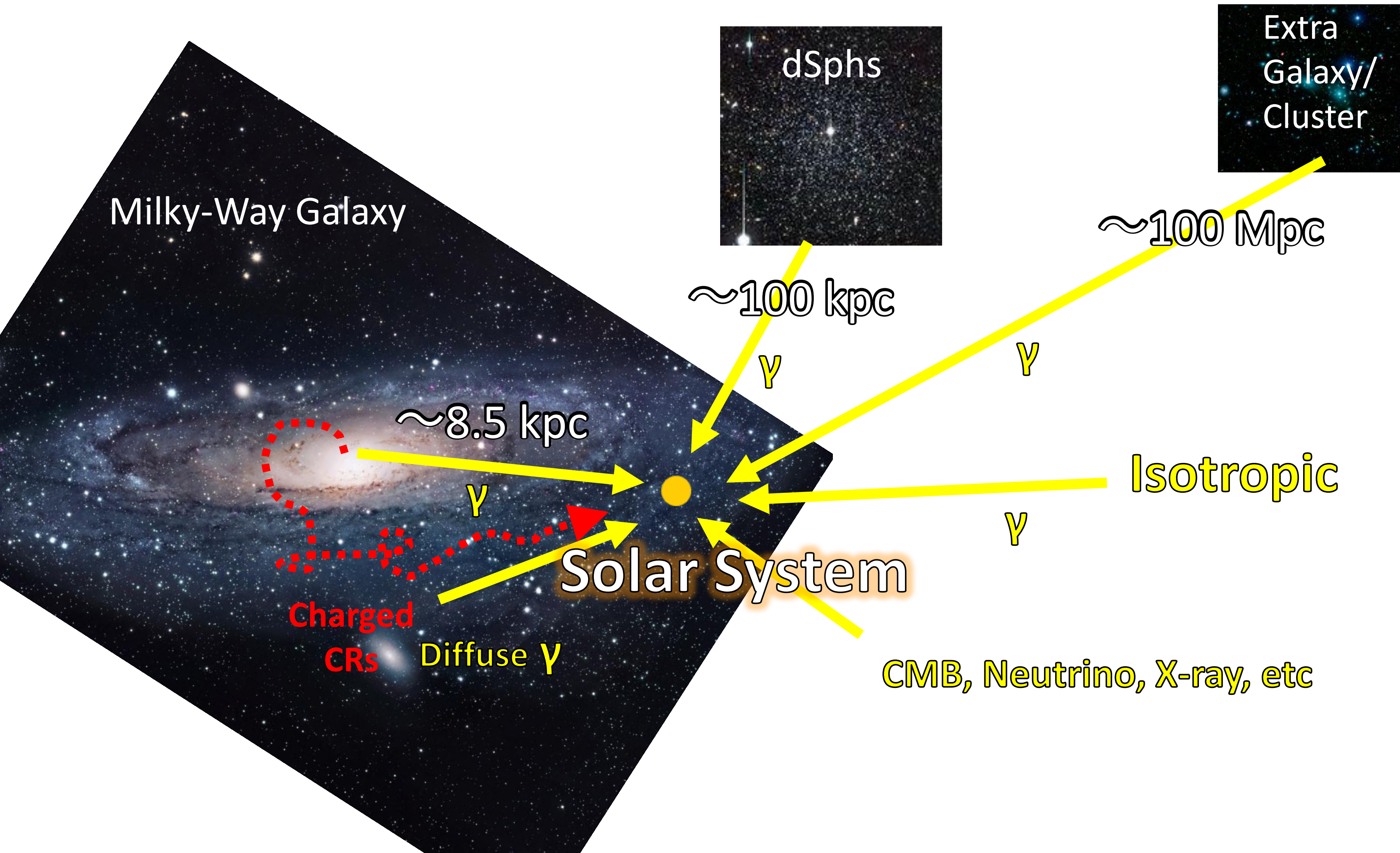

Signal Target

Null Signal → Constraint

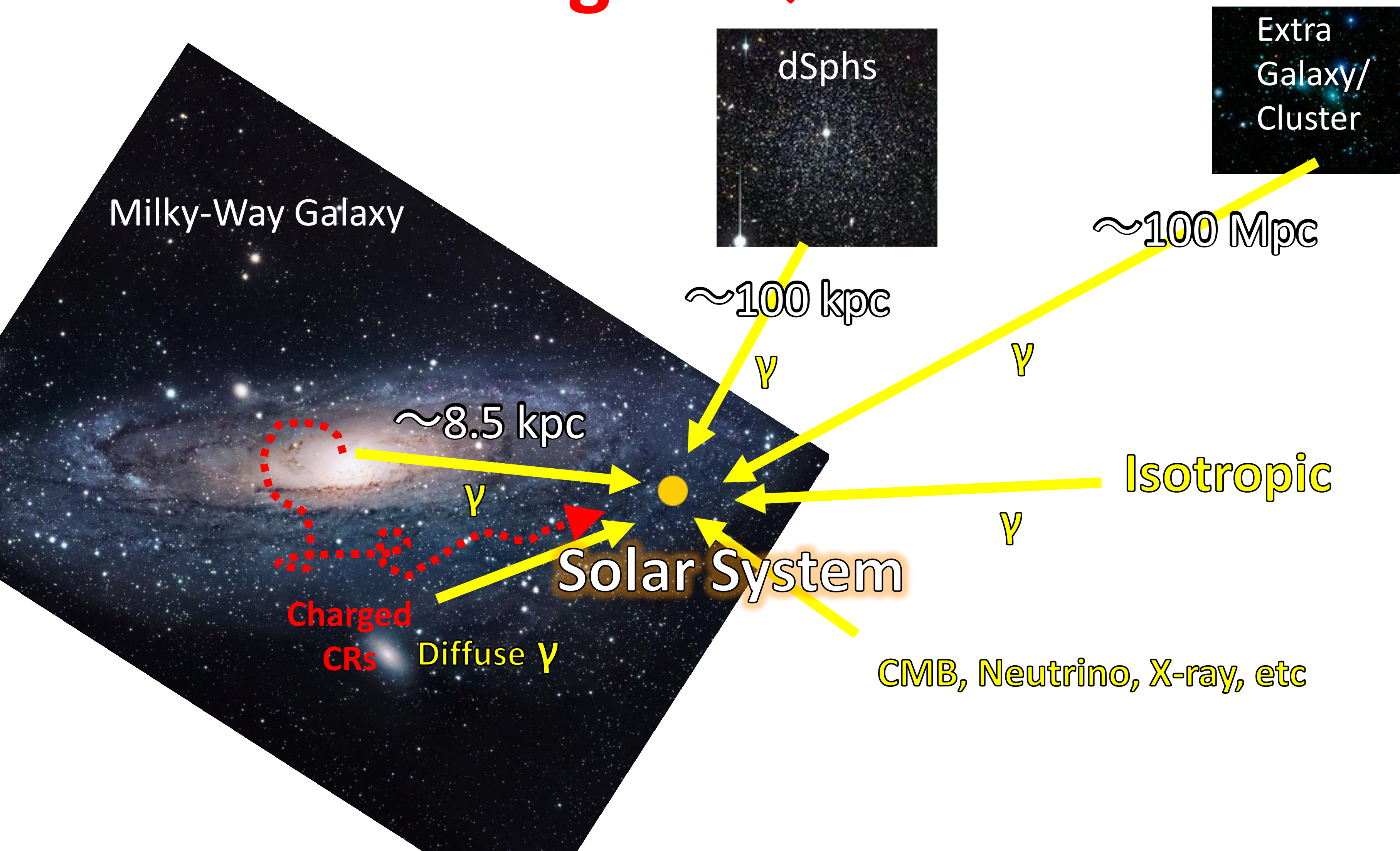

Current observational limit

Null Signal → Constraint

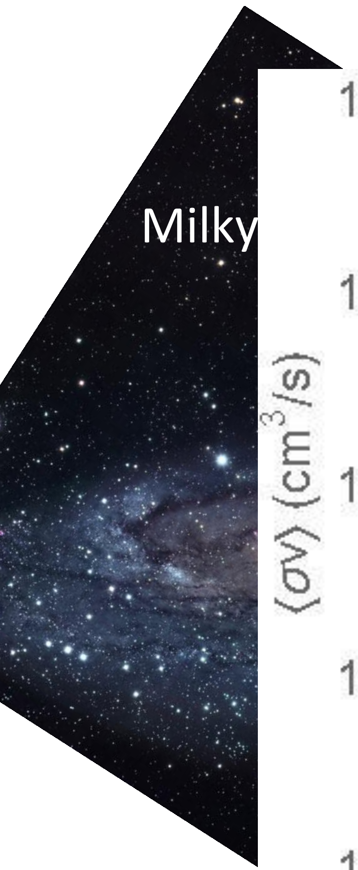

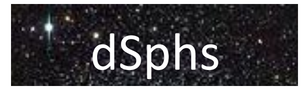

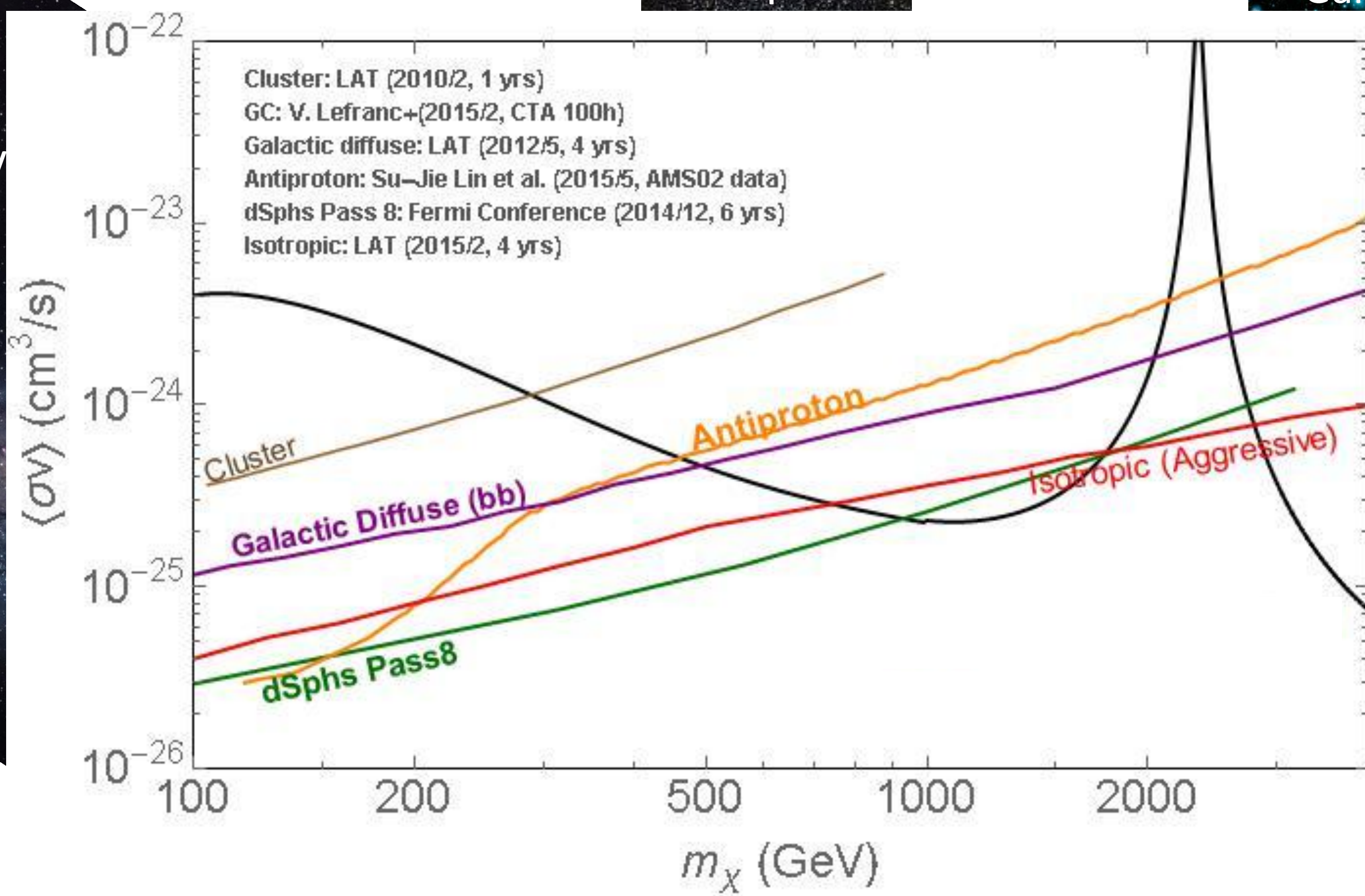

Current observational limit

Null Signal → Constraint

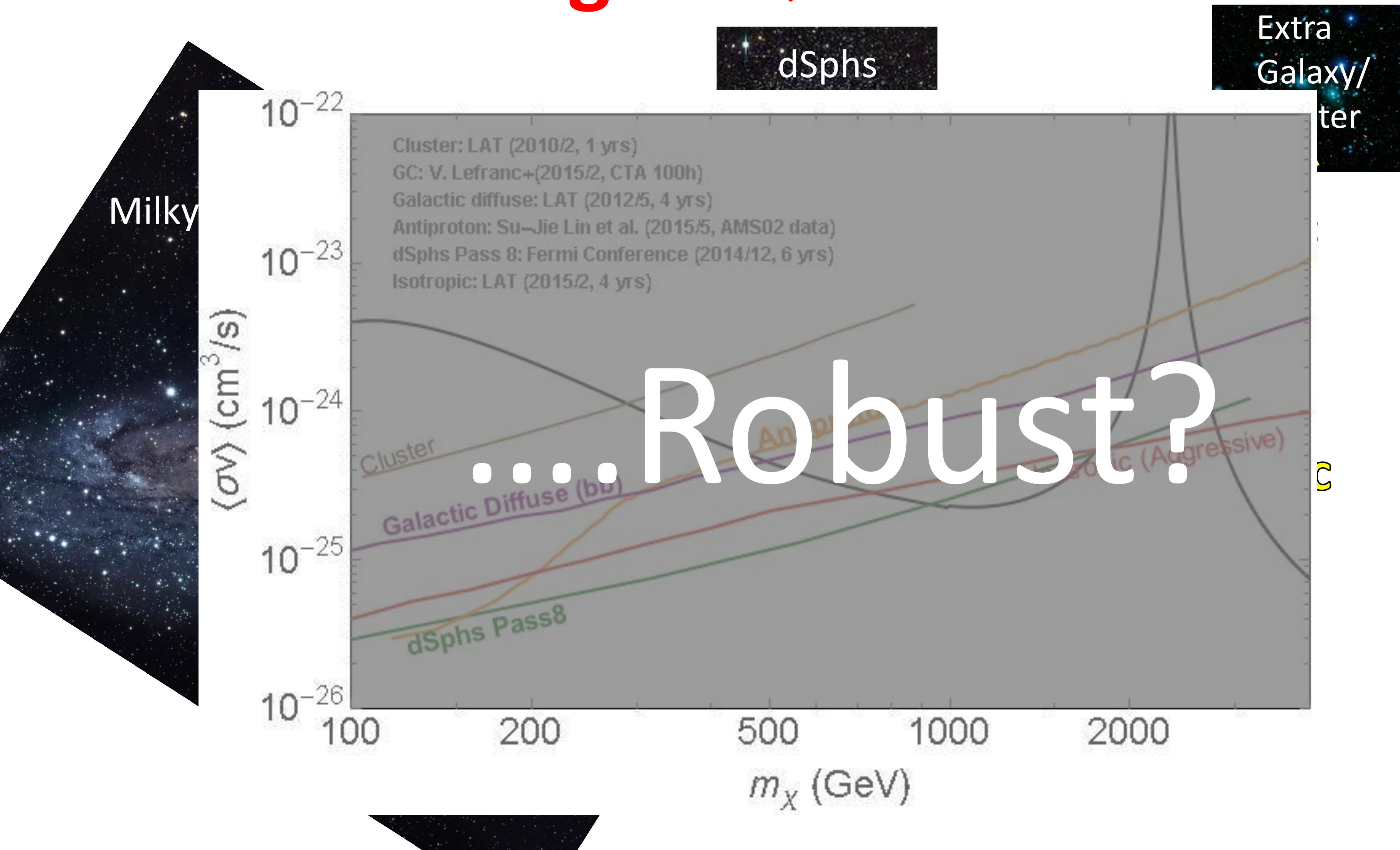

Current observational limit

Null Signal → Constraint

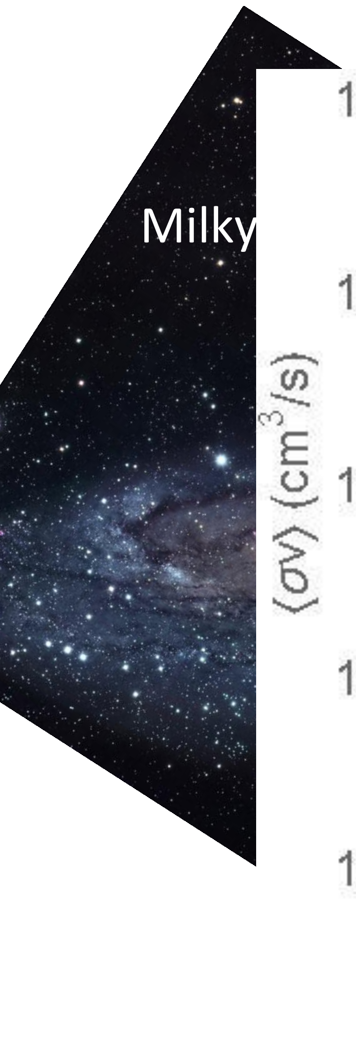

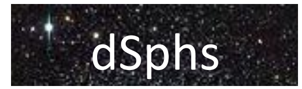

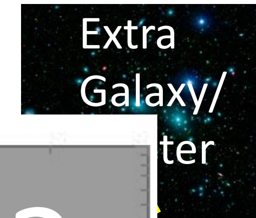

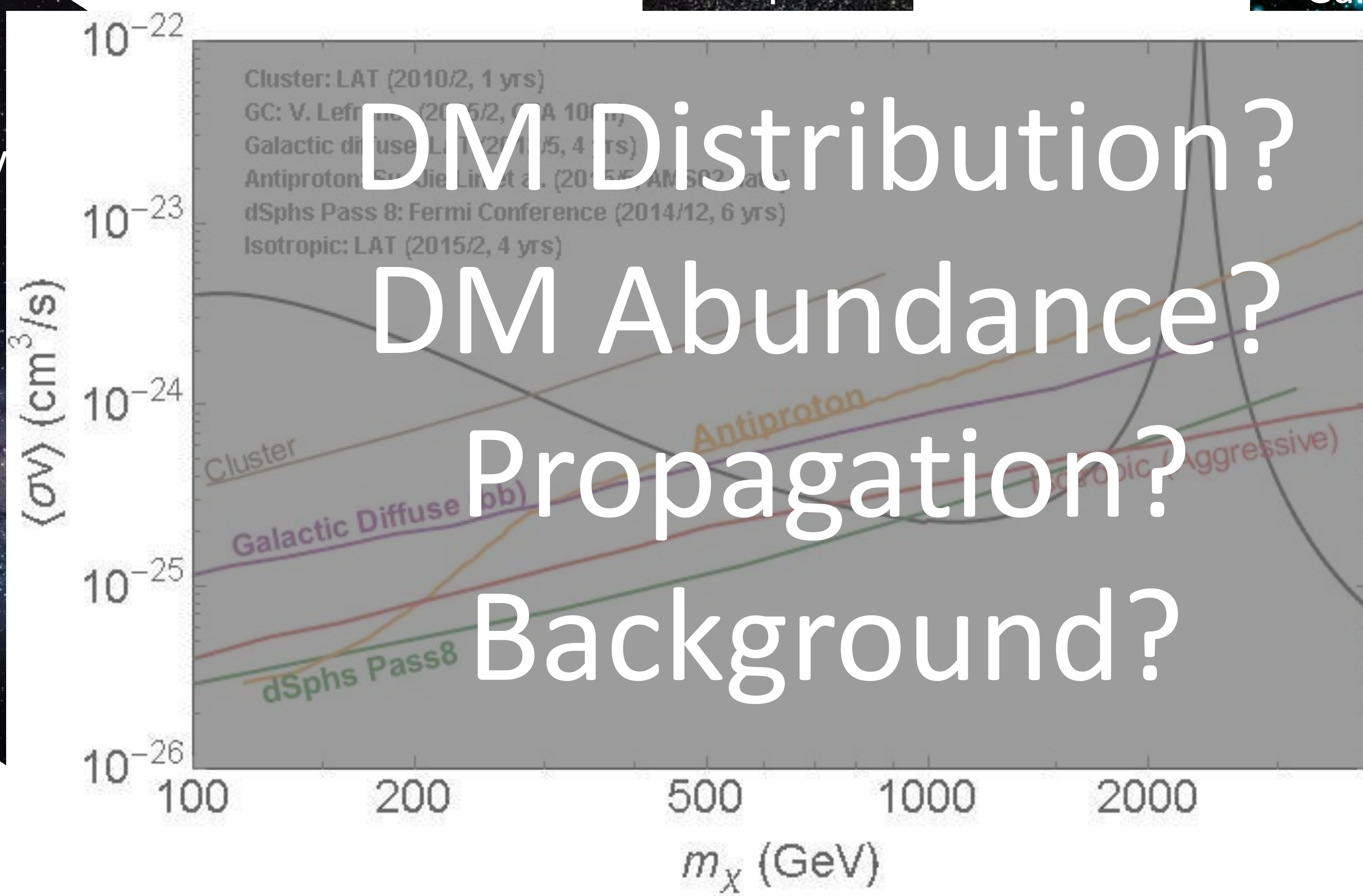

DM Distribution?

DM Abundance?

Propagation?

Background?

Current observational limit

Null Signal → Constraint

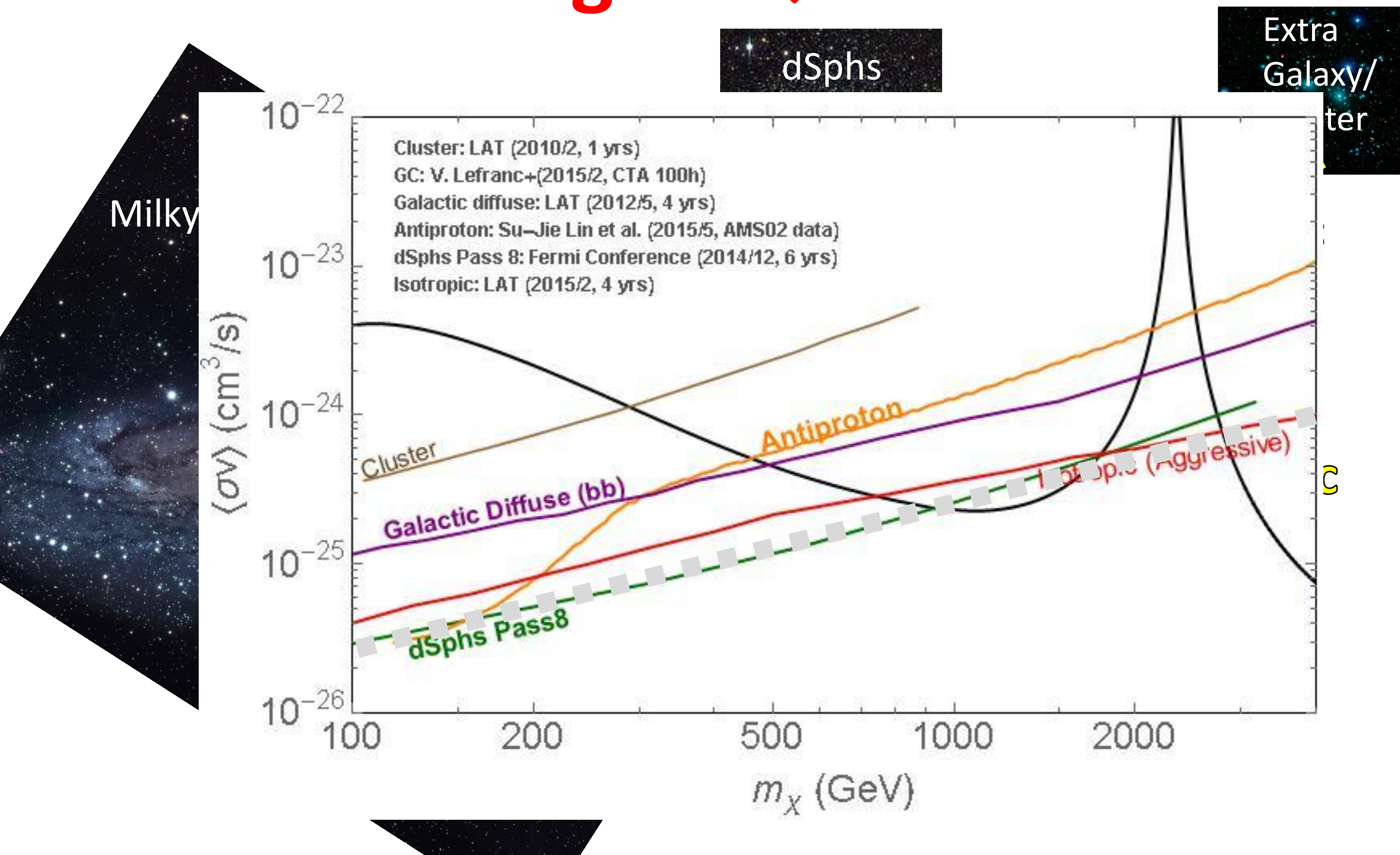

Current observational limit

Null Signal → Constraint

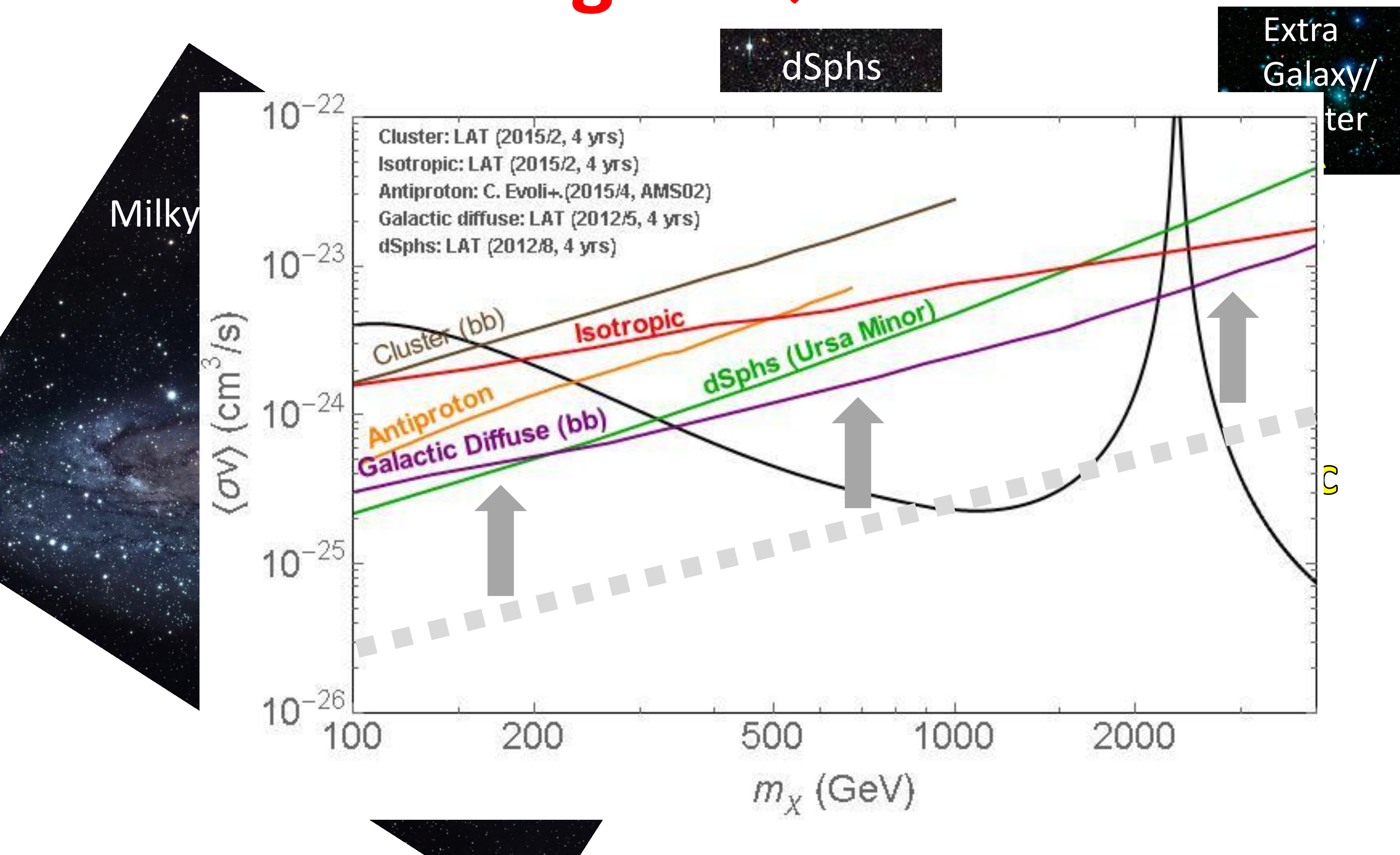

Current observational limit

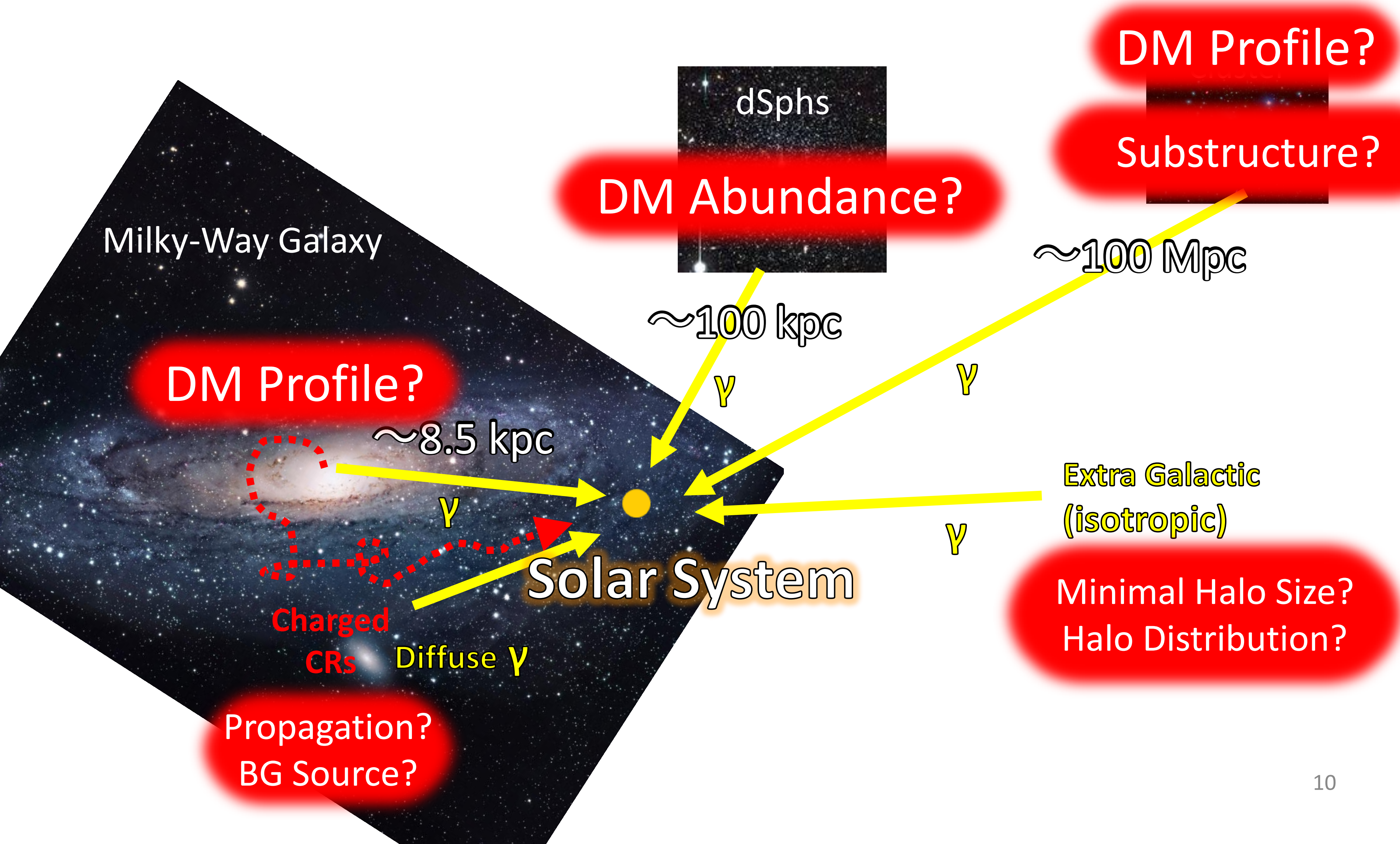

Current observational limit

Current observational limit

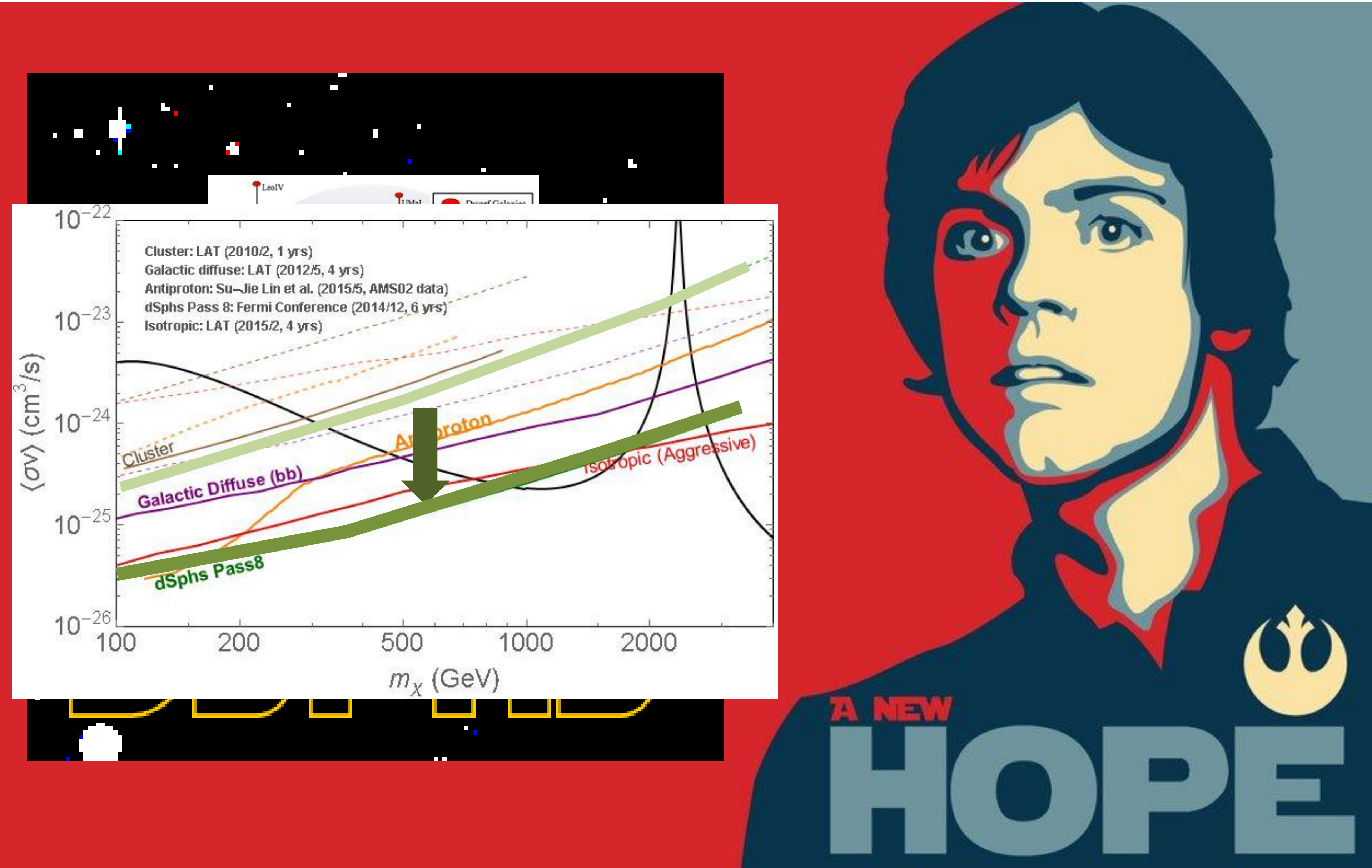

Current observational limit

Dwarf spheroidal galaxies

Satellite galaxies around MW
Small Luminosity
No gas
No Star Formation

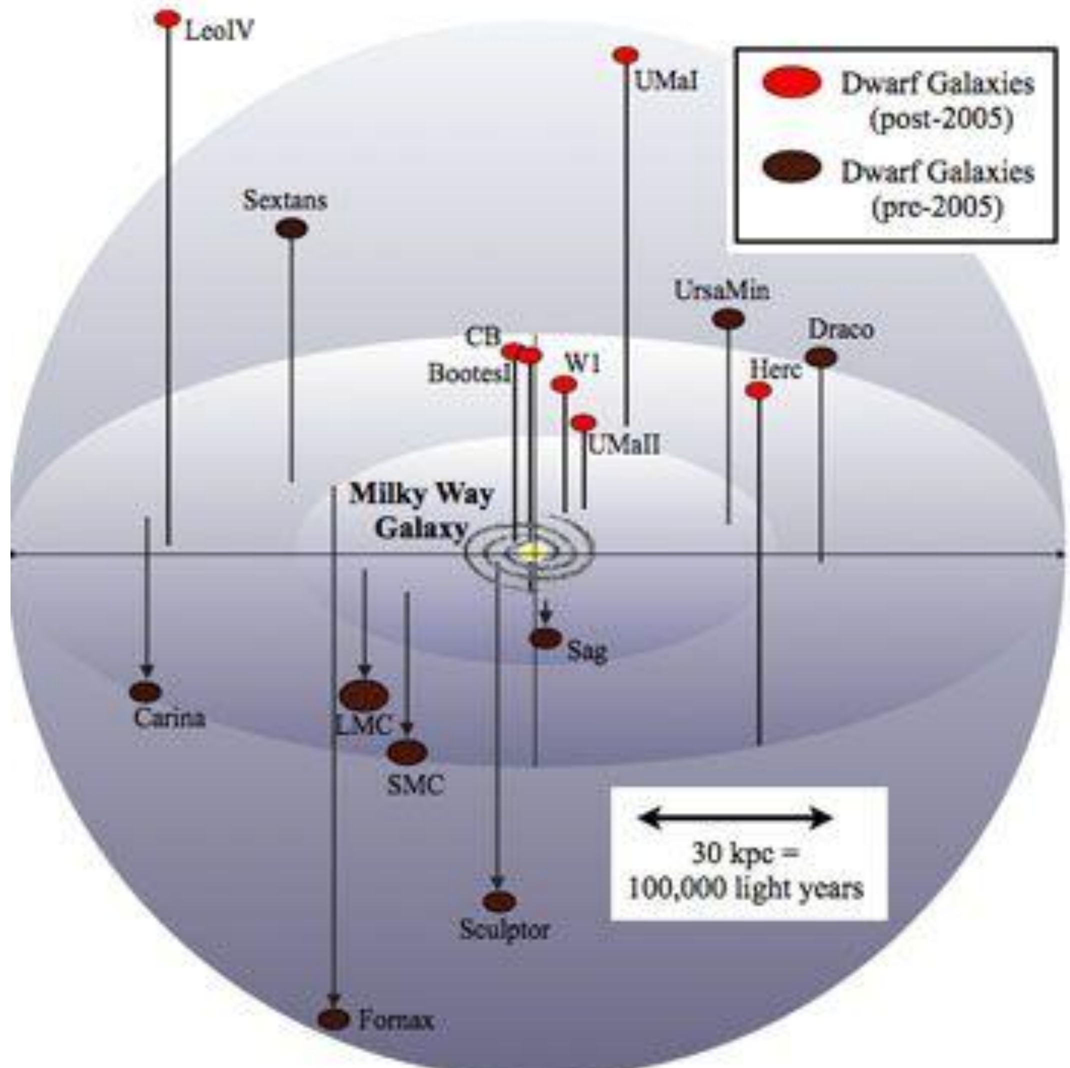

Dwarf spheroidal galaxies

dSphs:

1. **Neighbor** galaxies: 10~100kpc
2. Large Mass to Luminosity ratio = **DM rich**
3. Fewer gas containment

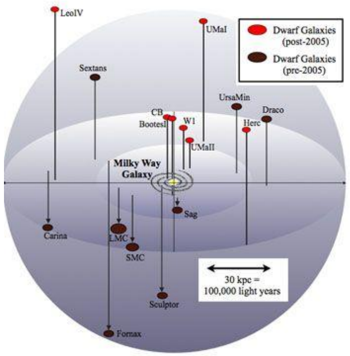

	Classical	Ultra-faint
#dSphs	8	>20
M/L ($M_\odot/L_\odot$)	10-100	100-1000
Distance (kpc)	60-250	10-60
#Obs Stars	150-2500	20-100
Characteristics	Brighter, farther	Darker, closer

See, e.g. Wolf et al (2010)

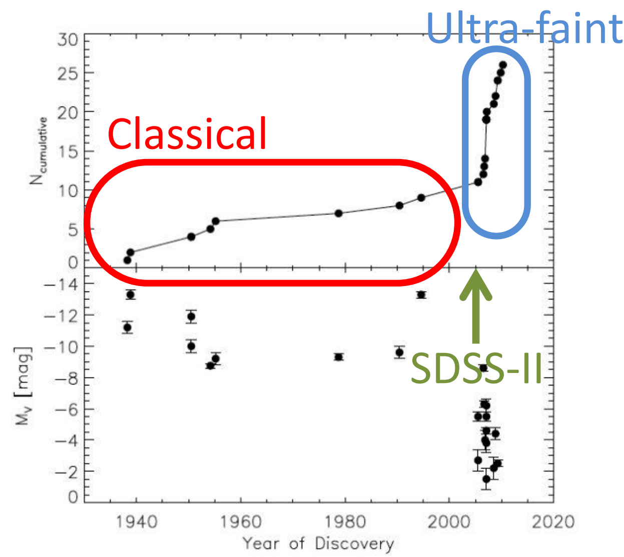

arXiv:0908.2995v6 [astro-ph.CO]

Uncertainty ?

How Robust?

How much will it be improved?

Signal Flux

$$\Phi(E,\Delta\Omega) = \left[\frac{\langle\sigma v\rangle}{8\pi m_{\tilde{w}}^2}\sum_f \mathrm{Br}(\tilde{w}^0\tilde{w}^0 \to f)\left(\frac{dN_\gamma}{dE}\right)_f\right]\left[\int_{\Delta\Omega} d\Omega \int_{l.o.s.} dl\,\rho^2(l,\Omega)\right]$$

Particle Physics Factor

Astrophysics Factor (J-factor)

$f = WW, ZZ, \gamma\gamma, Z\gamma$

Error: 1-10 % level

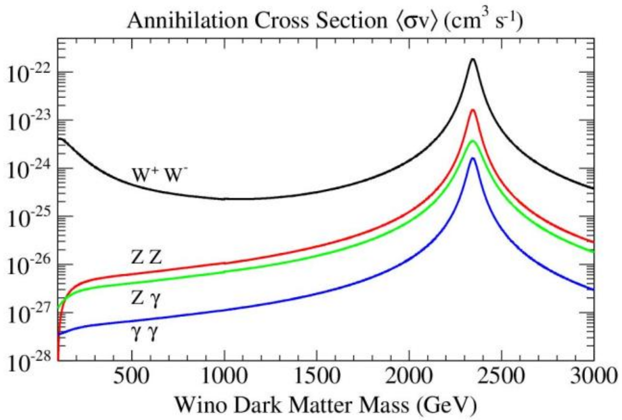

Hryczuk and Iengo (2012)
arXiv:1111.2916v4 [hep-ph]

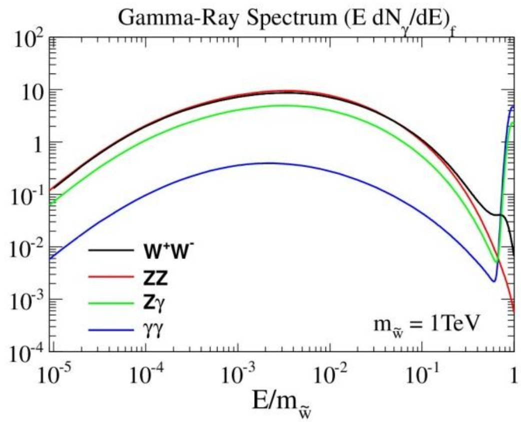

Cirelli et al. (2012)
arXiv:1012.4515 [hep-ph]

Large uncertainty:
Next Slide

$$J \simeq \frac{1}{D^2}\int_{\mathrm{Vol}} r^2\rho^2(r)\mathrm{d}r$$

Astrophysical Factor

DM Density profile

$$\rho(r) = \rho_s \, (r/r_s)^{-\gamma} \, [1 + (r/r_s)^{\alpha}]^{(\gamma-\beta)/\alpha}$$

$\rho_s (r/r_s)^{-1}(1+r/r_s)^{-2}$ Cusp

$\rho_s (1+r/r_s)^{-1}(1+r/r_s)^{-2}$ Cored

Stellar Density Profile: ν(r)

Jeans equation for stars

$$\frac{1}{\nu}\frac{d}{dr}(\nu \bar{v_r^2}) + 2\frac{\beta(r)\bar{v_r^2}}{r} = -\frac{GM(r)}{r^2}$$

$\sigma^{2\,(\mathrm{Theory})}_{\mathrm{l.o.s}}$ ⟷ $\sigma^{2\,(\mathrm{obs})}_{\mathrm{l.o.s}}$

Fit

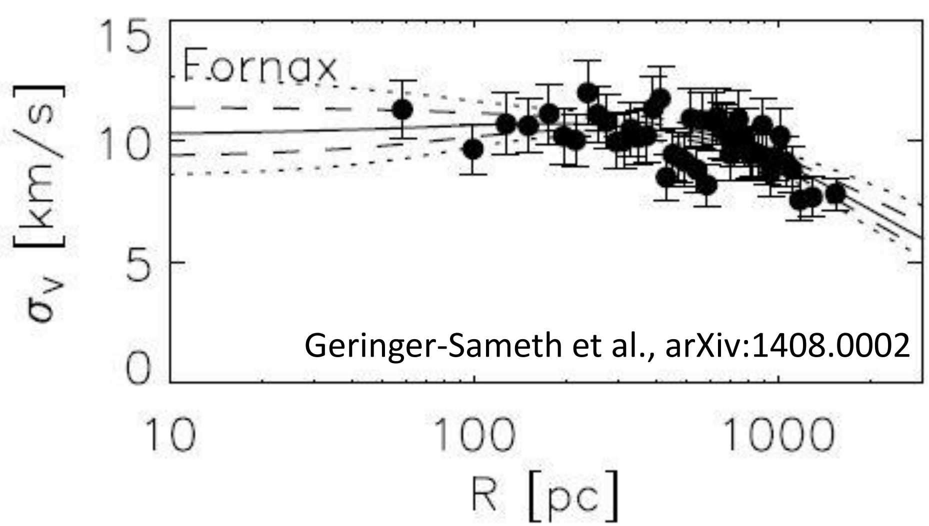

$$P(\theta|D) \propto P(D|\theta)P(\theta)$$

$$\sim \prod_{i}^{\mathrm{samples}} \exp\left[-\frac{(\sigma^2_{\mathrm{obs}}(r_i) - \sigma^2_{\mathrm{theory}}(r_i,\theta))^2}{2\delta^2}\right]$$

Astrophysical Factor

DM Density profile

$$\rho(r) = \rho_s\,(r/r_s)^{-\gamma}\,[1+(r/r_s)^{\alpha}]^{(\gamma-\beta)/\alpha}$$

$\rho_s (r/r_s)^{-1}(1+r/r_s)^{-2}$ Cusp

$\rho_s (1+r/r_s)^{-1}(1+r/r_s)^{-2}$ Cored

Stellar Density Profile: ν(r)

Jeans equation for stars

$$\frac{1}{\nu}\frac{d}{dr}(\nu \bar{v_r^2}) + 2\frac{\beta(r)\bar{v_r^2}}{r} = -\frac{GM(r)}{r^2}$$

$\sigma^{2\,(\mathrm{Theory})}_{\mathrm{l.o.s}}$ ↔ $\sigma^{2\,(\mathrm{obs})}_{\mathrm{l.o.s}}$

Fit

		long. (deg.)	lat. (deg.)	dist. (kpc)	α_s (deg.)	$\log_{10}[J(0.5°)/(\mathrm{GeV^2cm^{-5}sr})]$
Classical: Well-determined	Draco	86.4	34.7	76	$0.25^{+0.15}_{-0.09}$	18.8 ± 0.16
	Ursa Min.	105.0	44.8	76	$0.32^{+0.18}_{-0.12}$	18.8 ± 0.19
	Sculptor	287.5	-83.2	86	$0.25^{+0.25}_{-0.13}$	18.6 ± 0.18
	Sextans	243.5	42.3	86	$0.13^{+0.07}_{-0.05}$	18.4 ± 0.27
Ultra-faint: Not well-determined. Prior dependence	Segue 1	220.5	50.4	23	$0.40^{+0.86}_{-0.27}$	19.5 ± 0.29
	Ursa Maj. II	152.5	37.4	32	$0.32^{+0.48}_{-0.19}$	19.3 ± 0.28
	Willman 1	158.6	56.8	38	$0.25^{+0.54}_{-0.17}$	19.1 ± 0.31
	Coma B.	241.9	83.6	44	$0.25^{+0.54}_{-0.17}$	19.0 ± 0.25

Large ambiguity!

★Note: Insensitive to the halo shape

Name	GLON (deg)	GLAT (deg)	Distance (kpc)	$\log_{10}(J^{\rm NFW})^{\rm a}$ ($\log_{10}[{\rm GeV^2\,cm^{-5}\,sr}]$)	$\log_{10}(\alpha_s^{\rm NFW})$ ($\log_{10}[{\rm deg}]$)	$\log_{10}(J^{\rm Burkert})^{\rm a}$ ($\log_{10}[{\rm GeV^2\,cm^{-5}\,sr}]$)	$\log_{10}(\alpha_s^{\rm Burkert})$ ($\log_{10}[{\rm deg}]$)
Bootes I	358.1	69.6	66	18.8 ± 0.22	-0.6 ± 0.3	18.6 ± 0.17	-1.1 ± 0.2
Bootes II	353.7	68.9	42	–	–	–	–
Bootes III	35.4	75.4	47	–	–	–	–
Canes Venatici I	74.3	79.8	218	17.7 ± 0.26	-1.3 ± 0.2	17.6 ± 0.17	-1.6 ± 0.1
Canes Venatici II	113.6	82.7	160	17.9 ± 0.25	-1.1 ± 0.4	17.8 ± 0.19	-1.6 ± 0.2
Canis Major	240.0	-8.0	7	–	–	–	–
Carina	260.1	-22.2	105	18.1 ± 0.23	-1.0 ± 0.3	18.1 ± 0.16	-1.5 ± 0.1
Coma Berenices	241.9	83.6	44	19.0 ± 0.25	-0.6 ± 0.5	18.9 ± 0.21	-1.1 ± 0.3
Draco	86.4	34.7	76	18.8 ± 0.16	-0.6 ± 0.2	18.7 ± 0.17	-1.0 ± 0.2
Fornax	237.1	-65.7	147	18.2 ± 0.21	-0.8 ± 0.2	18.1 ± 0.22	-1.1 ± 0.1
Hercules	28.7	36.9	132	18.1 ± 0.25	-1.1 ± 0.4	17.9 ± 0.19	-1.6 ± 0.2
Leo I	226.0	49.1	254	17.7 ± 0.18	-1.1 ± 0.3	17.6 ± 0.17	-1.5 ± 0.2
Leo II	220.2	67.2	233	17.6 ± 0.18	-1.1 ± 0.5	17.5 ± 0.15	-1.9 ± 0.5
Leo IV	265.4	56.5	154	17.9 ± 0.28	-1.1 ± 0.4	17.8 ± 0.21	-1.6 ± 0.2
Leo V	261.9	58.5	178	–	–	–	–
Pisces II	79.2	-47.1	182	–	–	–	–
Sagittarius	5.6	-14.2	26	–	–	–	–
Sculptor	287.5	-83.2	86	18.6 ± 0.18	-0.6 ± 0.3	18.5 ± 0.17	-1.1 ± 0.2
Segue 1	220.5	50.4	23	19.5 ± 0.29	-0.4 ± 0.5	19.4 ± 0.24	-0.9 ± 0.2
Segue 2	149.4	-38.1	35	–	–	–	–
Sextans	243.5	42.3	86	18.4 ± 0.27	-0.9 ± 0.2	18.4 ± 0.16	-1.2 ± 0.1
Ursa Major I	159.4	54.4	97	18.3 ± 0.24	-1.0 ± 0.3	18.2 ± 0.18	-1.4 ± 0.2
Ursa Major II	152.5	37.4	32	19.3 ± 0.28	-0.5 ± 0.4	19.2 ± 0.21	-0.9 ± 0.2
Ursa Minor	105.0	44.8	76	18.8 ± 0.19	-0.5 ± 0.2	18.7 ± 0.20	-0.9 ± 0.2
Willman 1	158.6	56.8	38	19.1 ± 0.31	-0.6 ± 0.5	19.0 ± 0.28	-1.1 ± 0.2

[a] J-factors are calculated over a solid angle of $\Delta\Omega \sim 2.4$

Coma B.	241.9	83.6	44	$0.25^{+0.34}_{-0.17}$	*19.0 ± 0.25*

Large ambiguity!

Uncertainty (prior dependence)

$$P(\theta|D) \propto P(D|\theta)P(\theta)$$

$$\prod_i^{\text{samples}} \exp\left[-\frac{(\sigma_{\text{obs}}^2(r_i) - \sigma_{\text{theory}}^2(r_i,\theta))^2}{2\delta^2}\right]$$

ex: $P(v_{\max}) \propto v_{\max}^{-n} dv_{\max}$

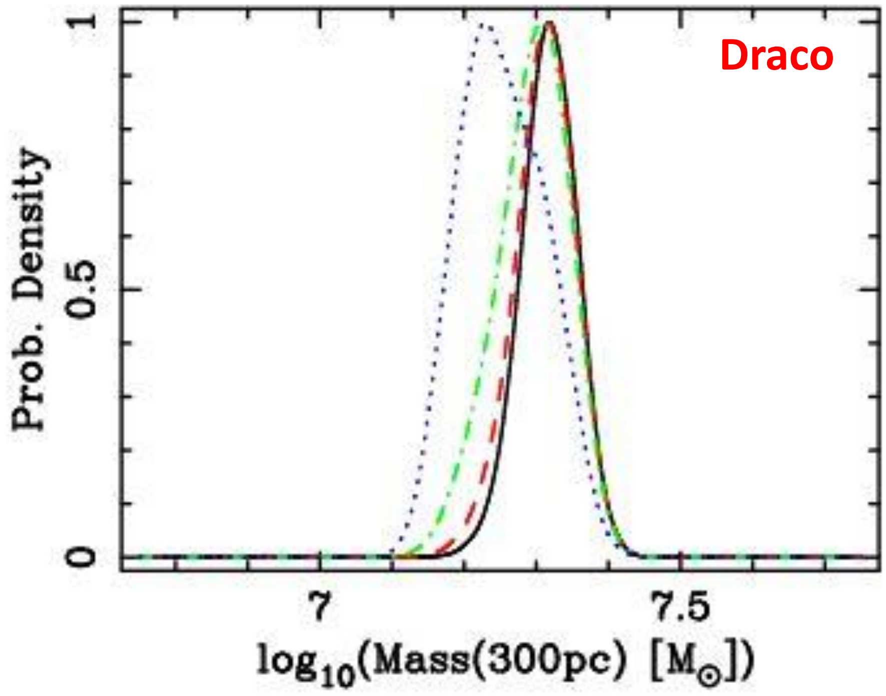

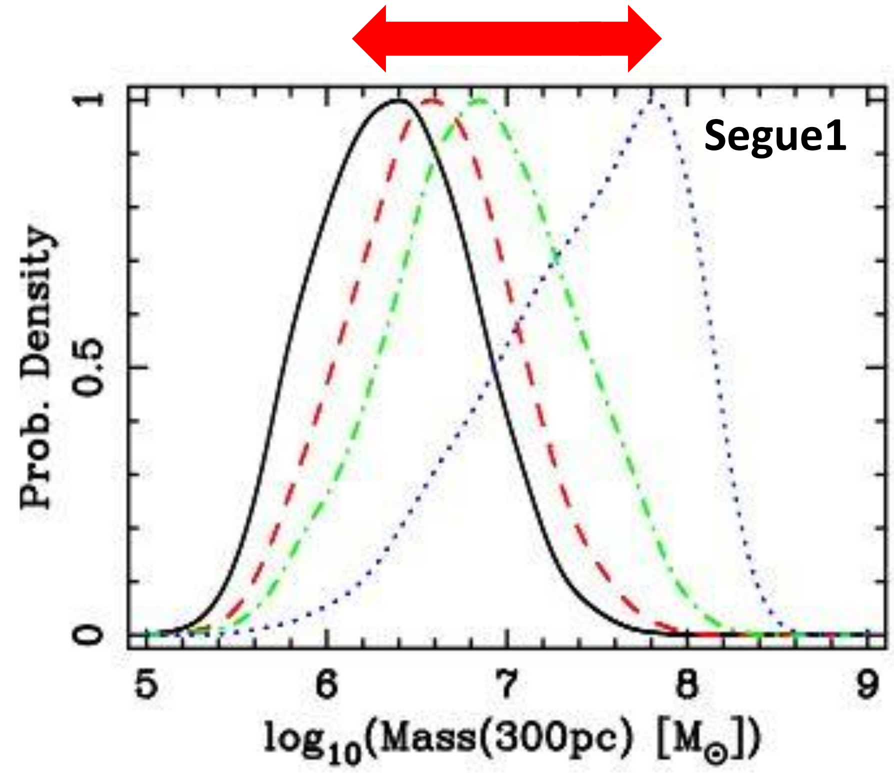

#Obs Stellar ～ 300

#Obs Stellar ～ 70

Martinez et al., arXiv: 0902.4715

Effect on sensitivity lines

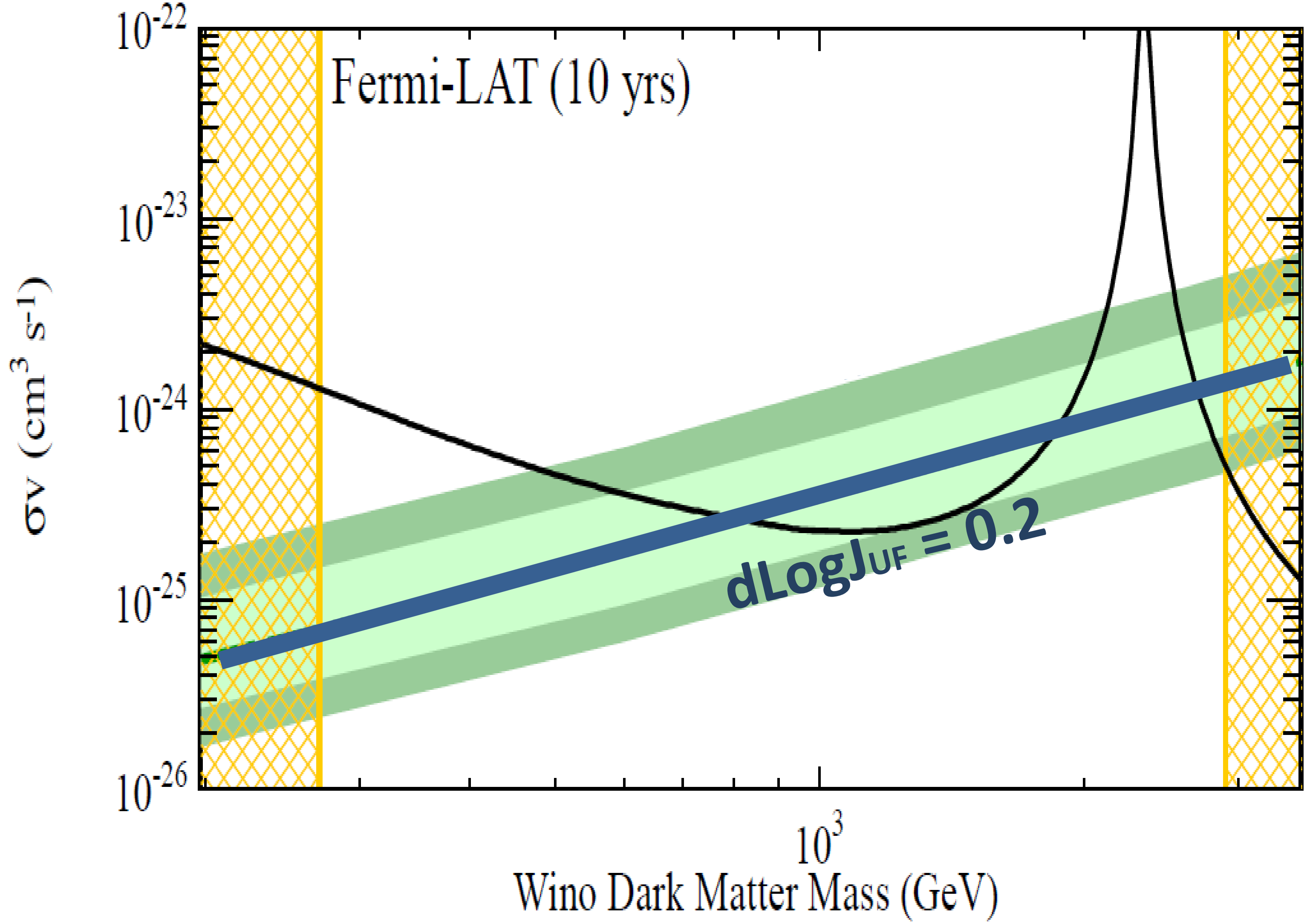

B. Bhattacherjee, M Ibe, KI, S Matsumoto, K Nishiyama, arXiv:1405.4914

Effect on sensitivity lines

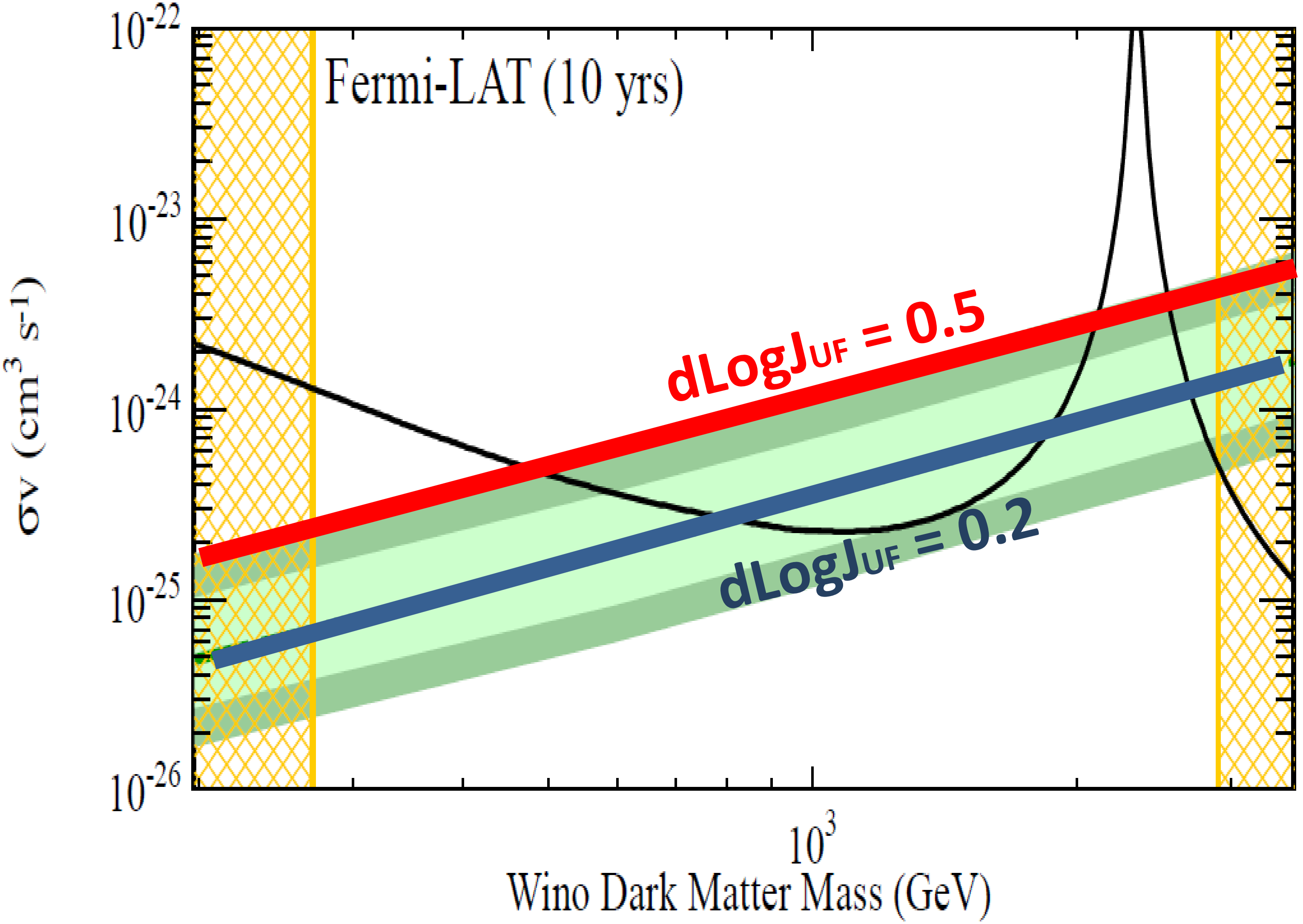

B. Bhattacherjee, M Ibe, KI, S Matsumoto, K Nishiyama, arXiv:1405.4914

Conservative vs Aggressive

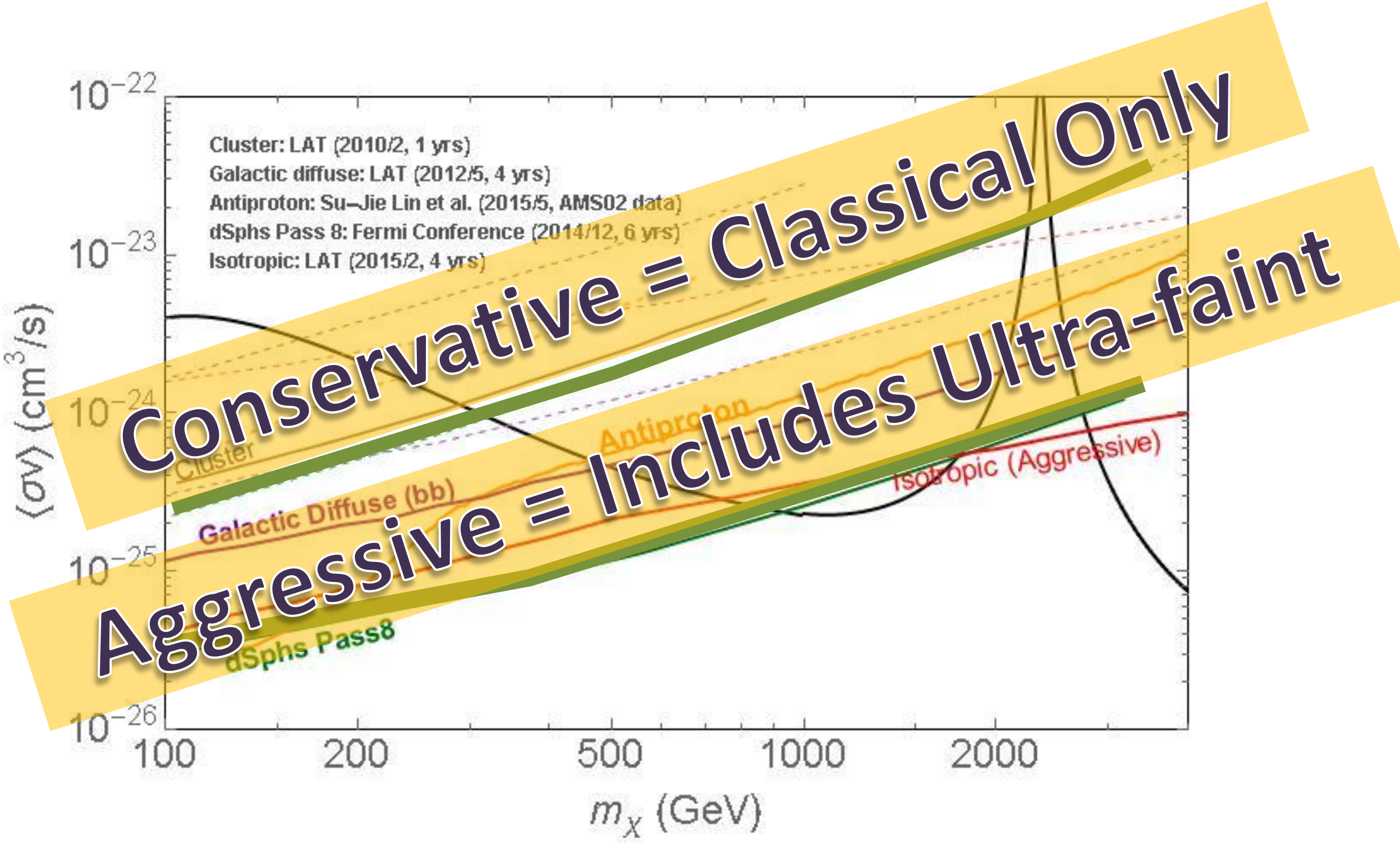

Question…

- How much can we improve the current profile uncertainty?
= How many new stellar kinematics will be measured by a Future Observation?

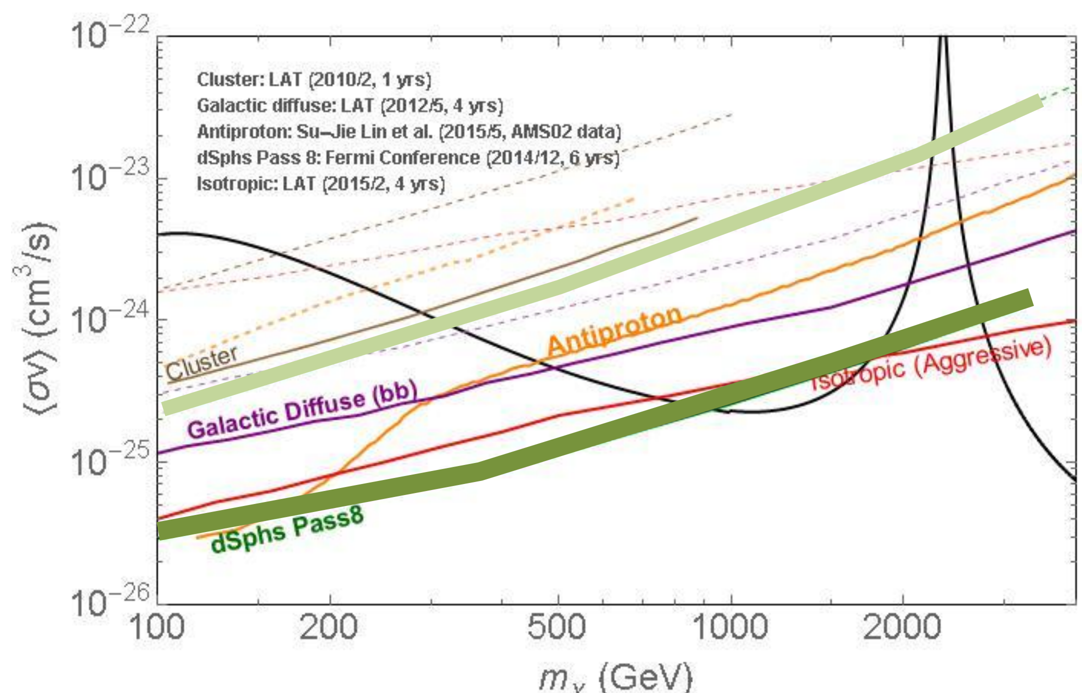

Prime Focus Spectroscopy

by SuMIRe Project of Subaru Telescope
（First Light: 2017）

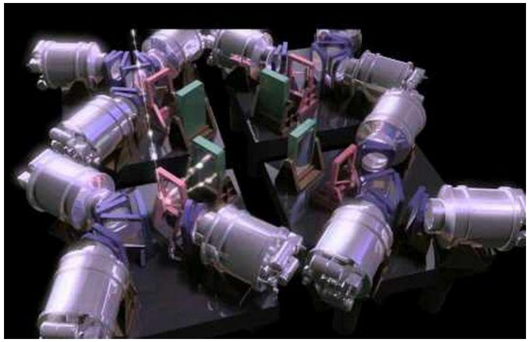

Large Field of View:
1.3 deg (diam)
with 2394 Fiber

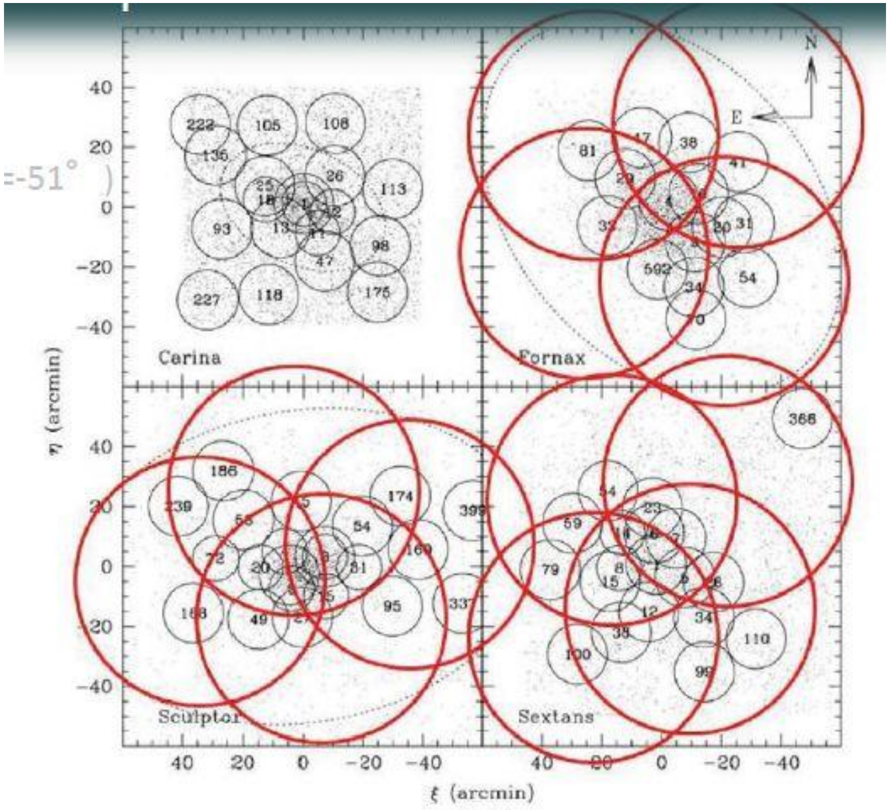

Prime Focus Spectroscopy

Classical (Ursa Minor)

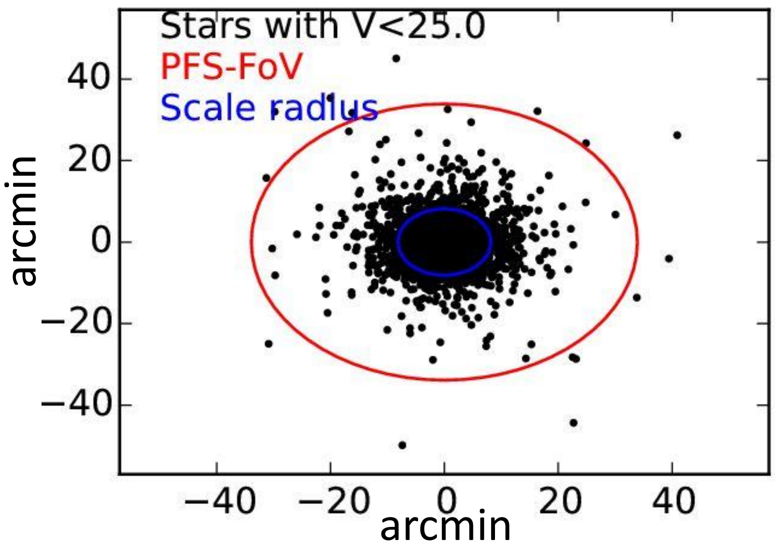

Ultra-faint (Segue 1)

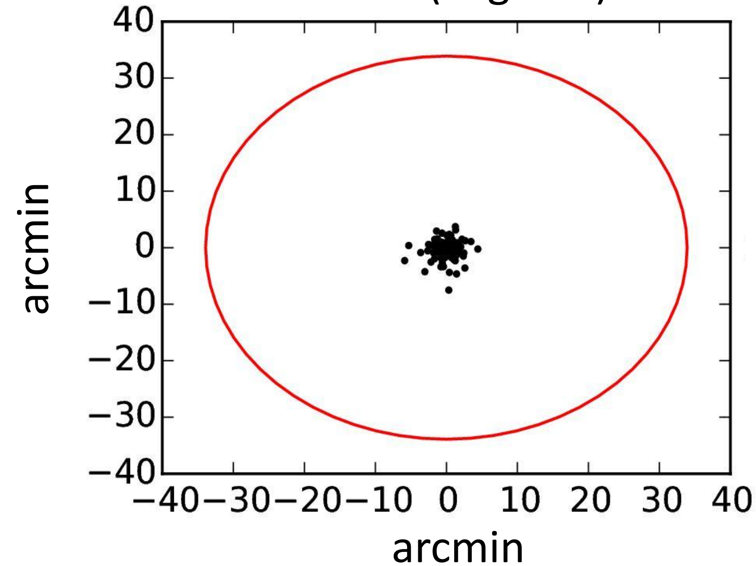

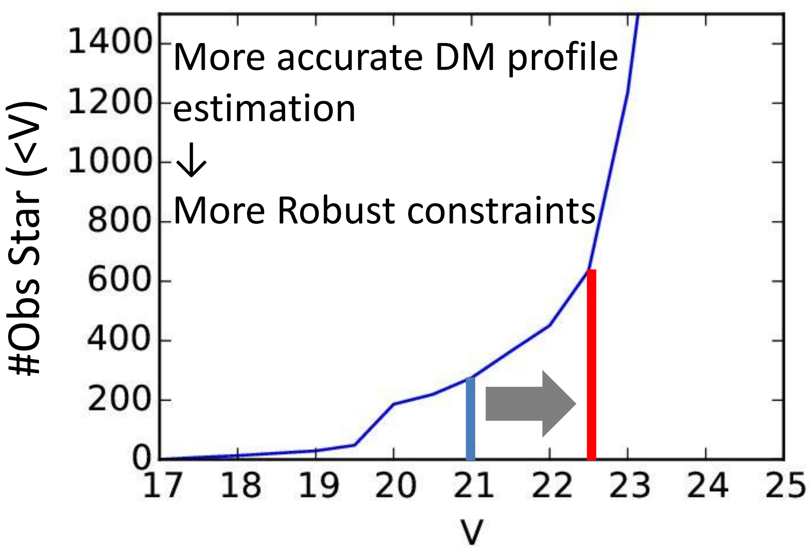

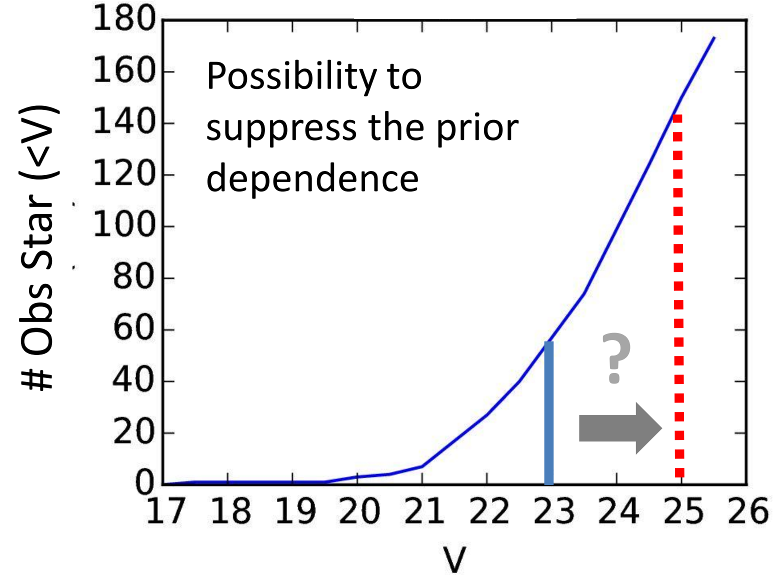

Strategy

1. Mock Observable:

(R, v, Metalicity, Luminosity)

= dSph Stellar + Foreground

dSph Stellar Mock

⇒Boltzmann Equation under DM profile

Foreground Mock

⇒Besancon Model (Robin+ (2003))

2. Detector Convolution:

⇒1. fix: dv = 3.0km/s

⇒2. Luminosity dependence for each stars

3. Fit:

(DM profile, anisotropy, dSph stellar profile, dSph v, foreground norm + metalicity)

⇒Fit to (v, r) probability density.

4. Implication:

Fermi 10 yr Exp (Pass 8?)

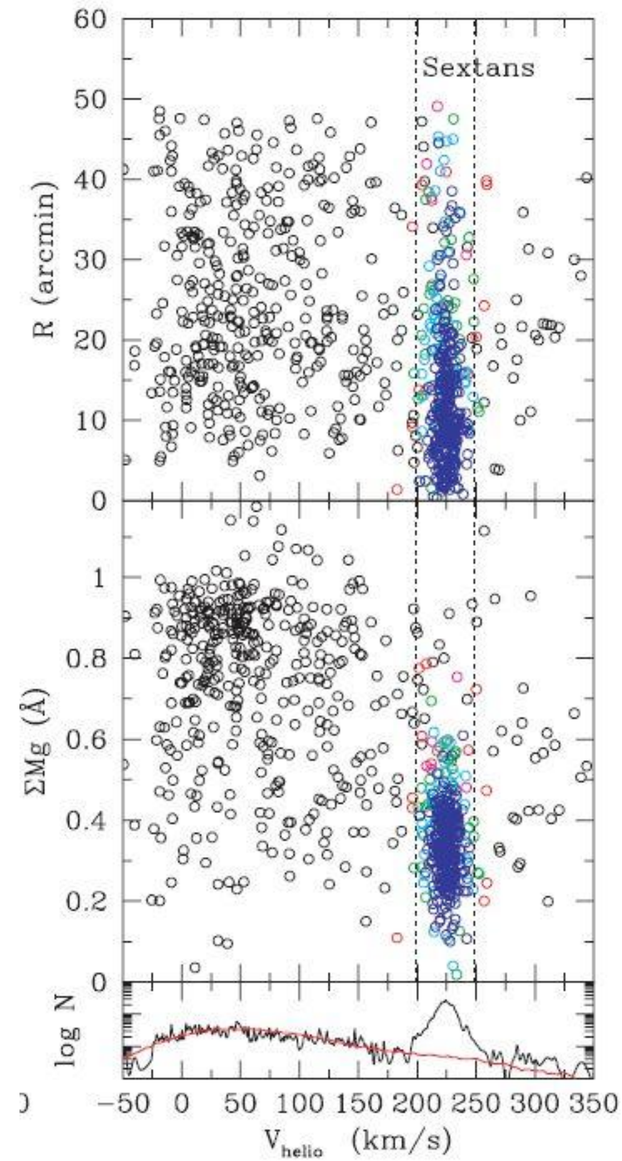

Walker+, AJ 137 (2009)

Strategy

1. Mock Observable:

(R, v, Metalicity, Luminosity)

= dSph Stellar + Foreground

dSph Stellar Mock

⇒Boltzmann Equation under DM profile

Foreground Mock

⇒Besancon Model (Robin+ (2003))

Coming Soon!

2. Detector Convolution:

⇒[illegible] d[illegible]km/s

⇒2. Luminosity dependence for each stars

3. Fit:

(DM profile, anisotropy, dSph stellar profile, dSph v, foreground norm + metalicity)

⇒Fit to (v, r) probability density.

4. Implication:

Fermi 10 yr Exp (Pass 8?)

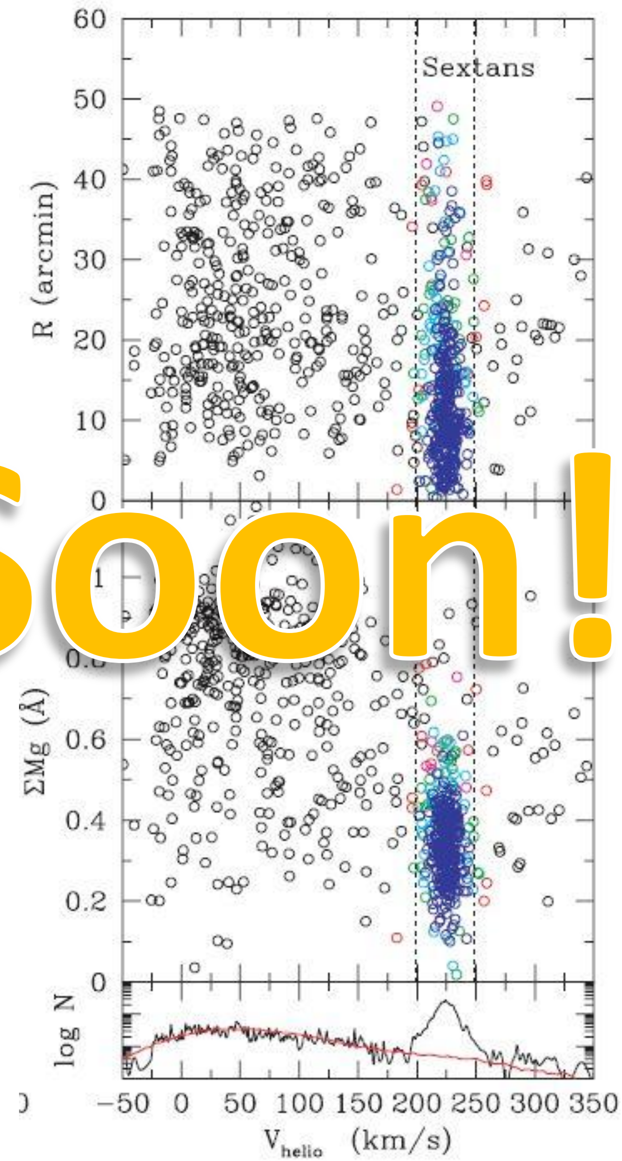

Walker+, AJ 137 (2009)

Summary

- Indirect detection is essential for DM search.
- Gamma-ray observation of dSph can give robust constraints on the DM annihilation cross section.
- Investigation of stellar kinematics is important.
- PFS will play a crucial role.

Thank You !

감사합니다

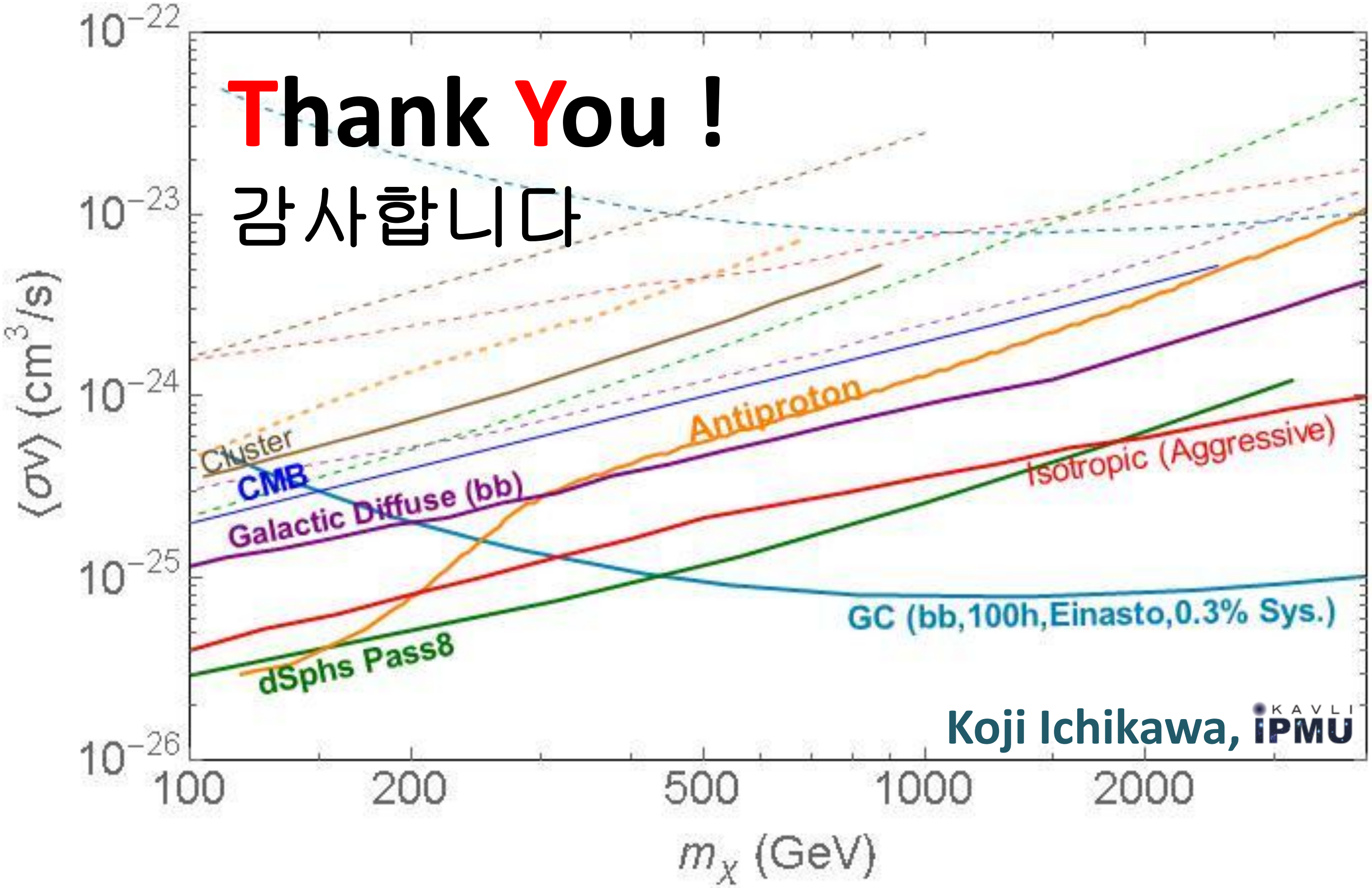

Koji Ichikawa, KAVLI IPMU

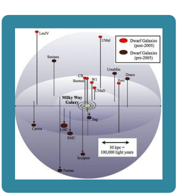
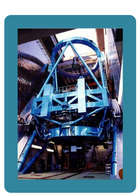


In collaboration with
Kohei Hayashi , Masahiro Ibe, Miho N. Ishigaki,
Shigeki Matsumoto and Hajime Sugai.

Back up

Detector

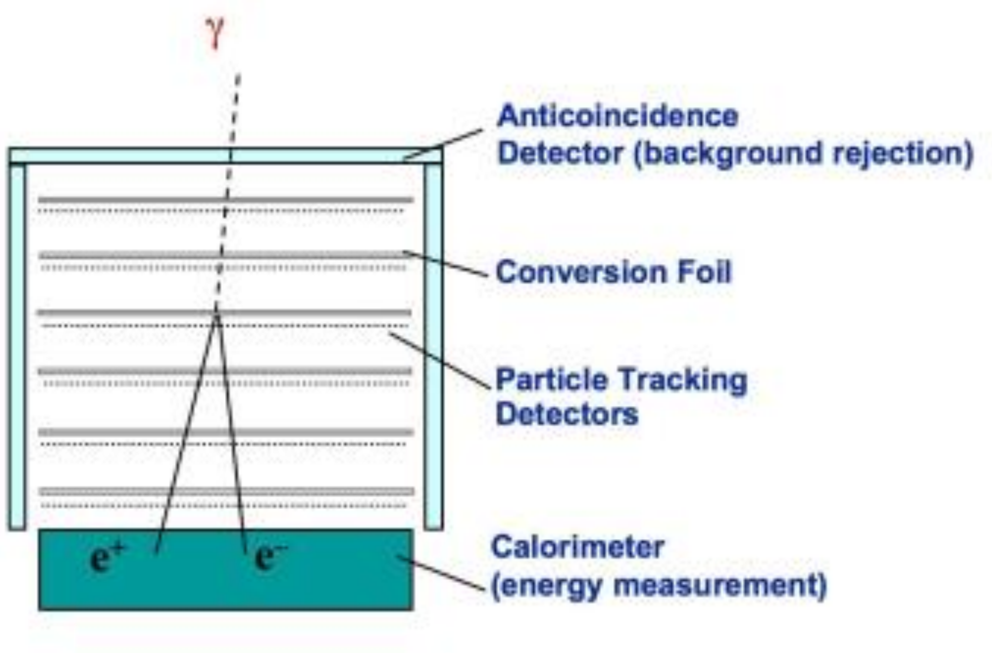

1.8 * 1.8 * 0.72 (m^3)
2789 kg

16 Tower:
37cm * 37cm * 66cm

Calorimeter 96 (8 layer)

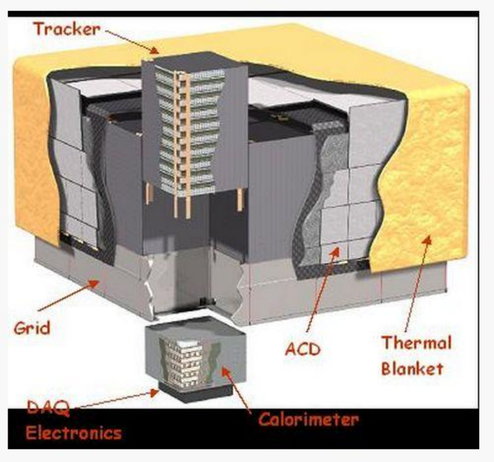

Detector

Tracker

Spark Chamber

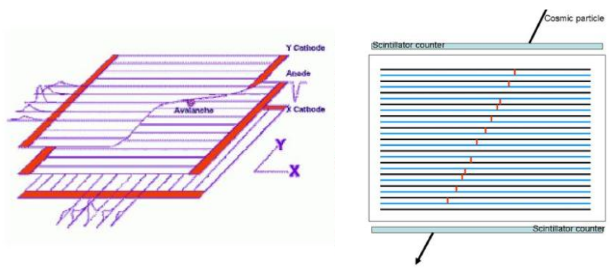

Silicon Strip

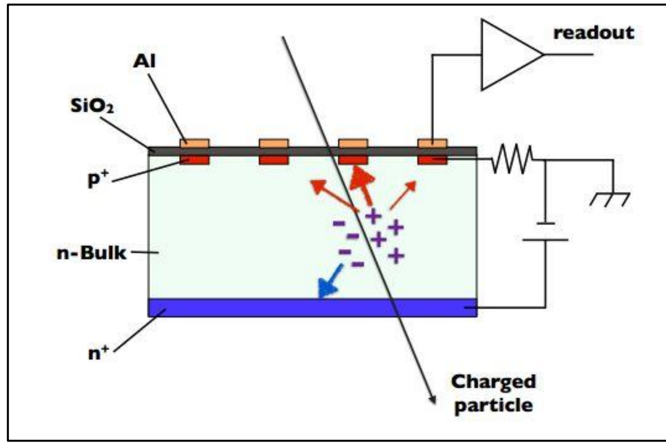

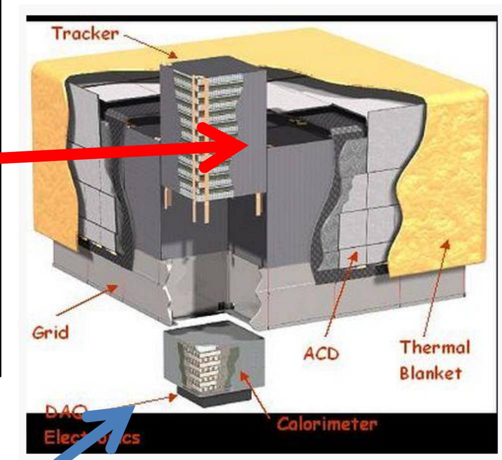

Calorimeter

CsI (Fermi-LAT)
326 × 26.7 × 19.9 mm lode
12 lodes × 8 layer
([arXive: 1206.1896])

Sensitivity Line (line gamma)

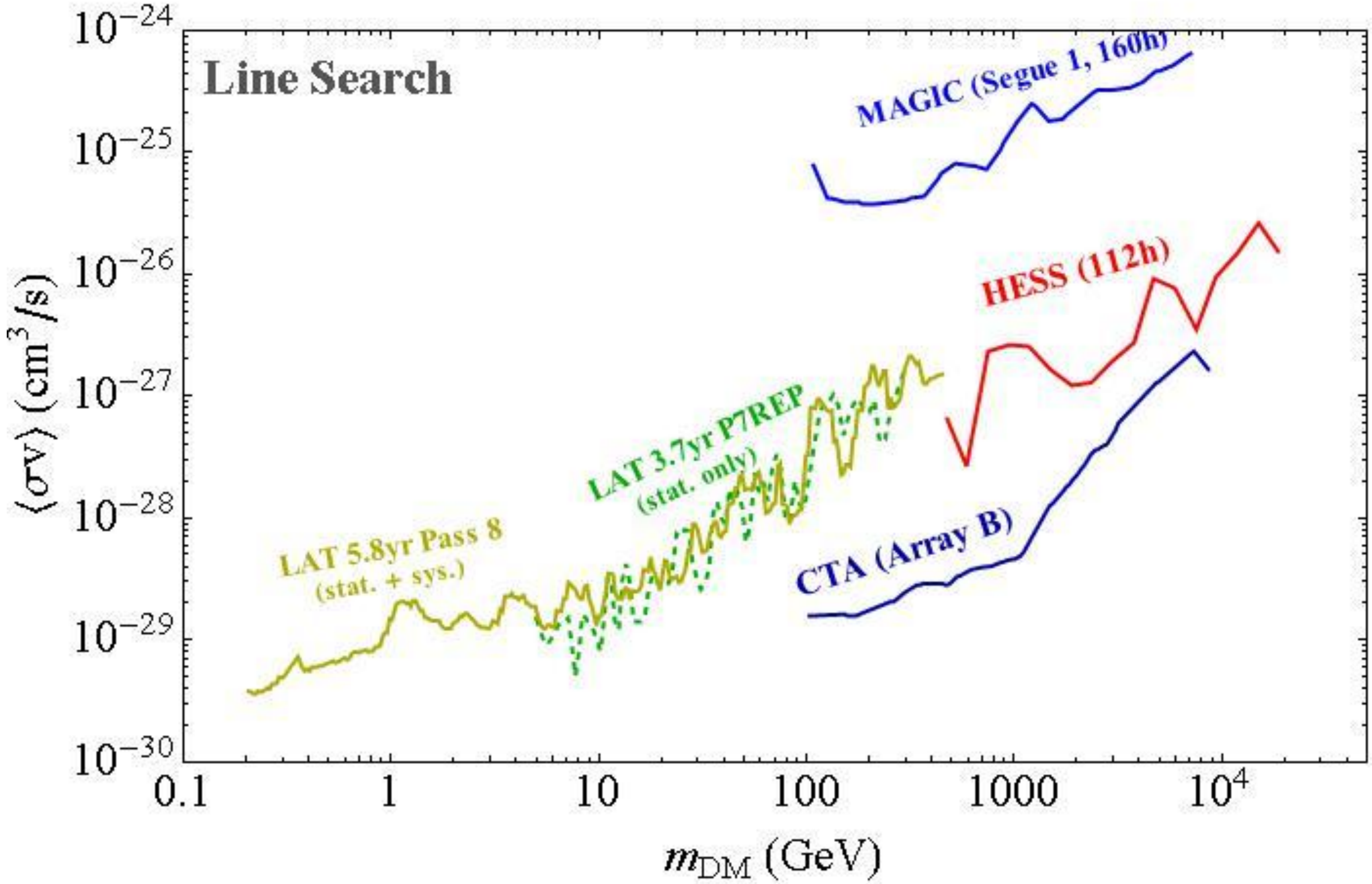

Observed Events

Signal: $$S_{ai} = t_{\rm obs} \times \int_{\Delta E_i} dE\, \mathcal{F}_a^{(\rm S)}(E, \Delta\Omega_i)\, A_{\rm eff}(E)$$

Background: $$B_{ai} = t_{\rm obs} \times \int_{\Delta E_i} dE\, \mathcal{F}_a^{(\rm B)}(E, \Delta\Omega_i)\, A_{\rm eff}(E)$$

a: dSph
i: Energy Bin

Energy Bin | ROI | Effective Area

Signal Flux: $F^{(S)}$ — Particle Factor, Astrophysical Factor

BG Flux: $F^{(B)}$ — Galactic Diffuse, Isotropic Diffuse, Point-like Source

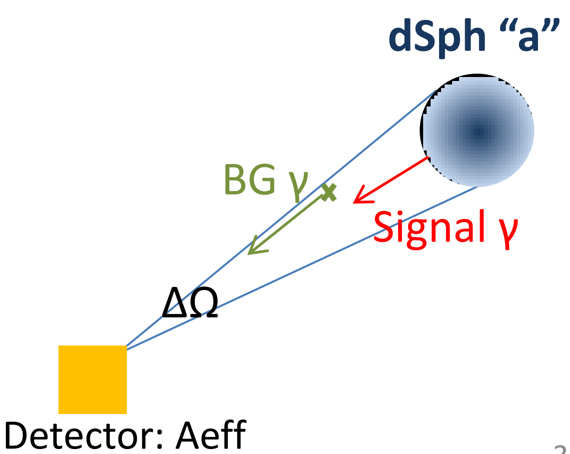

Background Flux

1. Galactic Diffuse

CR + ISM, Brems of CRe, IC (CRe + Interstellar radiation field)

→ Simulation (e.g. GALPROP) with ISM, ISRF, Large Scale Structure.

2. Isotropic Diffuse

AGN, Starburst, γ-Ray burst, unknown sources

→ Evaluated from $|b| > 30^o$ sky data

3. Point-like Source

AGN, SNR, Pulsars, Unidentified

→ Mask/Model

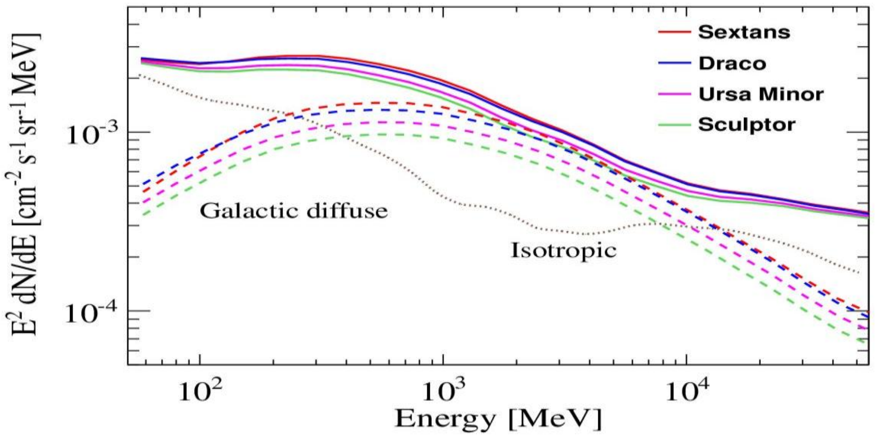

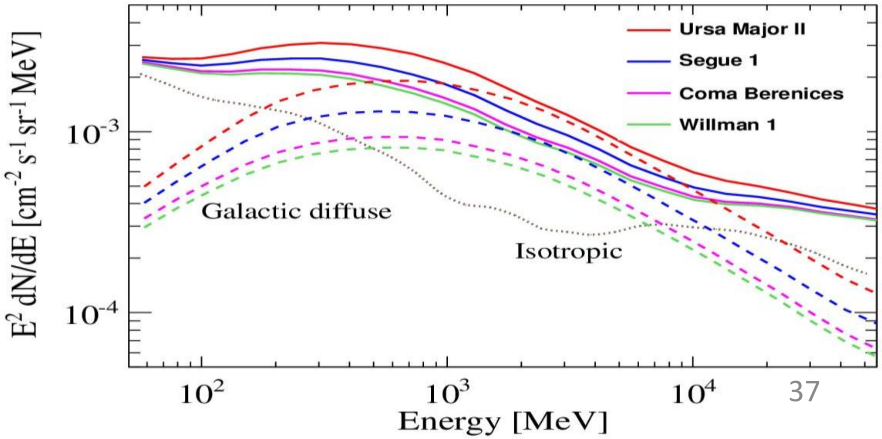

Detector Capabilities

Satellite- type Obs

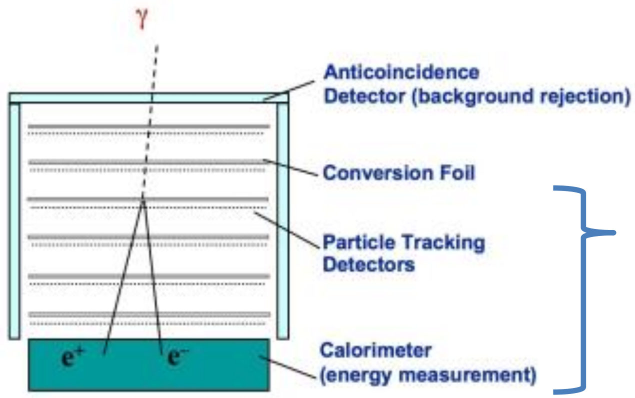

Direction Reconstruction

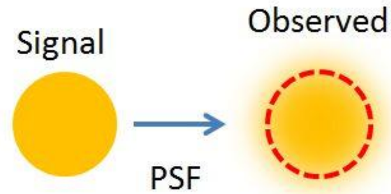

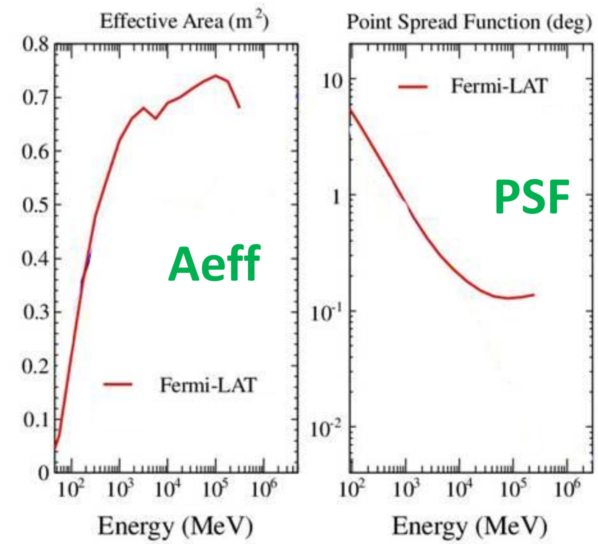

ROI: $\Delta\Omega_i = 2\pi(1 - \cos\alpha_i)$

$$\alpha_i = [(0.5^\circ)^2 + \psi_{68}^2(E_i)]^{1/2}$$

Typical dSphs Size PSF (68 % containment angle)

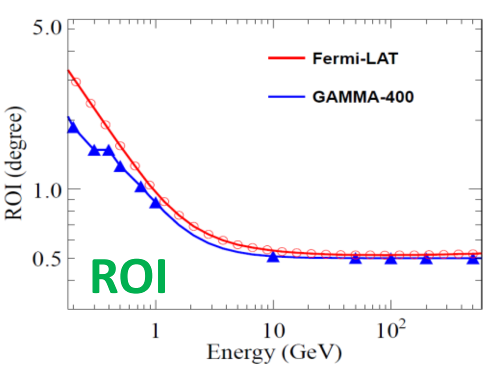

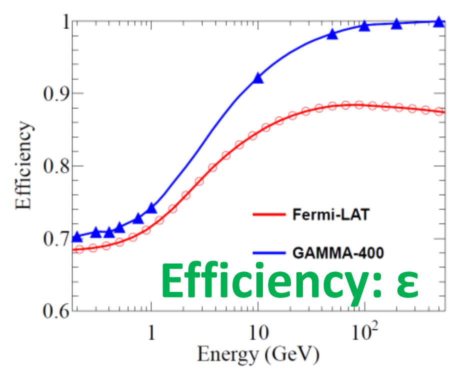

Signal Flux

$$\mathcal{F}_a^{(\mathrm{S})}(E, \Delta\Omega_i) = \epsilon(\Delta\Omega_i)\,\Phi_a(E, \Delta\Omega_i)$$

PSF effect -> efficiency ε

Background Flux

$$\mathcal{F}_a^{(\mathrm{B})}(E, \Delta\Omega_i) = \Delta\Omega_i\,(d\Phi_a^{\mathrm{B}}(E)/d\Omega)$$

Large ΔΩ -> Large Background

Sensitivity Line

Profile Likelihood

J-factor error is included

$$\mathcal{L}[\langle\sigma v\rangle, \{J_a\}] \equiv \prod_{a,i} \frac{P\left(N_{ai}; S_{ai}[\langle\sigma v\rangle, J_a] + B_{ai}\right)}{P\left(N_{ai}; N_{ai}\right)} G\left(J_a; \log_{10} J_a^{(\mathrm{obs})}, \delta(\log_{10} J_a^{(\mathrm{obs})})\right)$$

P(N:λ): Poisson
G(x: μ, σ): Log Gaussian
N_{ai}: Observed Events

Test (95% C.L)

$$-2\ln\mathcal{L}(\langle\sigma v\rangle, \{J_{\min}\}) + 2\ln\mathcal{L}(0, \{J_{\min}\}) = 2.71$$

2000 Pseudo Experiments for N_{ai} ($\{N^{(1)}_{ai}, N^{(2)}_{ai}, N^{(3)}_{ai} \ldots\}$)
(Poisson with the mean of B_{ai})

Each $N^{(i)}_{ai} \rightarrow \langle\sigma v\rangle^{(i)}$

Right Figure:
Mean and 68 (95) % band
for the set $\{\langle\sigma v\rangle^{(1)}, \langle\sigma v\rangle^{(2)}, \langle\sigma v\rangle^{(3)}, \ldots\}$

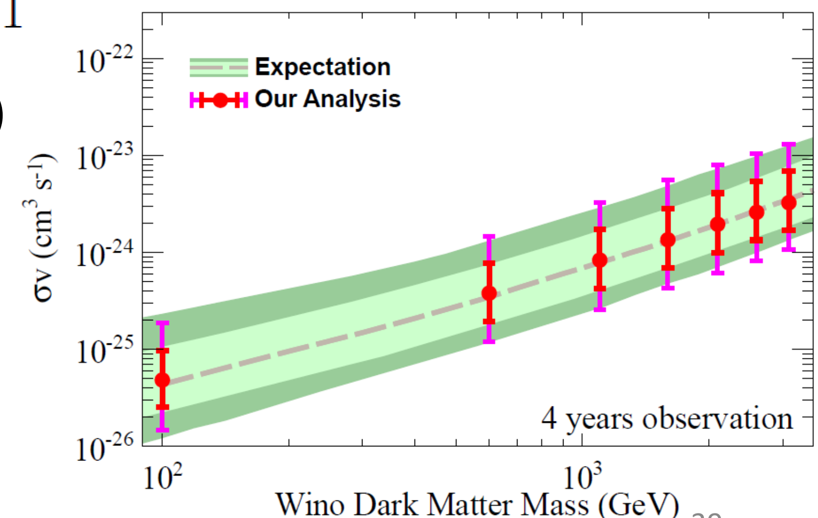

CMB

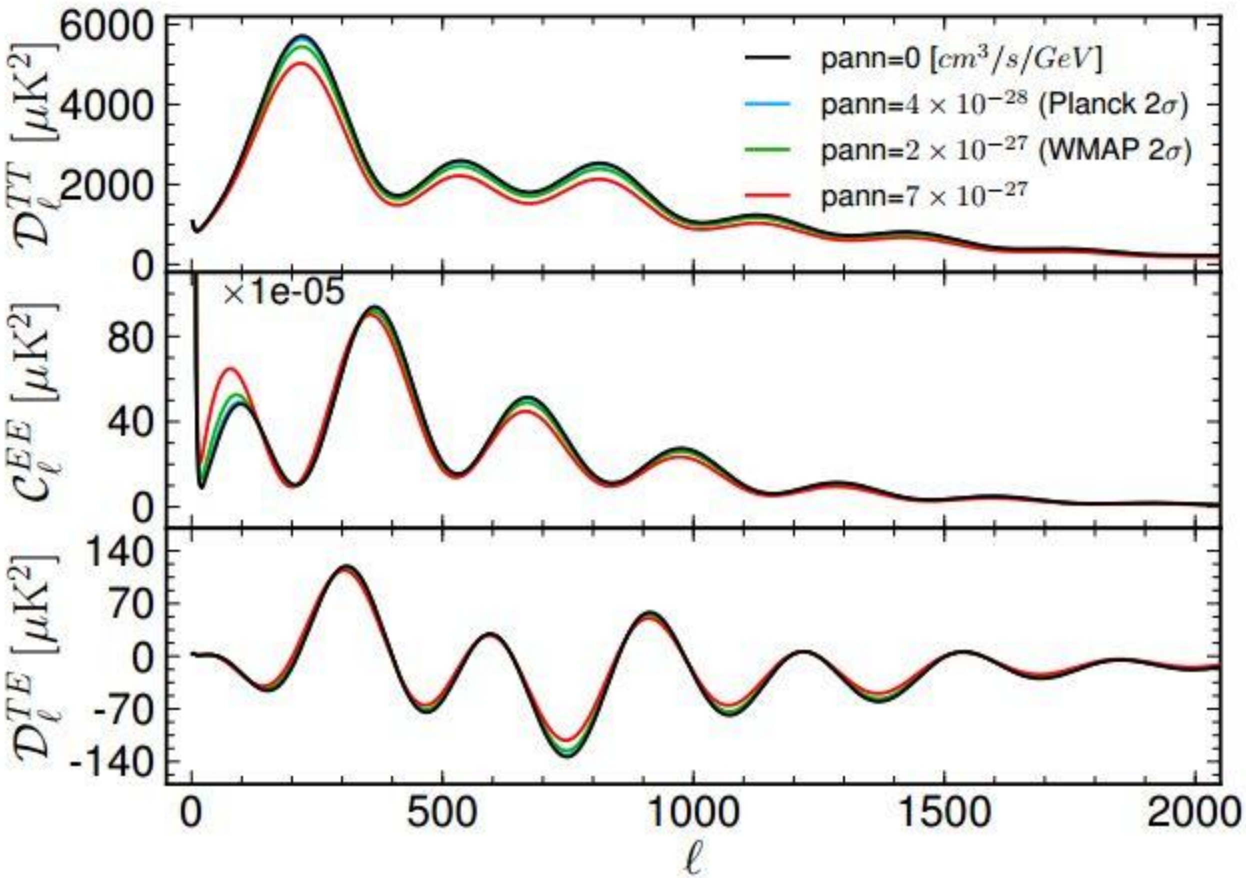

DM annihilation:

- Suppresses amplitude (very degenerate with other parameters).
- Enhances polarization at large scales (l<~300).

$$p_{ann} = f_{eff} \frac{<\sigma v>}{m_\chi}$$

S. Galli, Ferrara, 1 Dec 2014

Mean Free Path of gamma-ray

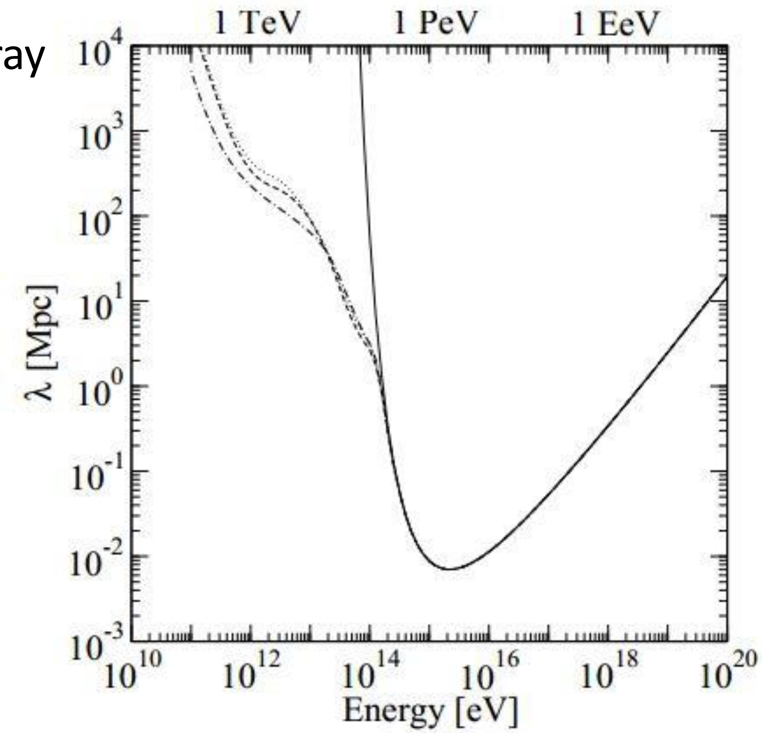

FIG. 1.— Pair production mean free path for VHE photons propagating through the present-day ($z = 0$) soft photon background as a function of energy for four different models of the background. *Solid:* Soft photon background consisting of only the CMB. *Dotted:* Soft photon background consisting of the CMB and the Gilmore et al. 2009 model of the EBL. *Dot-dashed:* Soft photon background consisting of the CMB and the Stecker et al. 2006 model of the EBL. *Dashed:* For comparison, the soft photon background consisting of the CMB and the Kneiske 2008 model of the EBL.

T. Venters, arXiv:1001.1363

BG photon component

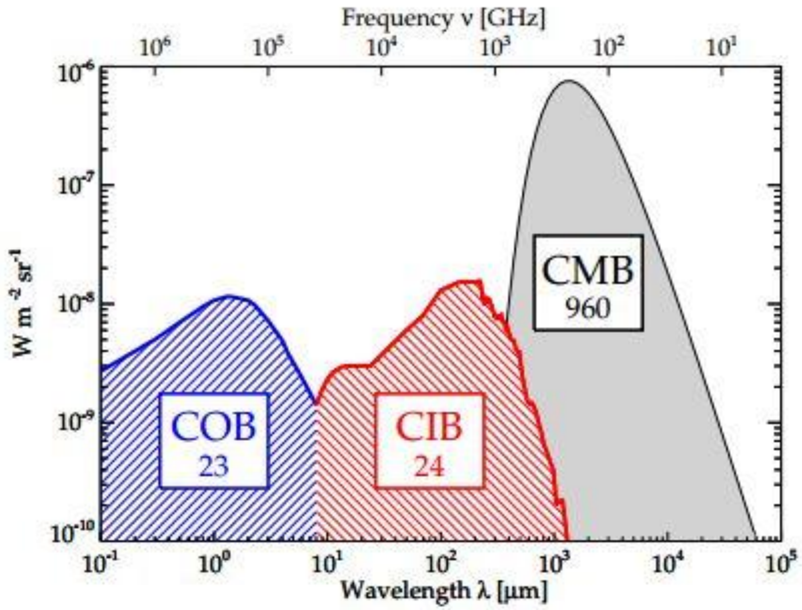

Fig. 14. Schematic Spectral Energy Distributions of the most important (by intensity) backgrounds in the universe, and their approximate brightness in nW m^{-2} sr^{-1} written in the boxes. From right to left: the Cosmic Microwave Background (CMB), the Cosmic Infrared Background (CIB) and the Cosmic Optical Background (COB).

H. Dole et al., astro-ph/0603208

Name	GLON (deg)	GLAT (deg)	Distance (kpc)	$\overline{\log_{10}(\mathrm{J}^{\mathrm{NFW}})}$ [a] ($\log_{10}[\mathrm{GeV}^2\,\mathrm{cm}^{-5}\,\mathrm{sr}]$)	$\overline{\log_{10}(\alpha_s^{\mathrm{NFW}})}$ ($\log_{10}[\mathrm{deg}]$)	$\overline{\log_{10}(\mathrm{J}^{\mathrm{Burkert}})}$ [a] ($\log_{10}[\mathrm{GeV}^2\,\mathrm{cm}^{-5}\,\mathrm{sr}]$)	$\overline{\log_{10}(\alpha_s^{\mathrm{Burkert}})}$ ($\log_{10}[\mathrm{deg}]$)
Bootes I	358.1	69.6	66	18.8 ± 0.22	-0.6 ± 0.3	18.6 ± 0.17	-1.1 ± 0.2
Bootes II	353.7	68.9	42	–	–	–	–
Bootes III	35.4	75.4	47	–	–	–	–
Canes Venatici I	74.3	79.8	218	17.7 ± 0.26	-1.3 ± 0.2	17.6 ± 0.17	-1.6 ± 0.1
Canes Venatici II	113.6	82.7	160	17.9 ± 0.25	-1.1 ± 0.4	17.8 ± 0.19	-1.6 ± 0.2
Canis Major	240.0	-8.0	7	–	–	–	–
Carina	260.1	-22.2	105	18.1 ± 0.23	-1.0 ± 0.3	18.1 ± 0.16	-1.5 ± 0.1
Coma Berenices	241.9	83.6	44	19.0 ± 0.25	-0.6 ± 0.5	18.9 ± 0.21	-1.1 ± 0.3
Draco	86.4	34.7	76	18.8 ± 0.16	-0.6 ± 0.2	18.7 ± 0.17	-1.0 ± 0.2
Fornax	237.1	-65.7	147	18.2 ± 0.21	-0.8 ± 0.2	18.1 ± 0.22	-1.1 ± 0.1
Hercules	28.7	36.9	132	18.1 ± 0.25	-1.1 ± 0.4	17.9 ± 0.19	-1.6 ± 0.2
Leo I	226.0	49.1	254	17.7 ± 0.18	-1.1 ± 0.3	17.6 ± 0.17	-1.5 ± 0.2
Leo II	220.2	67.2	233	17.6 ± 0.18	-1.1 ± 0.5	17.5 ± 0.15	-1.9 ± 0.5
Leo IV	265.4	56.5	154	17.9 ± 0.28	-1.1 ± 0.4	17.8 ± 0.21	-1.6 ± 0.2
Leo V	261.9	58.5	178	–	–	–	–
Pisces II	79.2	-47.1	182	–	–	–	–
Sagittarius	5.6	-14.2	26	–	–	–	–
Sculptor	287.5	-83.2	86	18.6 ± 0.18	-0.6 ± 0.3	18.5 ± 0.17	-1.1 ± 0.2
Segue 1	220.5	50.4	23	19.5 ± 0.29	-0.4 ± 0.5	19.4 ± 0.24	-0.9 ± 0.2
Segue 2	149.4	-38.1	35	–	–	–	–
Sextans	243.5	42.3	86	18.4 ± 0.27	-0.9 ± 0.2	18.4 ± 0.16	-1.2 ± 0.1
Ursa Major I	159.4	54.4	97	18.3 ± 0.24	-1.0 ± 0.3	18.2 ± 0.18	-1.4 ± 0.2
Ursa Major II	152.5	37.4	32	19.3 ± 0.28	-0.5 ± 0.4	19.2 ± 0.21	-0.9 ± 0.2
Ursa Minor	105.0	44.8	76	18.8 ± 0.19	-0.5 ± 0.2	18.7 ± 0.20	-0.9 ± 0.2
Willman 1	158.6	56.8	38	19.1 ± 0.31	-0.6 ± 0.5	19.0 ± 0.28	-1.1 ± 0.2

[a] J-factors are calculated over a solid angle of $\Delta\Omega \sim 2.4 \times 10^{-4}$ sr.

Fermi-LAT arXiv:1310.0828v1 [astro-ph.HE]

TABLE 1
PROPERTIES OF MILKY WAY SATELLITES* AND STELLAR-KINEMATIC SAMPLES

object	RA (J2000) [hh:mm:ss]	Dec. (J2000) [dd:mm:ss]	Distance [kpc]	M_V [mag]	R_{half} [pc]	N_{sample} [pc]	r_{max} [pc]
Carina	06:41:36.7	−50:57:58	105 ± 6	-9.1 ± 0.5	250 ± 39	774	2224^{+885}_{-441}
Draco	17:20:12.4	+57:54:55	76 ± 6	-8.8 ± 0.3	221 ± 19	292	1866^{+715}_{-317}
Fornax	02:39:59.3	−34:26:57	147 ± 12	-13.4 ± 0.3	710 ± 77	2483	6272^{+2616}_{-1366}
Leo I	10:08:28.1	+12:18:23	254 ± 15	-12.0 ± 0.3	251 ± 27	267	1948^{+794}_{-407}
Leo II	11:13:28.8	+22:09:06	233 ± 14	-9.8 ± 0.3	176 ± 42	126	824^{+345}_{-178}
Sculptor	01:00:09.4	−33:42:33	86 ± 6	-11.1 ± 0.5	283 ± 45	1365	2673^{+1099}_{-569}
Sextans	10:13:03.0	−01:36:53	86 ± 4	-9.3 ± 0.5	695 ± 44	441	2544^{+1109}_{-587}
Ursa Minor	15:09:08.5	+67:13:21	76 ± 3	-8.8 ± 0.5	181 ± 27	313	1580^{+626}_{-312}
Bootes I	14:00:06.0	+14:30:00	66 ± 2	-6.3 ± 0.2	242 ± 21	37	544^{+252}_{-135}
Canes Venatici I	13:28:03.5	+33:33:21	218 ± 10	-8.6 ± 0.2	564 ± 36	214	2030^{+884}_{-468}
Canes Venatici II	12:57:10.0	+34:19:15	160 ± 4	-4.9 ± 0.5	74 ± 14	25	352^{+105}_{-28}
Coma Berenices	12:26:59.0	+23:54:15	44 ± 4	-4.1 ± 0.5	77 ± 10	59	238^{+103}_{-53}
Hercules	16:31:02.0	+12:47:30	132 ± 12	-6.6 ± 0.4	330^{+75}_{-52}	30	638^{+295}_{-147}
Leo IV	11:32:57.0	−00:32:00	154 ± 6	-5.8 ± 0.4	206 ± 37	18	443^{+197}_{-95}
Leo V	11:31:09.6	+02:13:12	178 ± 10	-5.2 ± 0.4	135 ± 32	5	201^{+95}_{-43}
Leo T	09:34:53.4	+17:03:05	417 ± 19	-8.0 ± 0.5	120 ± 9	19	534^{+183}_{-60}
Segue 1	10:07:04.0	+16:04:55	23 ± 2	-1.5 ± 0.8	29^{+8}_{-5}	70	139^{+56}_{-28}
Segue 2	02:19:16.0	+20:10:31	35 ± 2	-2.5 ± 0.3	35 ± 3	25	119^{+45}_{-18}
Ursa Major I	10:34:52.8	+51:55:12	97 ± 4	-5.5 ± 0.3	319 ± 50	39	732^{+338}_{-181}
Ursa Major II	08:51:30.0	+63:07:48	32 ± 4	-4.2 ± 0.6	149 ± 21	20	294^{+139}_{-74}

Geringer-Sameth et al., arXiv:1408.0002

Fragmentation

Simulation Code: Pythia, HERWIG…

Tuned by Collider Exp at High Energy Region

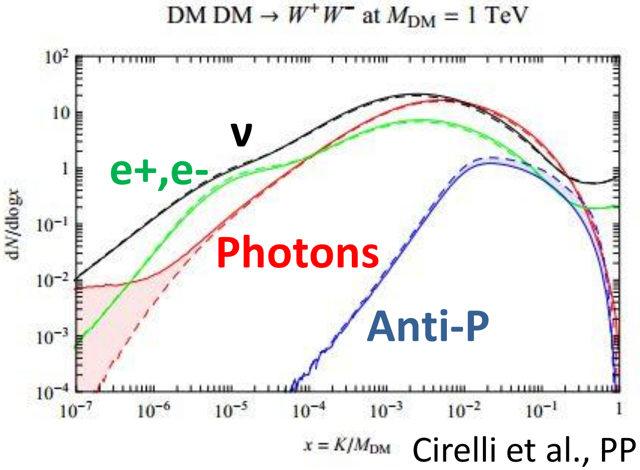

Cirelli et al., PPPC4

100 GeV DM anni -> WW-> γ (Cembranos et al., 2013)

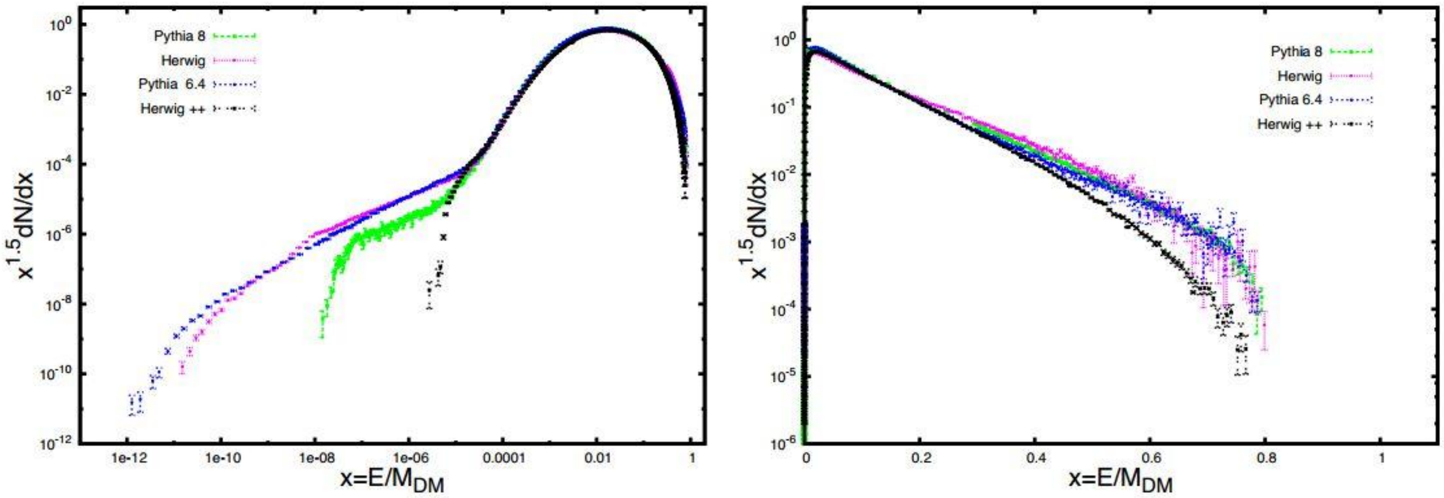

Point-like Source

Origin

AGN	-1000 (Blazar: 800)
Unknown	-600
SN	-60
Pulsar	-100

Table 6. LAT 2FGL Source Classes

Description	Identified Designator	Identified Number	Associated Designator	Associated Number
Pulsar, identified by pulsations	PSR	83	...	...
Pulsar, no pulsations seen in LAT yet	...	...	psr	25
Pulsar wind nebula	PWN	3	pwn	0
Supernova remnant	SNR	6	snr	4
Supernova remnant / Pulsar wind nebula	...	...	†	58
Globular cluster	GLC	0	glc	11
High-mass binary	HMB	4	hmb	0
Nova	NOV	1	nov	0
BL Lac type of blazar	BZB	7	bzb	429
FSRQ type of blazar	BZQ	17	bzq	353
Non-blazar active galaxy	AGN	1	agn	10
Radio galaxy	RDG	2	rdg	10
Seyfert galaxy	SEY	1	sey	5
Active galaxy of uncertain type	AGU	0	agu	257
Normal galaxy (or part)	GAL	2	gal	4
Starburst galaxy	SBG	0	sbg	4
Class uncertain	...	...	...	1
Unassociated	...	...	...	575
Total	...	127	...	1746

Note. — The designation '†' indicates potential association with SNR or PWN (see Table 11). Designations shown in capital letters are firm identifications; lower case letters indicate associations. In the case of AGN, many of the associations have high confidence (Ackermann et al. 2011b). Among the pulsars, those with names beginning with LAT were discovered with the LAT. In the FITS version of the 2FGL catalog, the † designator is replaced with 'spp'; see Appendix C.

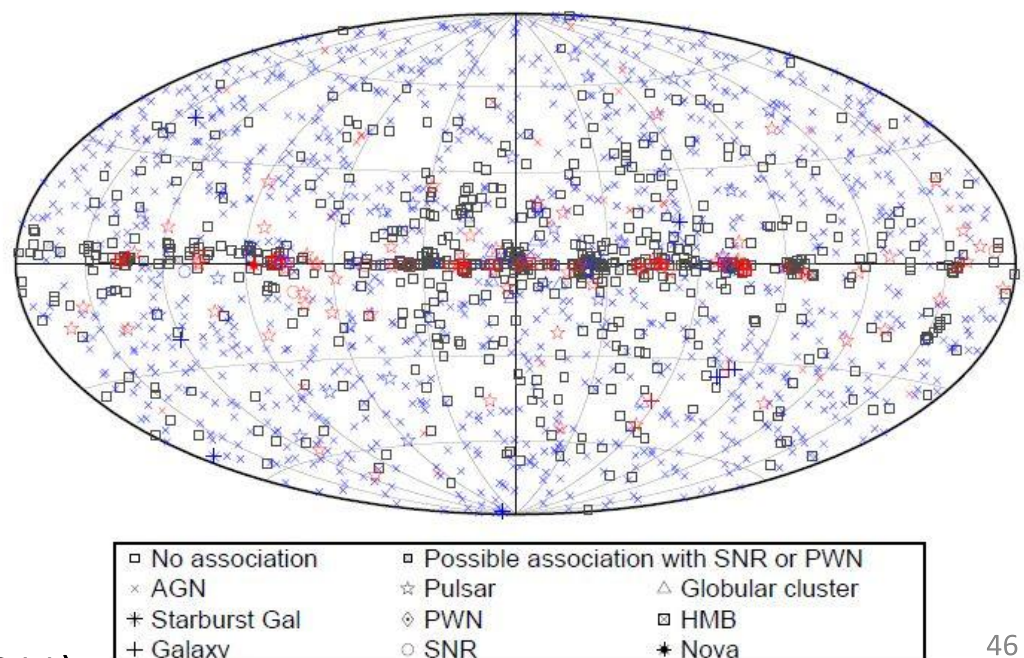

LAT 2FGL (2011)

Galactic Diffuse

Origin

Decay of π^0 (CR + ISM)
Bremsstrahlung (CRe + ISM)
Inverse Compton scattering in Interstellar radiation field (ISRF)
(Large Scale Structure (Loop I, Fermi Bubbles))

Model: GALPROP + Input

Interstellar gas distribution (mainly HI, HII at high latitude)
ISRF model
Large Scale Structure Templates
Parameters of diffusion equation

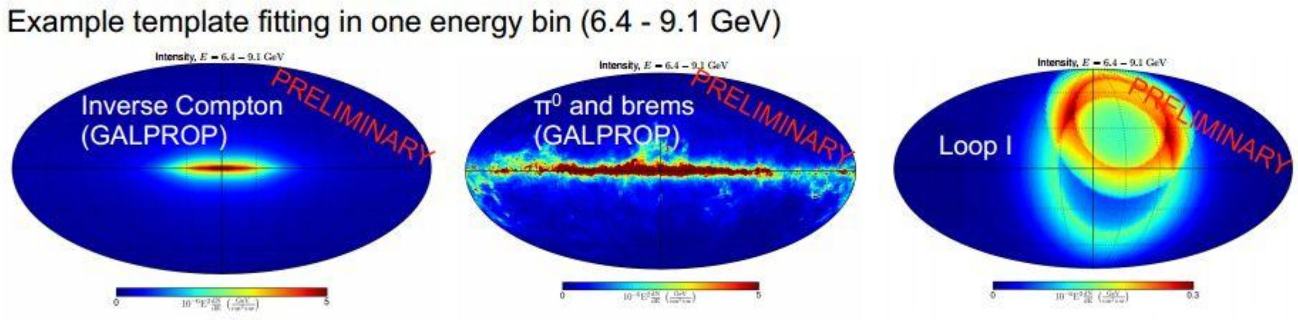

Fermi-LAT, “Two Methods to Study the Fermi Bubbles”

A. Sellerholm, "Cosmological Dark Matter and the Isotropic Gamma-Ray Background"

HI

H2

HII

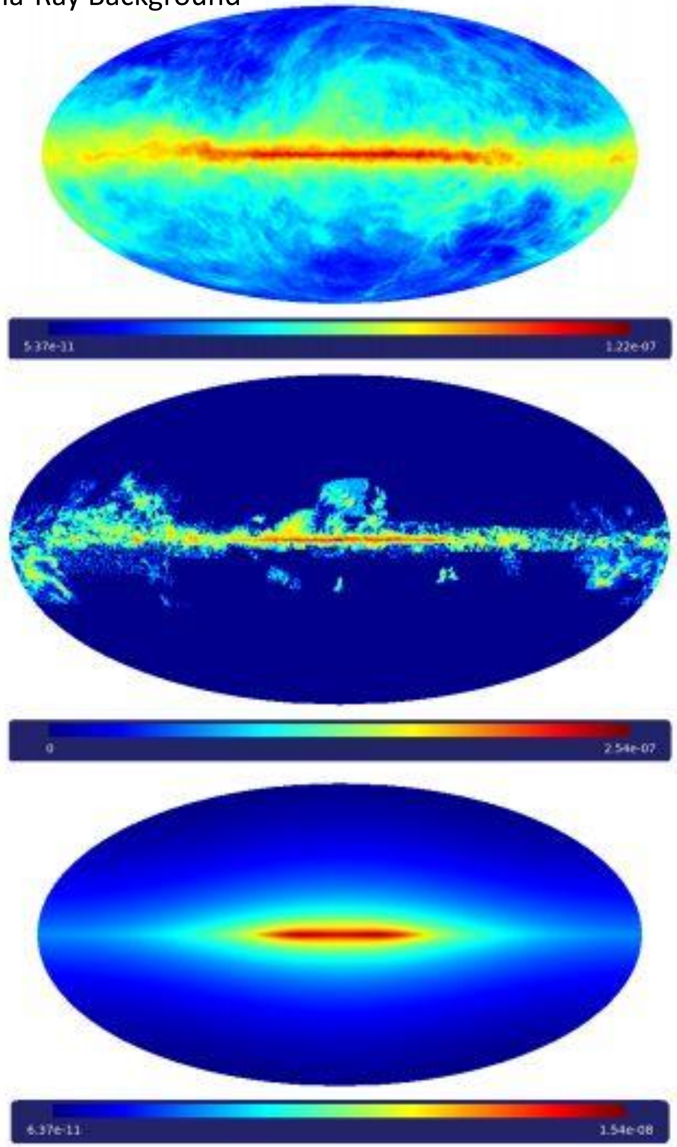

Figure 4.2: Spatial distribution of the differential energy spectrum of gamma-rays, at 1.2 GeV, originating from the HI (top), H_2 (middle) and HII (bottom), through bremsstrahlung and π^0-decay. The maps are in galactic co-ordinates and the colour scale is logarithmic. They were generated using GALPROP and the differential energy spectra can be seen in figure 4.5.

Interstellar gas maps

- use gas maps as in the GALPROP code (http://galprop.stanford.edu/webrun.php)

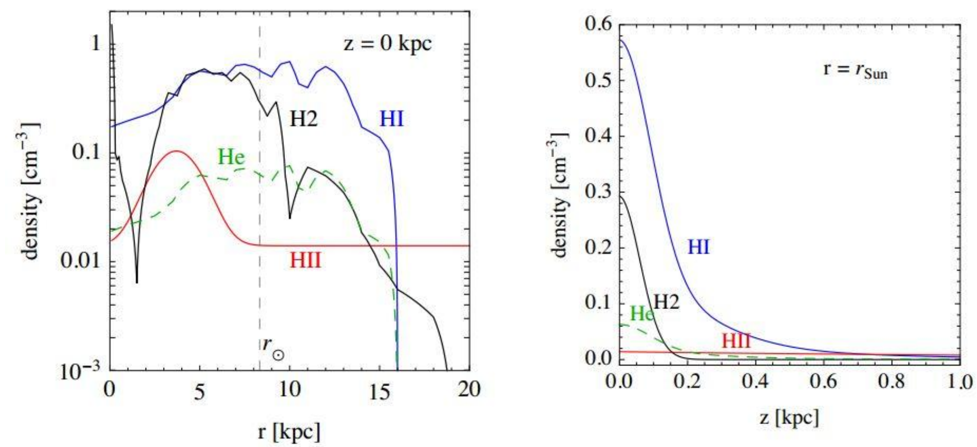

[Gordon & Burton, ApJ 208 (1976); Dickey & Lockman, Ann. Rev. Astron. Astrophys. 28 (1990); Cox+, A&A, 155 (1986); Bronfman+, Astrophys. J. 324 (1988); Wouterloot+, A&A 230 (1990); Gaensler+, Publ. Astron. Soc. of Australia 25 (2008)]

M. Cirelli et al., **JCAP 1311 (2013) 035** [arXiv: 1307:7152]

Diffuse components

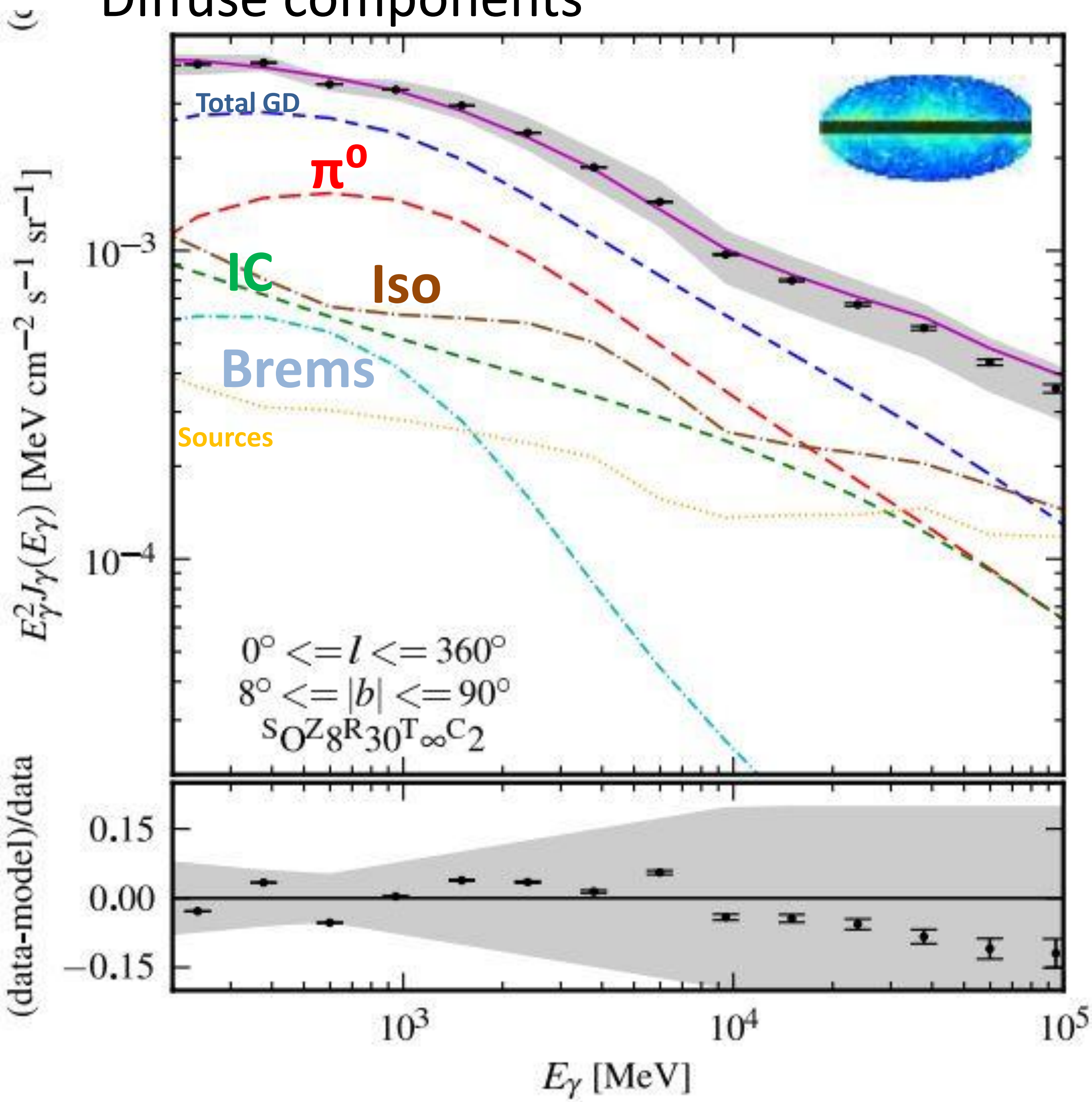

LAT 2012
ApJ. 750

Isotropic Diffuse

Origin:

Unsolved Extragalactic source

AGN, Starburst galaxies, γ-ray burst…

Model:

(Obs) – (Galactic Diffuse) – (Point Sources)

Uncertainty:

- GD model (Gas, ISRF, diffusion params
- Unknown Source

  -> Less than 10-20 %
- Miss identified CR (>10 GeV)

  -> Event Selection Dependence

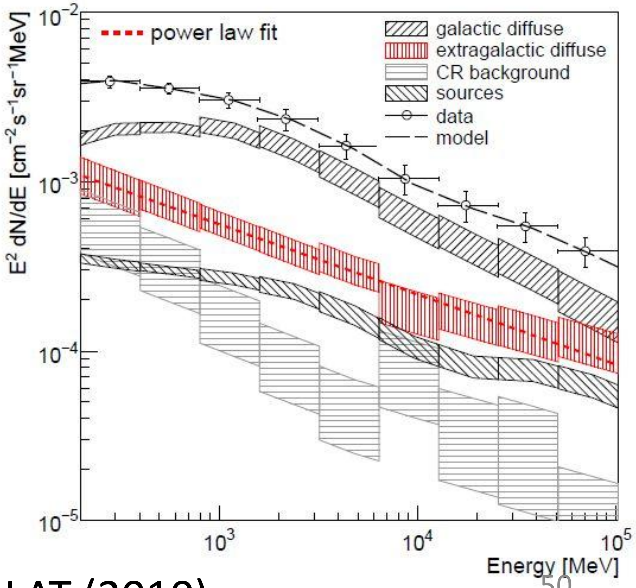

LAT (2010)

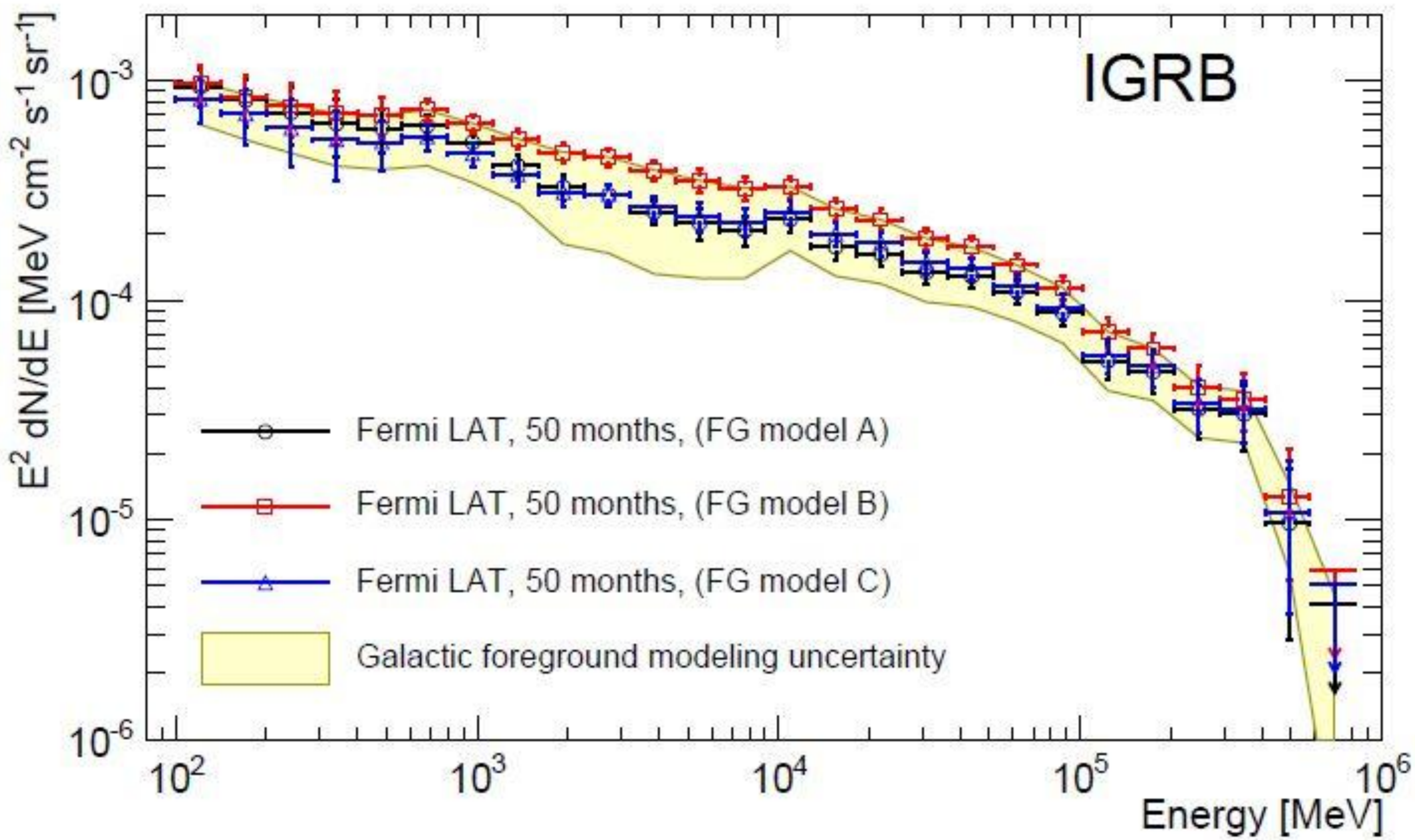

Fermi LAT, arXiv:1410.3696

Direct Detection for Wino

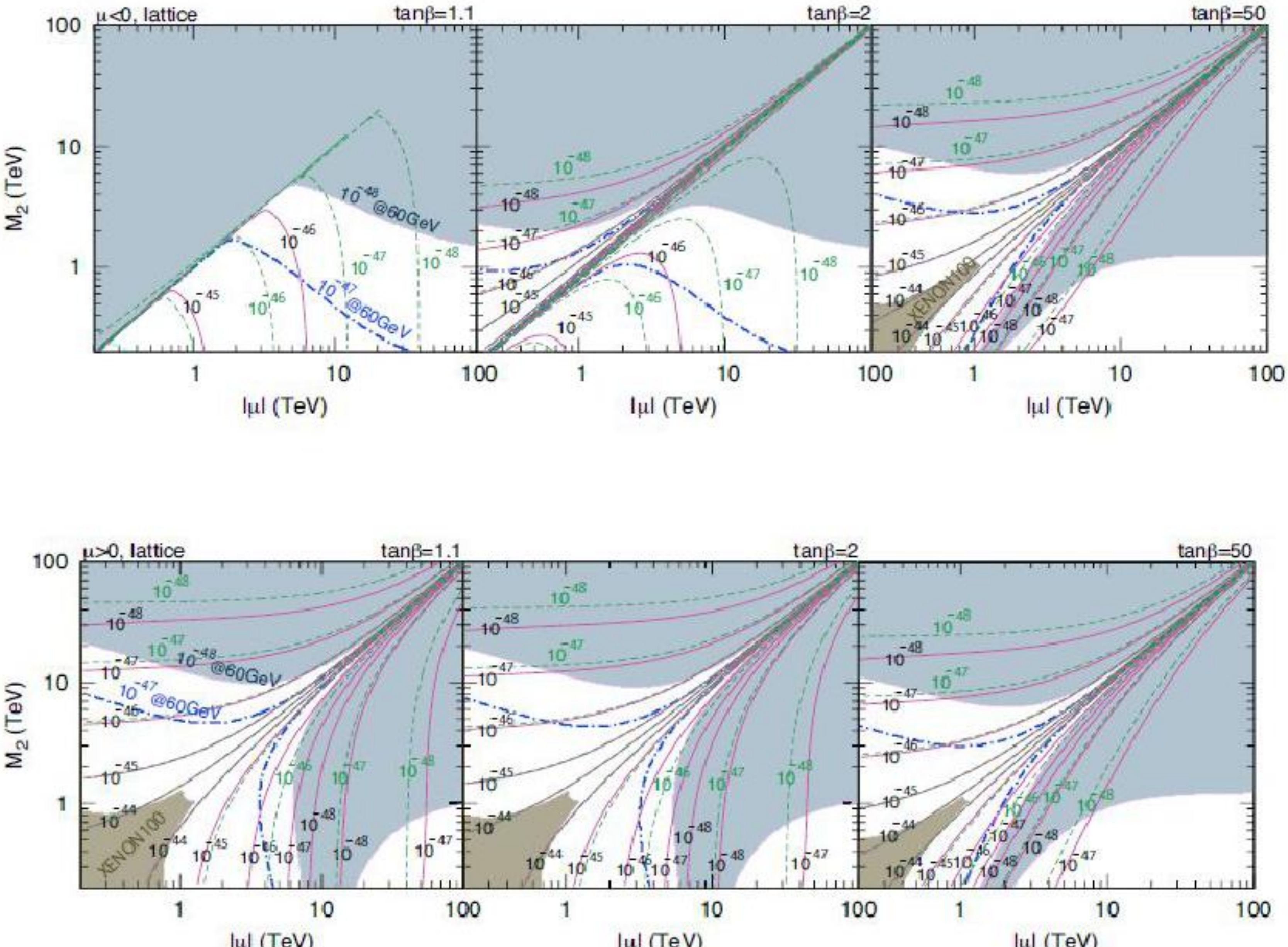

Purple
Numer
Result

Dark S
Exclus
by XE

Blue D
Future
(a ton-
Xenon
exp)

Astrophysical Factor

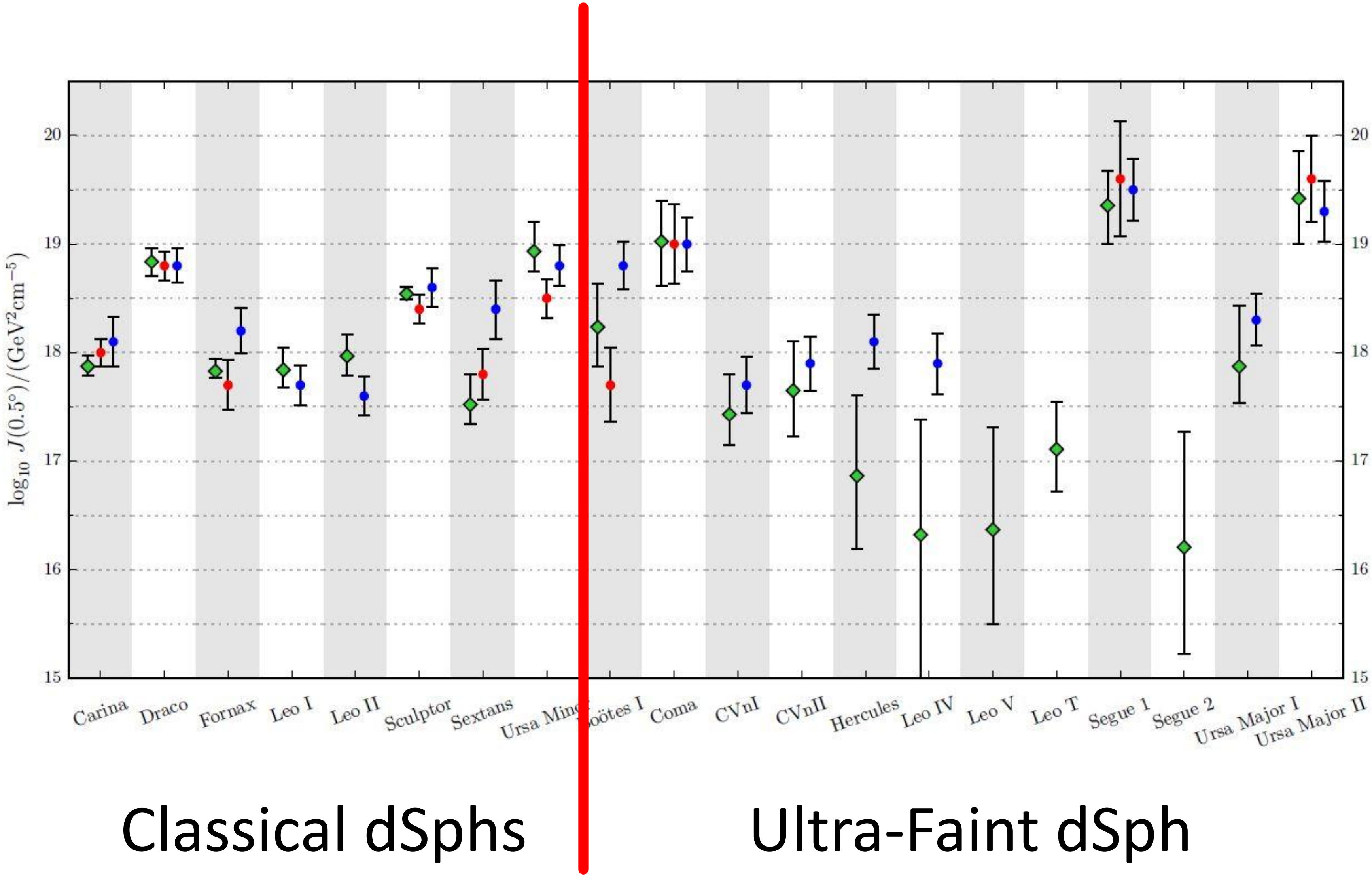

Classical dSphs

Ultra-Faint dSph

Geringer-Sameth et al., arXiv:1410.2242

Astrophysical Factor

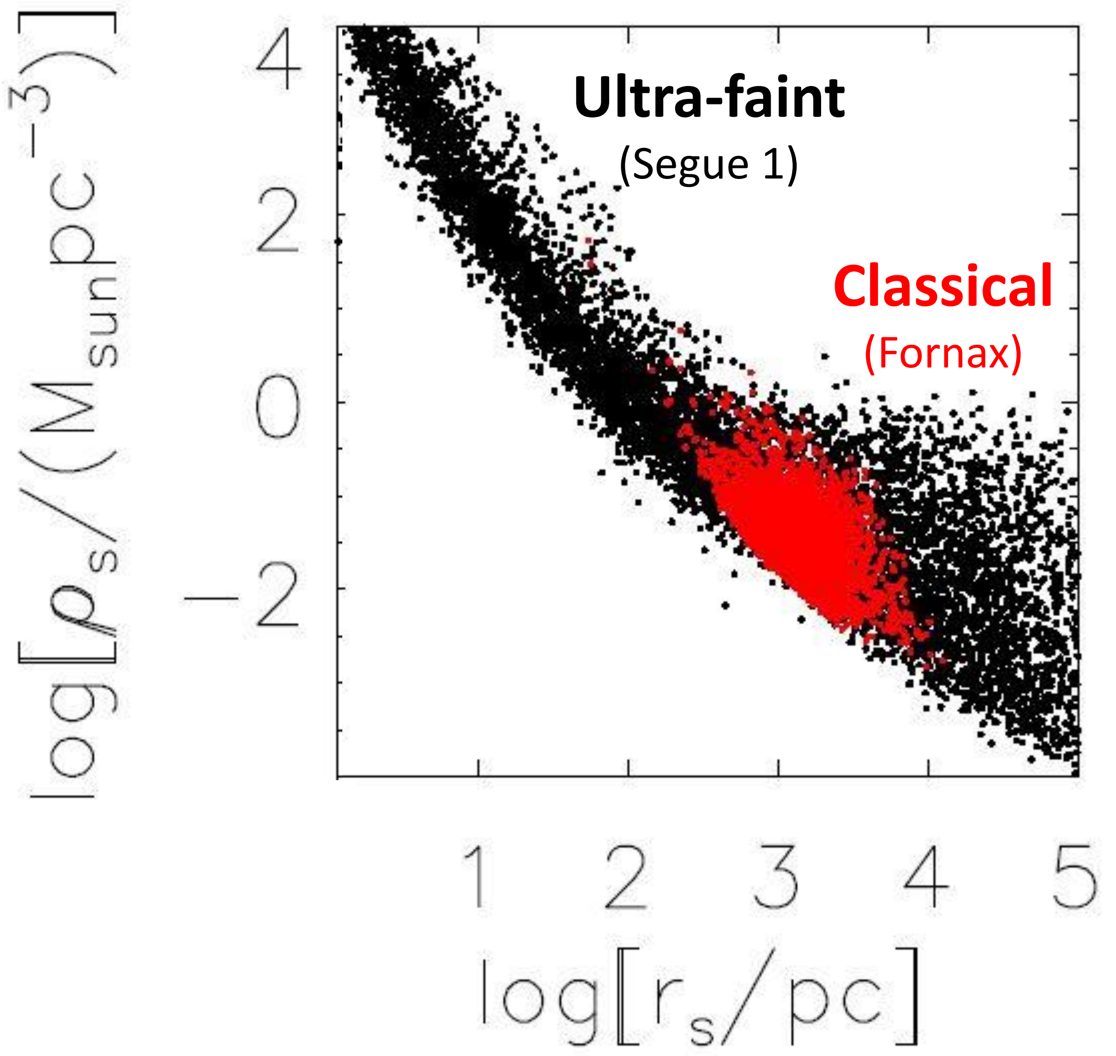

Geringer-Sameth et al., arXiv:1408.0002

Astrophysical Factor

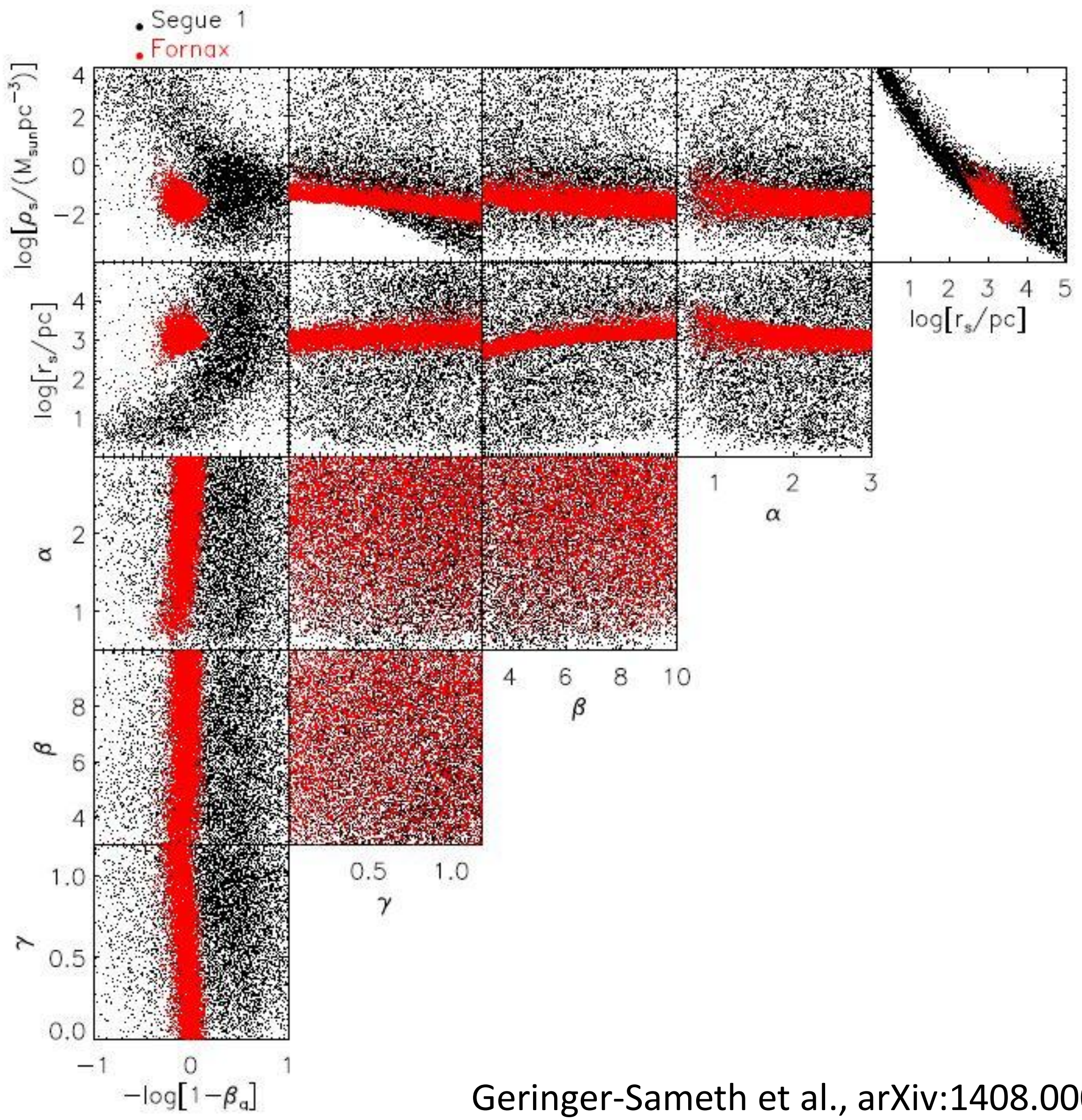

Geringer-Sameth et al., arXiv:1408.0002

Astrophysical Factor

Mock Data => J-factor: Sample dependence

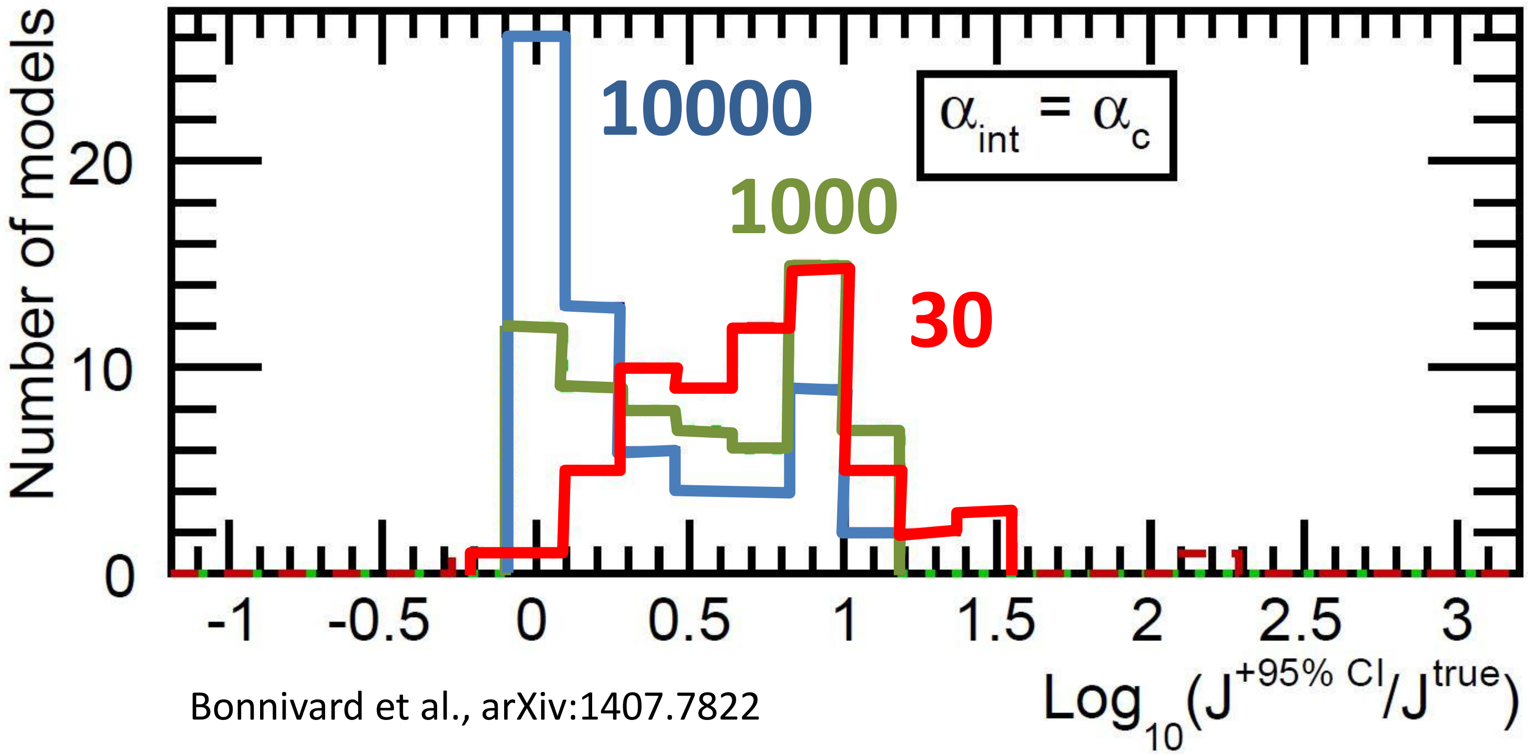

Bonnivard et al., arXiv:1407.7822

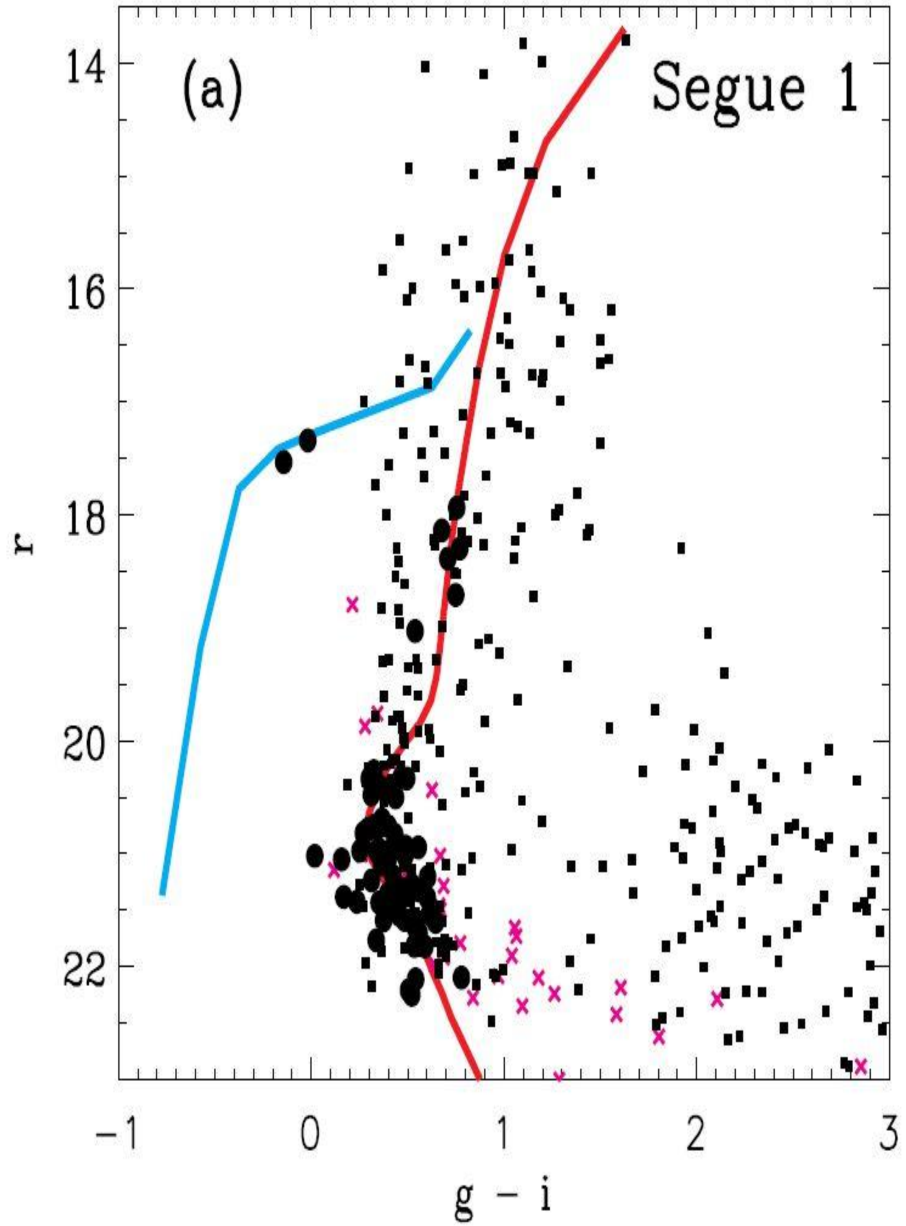

J. D. Simon et al., (2011)

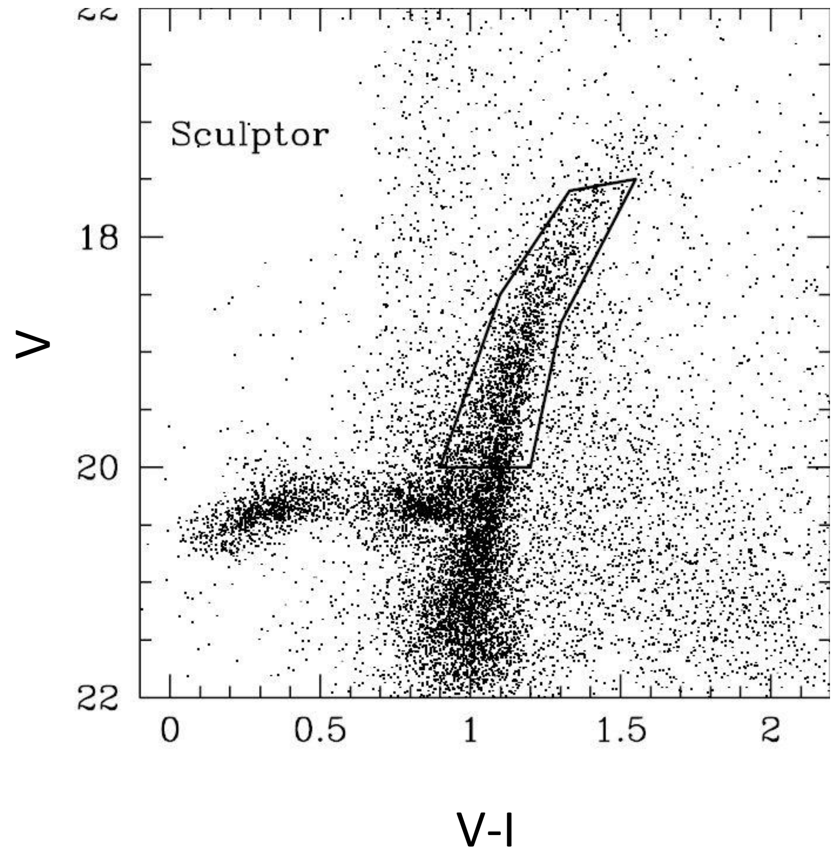

M. G. Walker et al,. (2007)

LAM
LABORATOIRE D'ASTROPHYSIQUE DE MARSEILLE

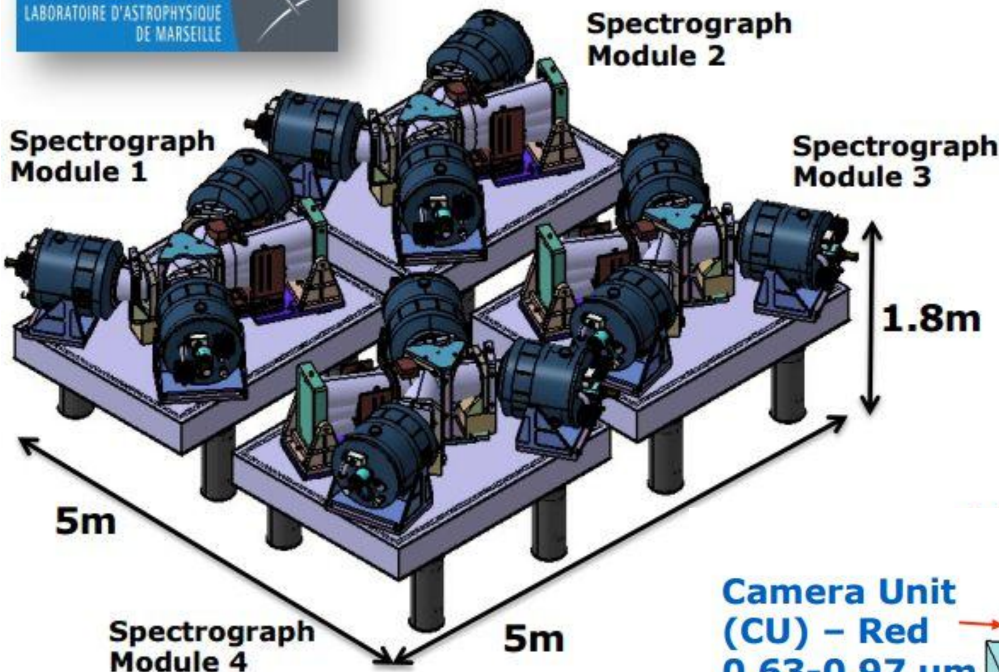

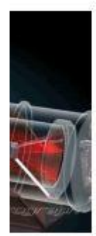

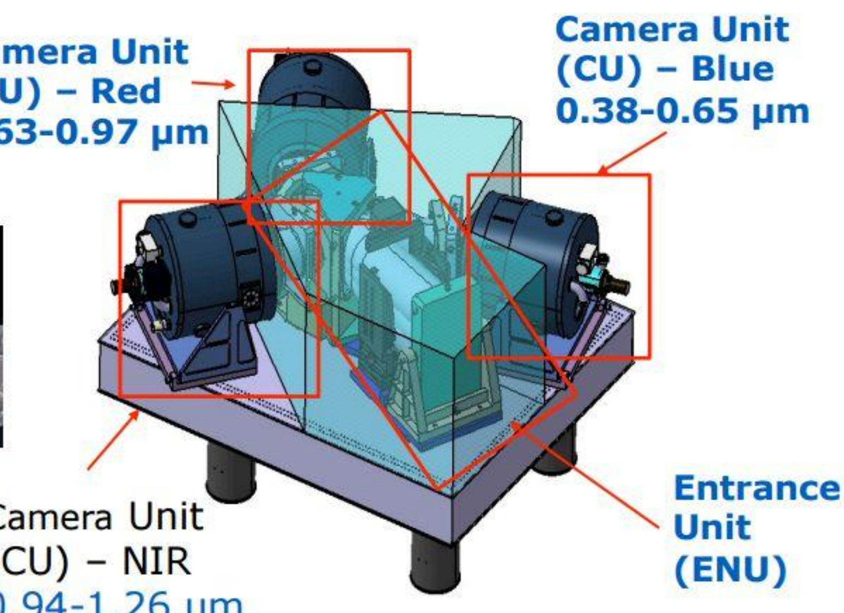

L. Tresse (Slide)

Draco	× [3] [4]	Walker et al. (2009b) Charbonnier et al. (2011)	Magellan/MMFS.
Ursa Minor	× [3] [4]	Walker et al. (2009b) Charbonnier et al. (2011)	Magellan/MMFS.
Sextans	[5]	Walker, Mateo & Olszewski (2009)	Magellan/MMFS.
Fornax	[5]	Walker, Mateo & Olszewski (2009)	Magellan/MMFS.
Sculptor	[5]	Walker, Mateo & Olszewski (2009)	Magellan/MMFS.
Carina	[5]	Walker, Mateo & Olszewski (2009)	Magellan/MMFS.
LeoI	[6]	Mateo et al. (2008)	MMT/Hectochelle.
LeoII	× [3] [4]	Walker et al. (2009b) Charbonnier et al. (2011)	Magellan/MMFS.

Coma Berenices	× [7]	Simon & Geha (2007)	Keck/DEIMOS.
Canes Venatici I	× [7]	Simon & Geha (2007)	Keck/DEIMOS.
Canes Venatici II	× [7]	Simon & Geha (2007)	Keck/DEIMOS.
Leo IV, Leo T	× [7]	Simon & Geha (2007)	Keck/DEIMOS.
Ursa Major I	× [7]	Simon & Geha (2007)	Keck/DEIMOS.
Ursa Major II	× [7]	Simon & Geha (2007)	Keck/DEIMOS.
Hercules	[8]	Aden et al. (2009b)	VLT/FLAMES+GIRAFFE.
Bootes I	[9]	Koposov et al. (2011)	VLT/FLAMES+GIRAFFE.
Leo V	[10]	Walker et al. (2009a)	MMT/Hectochelle.
Segue 1	[11]	Simon et al. (2011)	Keck/DEIMOS.
Segue 2	[12]	Kirby et al. (2013)	Keck/DEIMOS.
Sagittarius	[13] [14]	Not used	tidal disruption and/or non-equilibrium
Willman 1	[13] [14]	Not used	tidal disruption and/or non-equilibrium

Spectrograph	MMFS	Hectochelle	DEIMOS	FLAMES +GIRAFFE	PFS
Telescope	Magellan/Caly	MMT	Keck	VLT	Subaru
Caliber [m]	6.5	6.5	10	8.2	8.2
FoV (diam)					
[arcmin]	20	60	5×16.6	25	78
[deg]	0.33	1.0	(rectangle)	0.42	1.3
Resolution					
R	Blue: 25000 Red: 20000	25000	6000	6500	2500-5000
Range [Å]	Blue: 3200-5000 Red: 4900-10000	3800 - 9000	6500-9000	8180-9375	3800-12600
Fibler	Blue: 128 Red: 128	224	Slits	130	2394
dSphs	7 Classicals	Leo I, V	8 UFs	Hercules, Bootes I	—
Refs	URL1, URL2	URL1, URL2	URL1	[8] [9]	URL1

主鏡タイプ(所属: 設置場所):

分割鏡(セグメント鏡)

- GTC 10.4m (IAC: ORM, スペイン)
- Keck 10m x 2 (WMKO: Mauna Kea, 合衆国)
- HET 9.5m (MacDonald Obs.: Mt. Fowlkes, 合衆国)

メニスカス鏡

- Subaru 8.3m (国立天文台: Mauna Kea, 合衆国)
- VLT 8.2m x 4 (ESO: Cerro Paranal, チリ)
- Gemini 8.2m x 2 (Gemini Obs.: Mauna Kea, 合衆国
Cerro Pachon, チリ)

ハニカム鏡

- LBT 8.4m + 8.4m (アリゾナ大など:Mt.Graham, 合衆国)
- MMT 6.5m (Steward Obs.: Mt.Hopkins, 合衆国)
- Magellan 6.5m x 2 (OCIW: Cerro Manqui, チリ)

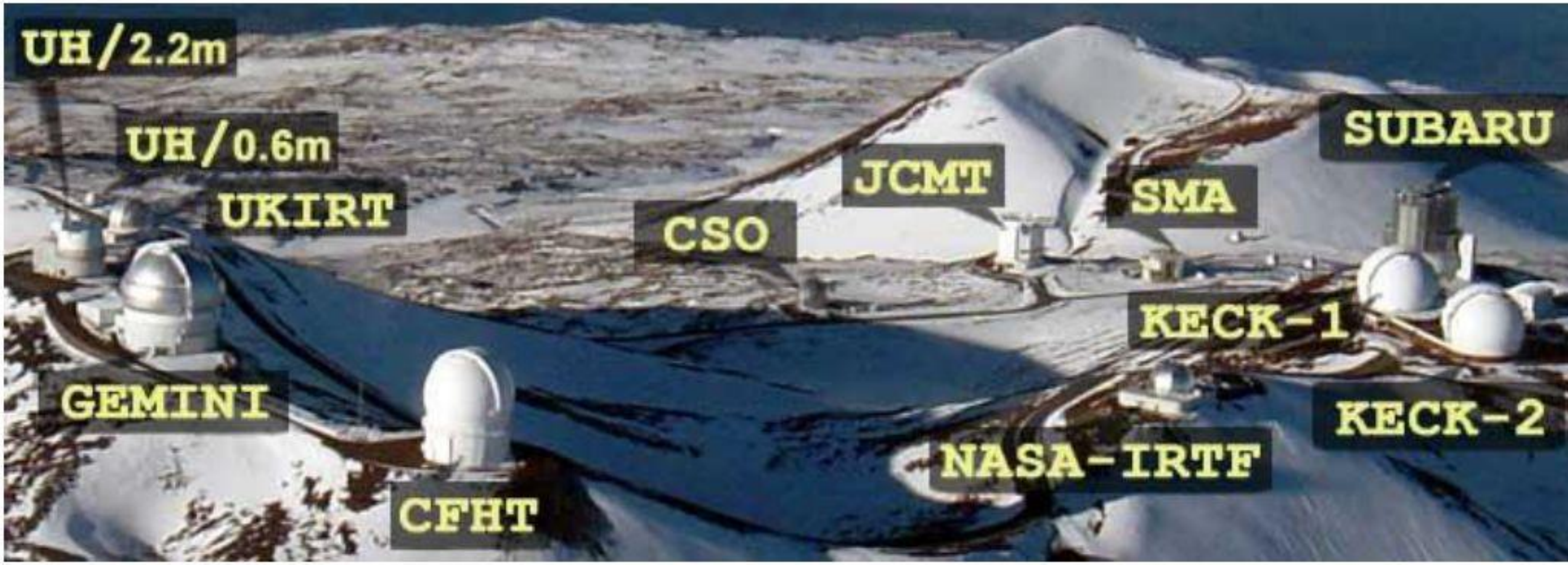

http://www.skymerica.com/Bigisland/subaru/

<u>/ith sound</u>

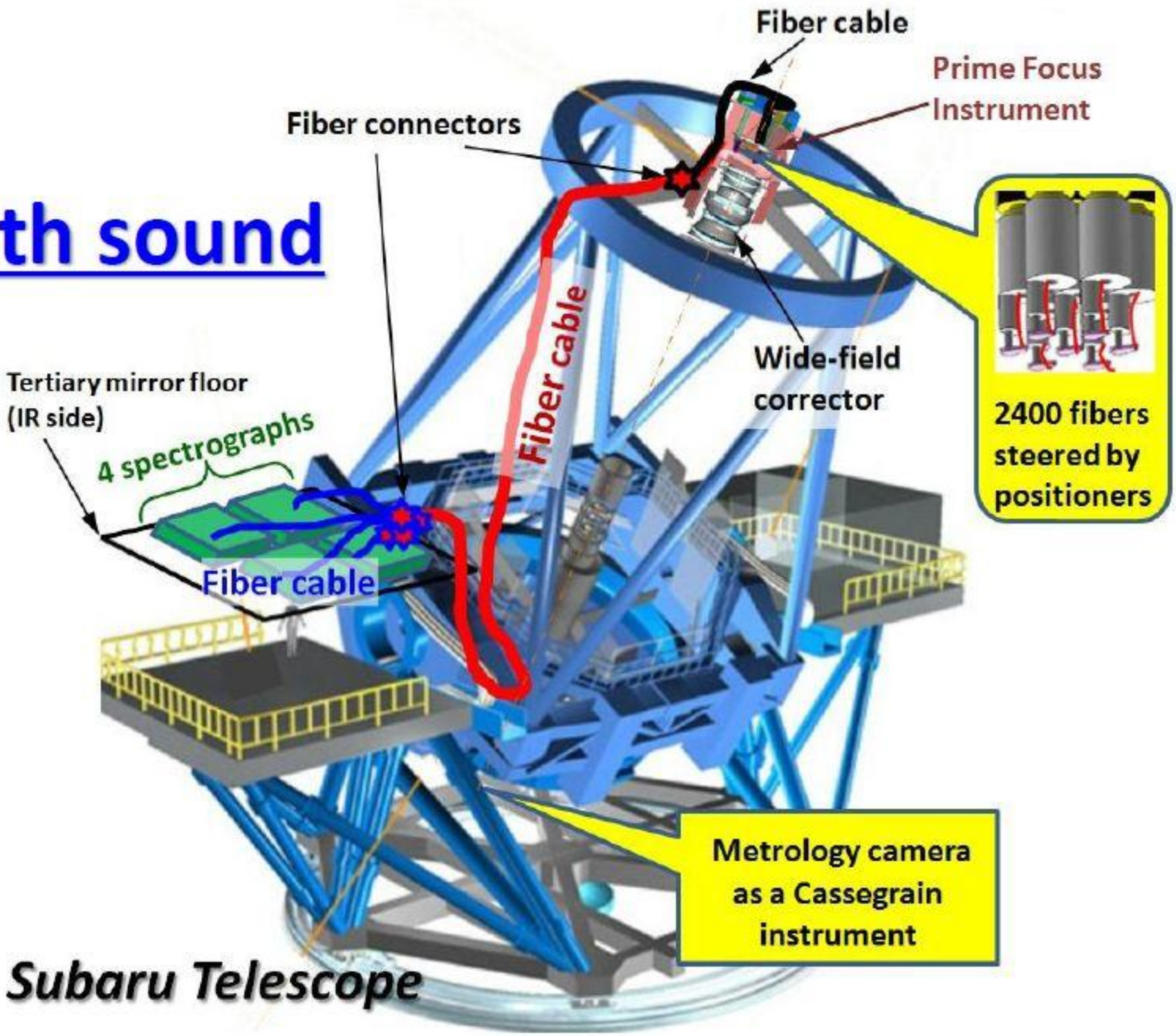
Fiber cable
Prime Focus Instrument
Fiber connectors
Fiber cable
Wide-field corrector
2400 fibers steered by positioners
Tertiary mirror floor (IR side)
4 spectrographs
Fiber cable
Metrology camera as a Cassegrain instrument
Subaru Telescope

生のObject画像

右が試験観測で取得されたIRS1の低分散モードでの生画像である。
横が波長分散方向で、0.9−1.8μ mを一度にカバーしている。縦が空間方向で、200ファイバー分のスペクトルが並び、20本毎のギャップは背景光補正に利用される。

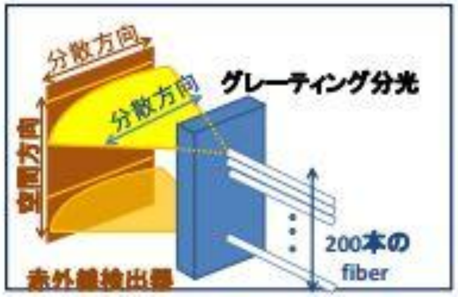

IRS1-LR,
exposure time : 15min
GOODSN
10/04/21 (HST)

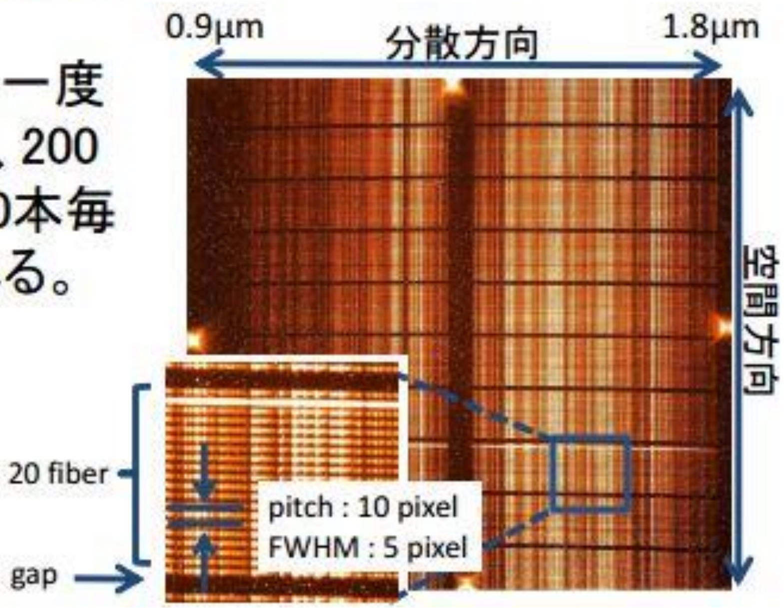

Arm	Coverage[nm]	Resolution[$\lambda/\delta\lambda$]
Blue	380 - 650	2500
Red	630 - 970	3200 (Medium resolution mode 710-885nm; R=5000)
NIR	940-1260	4500

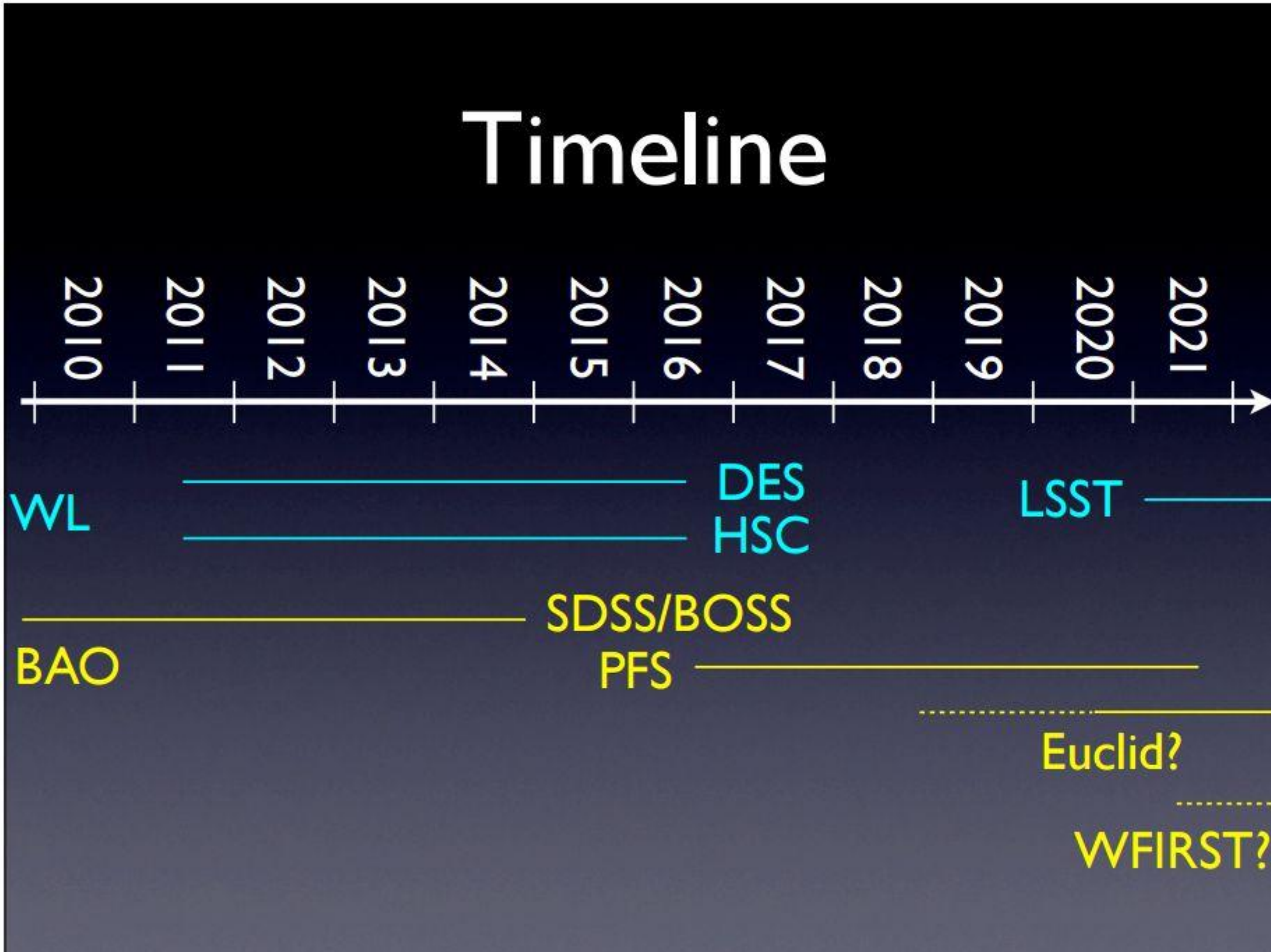
Timeline
2010
2011
2012
2013
2014
2015
2016
2017
2018
2019
2020
2021
WL
DES
HSC
LSST
BAO
SDSS/BOSS
PFS
Euclid?
WFIRST?

Models of dSph galaxy from Walker et al.

1. systemic v_z velocity (km/s)
2. $\langle Mg \rangle_1 = \langle Mg \rangle_2$ (Angstroms; difference in mean Mg index between inner (subscript 1) and outer (subscript 2) components)
3. $N_{\rm sample}$, number of stars in sample
4. $N_{\rm members}/N_{\rm sample}$; stars that are not members are drawn from foreground model
5. fraction of members that belong to member component 1 (as many as two member components are considered)
6. μ_α (mas/century); systemic proper motion in RA direction
7. μ_δ (mas/century); systemic proper motion in Dec direction
8. γ_*, component 1
9. β_*, component 1
10. r_*, component 1 (pc)
11. r_a/r_*, component 1 (assumes Osipkov-Merritt anisotropy profile; note that isotropic models have a large value of 10^4)
12. γ_*, component 2
13. β_*, component 2
14. r_*, component 2 (pc)
15. r_a/r_*, component 2 (assumes Osipkov-Merritt anisotropy profile, note that isotropic models have a large value of 10^4)
16. $\gamma_{\rm DM}$
17. $\beta_{\rm DM}$
18. $r_{\rm DM}$ (pc)
19. $\alpha_{\rm DM}$
20. ρ_0 ($M_\odot$/pc^3)
21. distance to center of galaxy (pc)
22. not applicable
23. not applicable
24. $\langle Mg \rangle_1$ (Angstroms)
25. binary fraction–i.e., fraction of member stars for which z velocity received contribution from binary motions.

星密度分布

速度非等方性

ダークマター

Mock data for individual stars

1. x position (pc)
2. y position (pc)
3. z position (pc)
4. v_x velocity (km/s; includes observational error)
5. v_y velocity (km/s; includes observational error)
6. v_z velocity (km/s; includes observational error, perspective effect due to systemic proper motion and los-component of binary-orbital motion)
7. $\delta(v_x)$ (km/s; observational error for x velocity in column 4)
8. $\delta(v_y)$ (km/s; observational error for y velocity in column 5)
9. $\delta(v_z)$ (km/s; observational error for z velocity in column 6)
10. v_x velocity as drawn directly from DF (i.e., before including observational errors and perspective effect; km/s)
11. v_y velocity as drawn directly from DF (i.e., before including observational errors and perspective effect; km/s)
12. v_z velocity as drawn directly from DF (i.e., before including observational errors, perspective effect and/or binary motions; km/s)
13. v_b (km/s; LOS velocity due to binary orbital motion; this is already included in the v_z velocity given in column 6)
14. Mg index (Angstroms)
15. $\delta(Mg)$ (Angstroms, observational error for Mg index in column 15)
16. Right Ascension (radians)
17. Declination (radians)
18. Right Ascension of center of galaxy (radians; will be either Fornax's or Sculptor's)
19. Declination of center of galaxy (radians; will be either Fornax's or Sculptor's)
20. probability of membership (evaluated using EM algorithm of Walker et al. (2009)
21. Which component is star drawn from (1=member component 1, 2=member component 2, 3=foreground)?

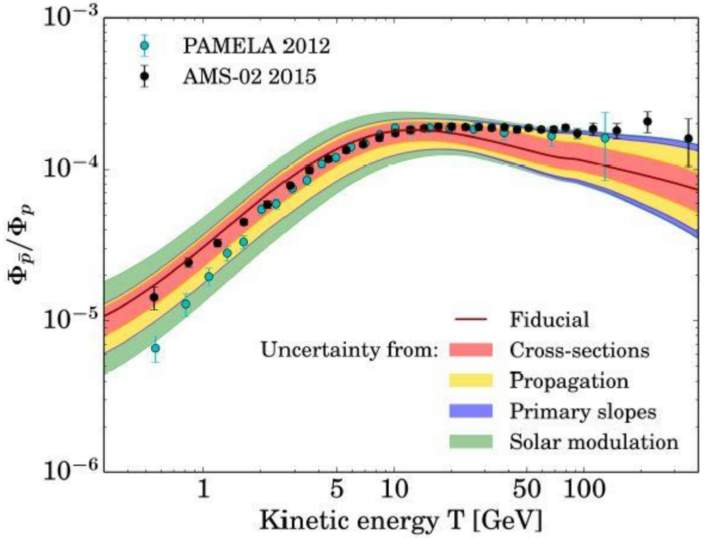

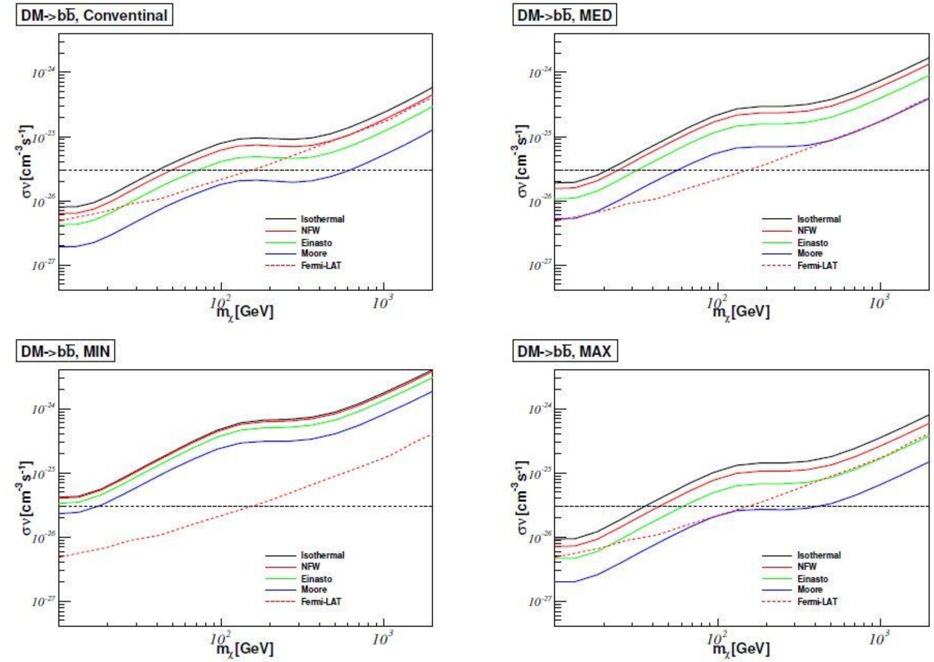

Jin+, arXiv: 1504.04604

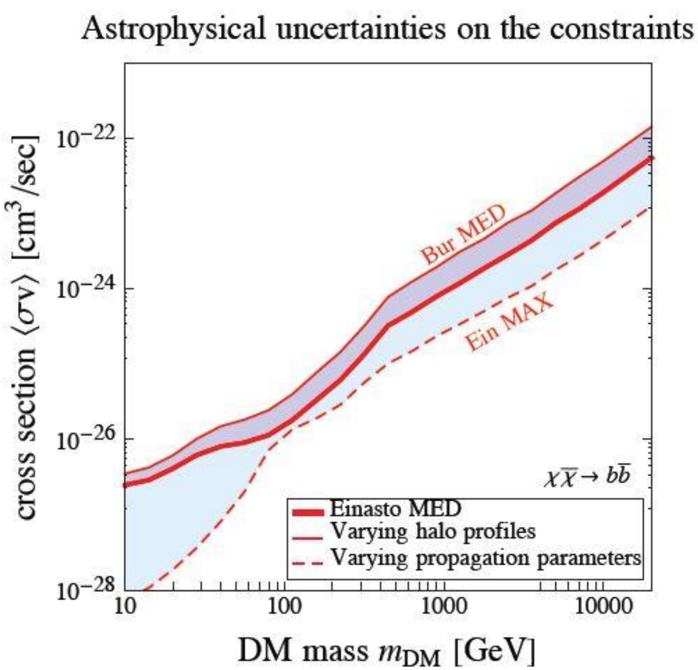

Gaelle+, arXiv: 1504.04276

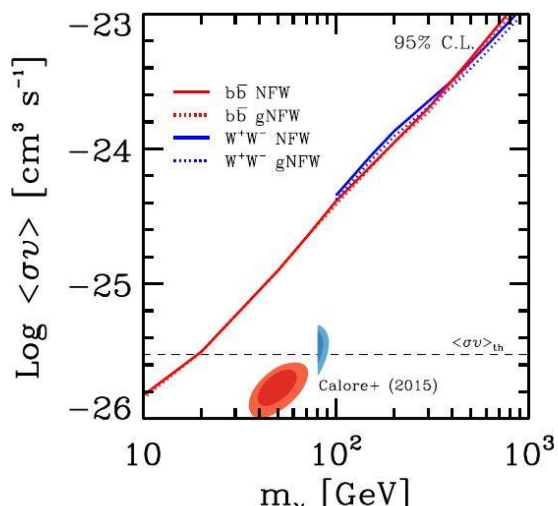

Evoli+, arXiv: 1504.05175

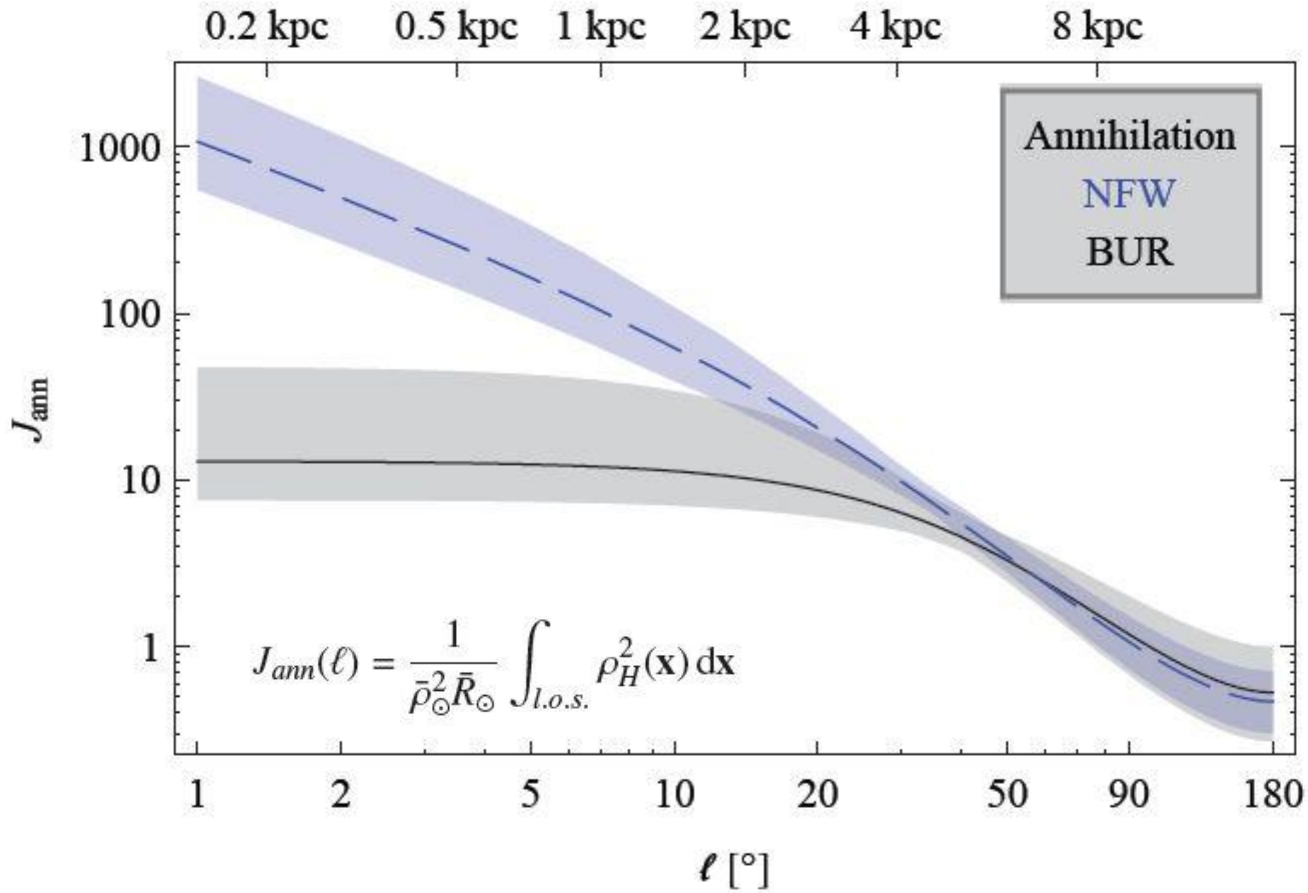

Nesti and Salucci, arXiv: 1304.5127

Subhalo distribution

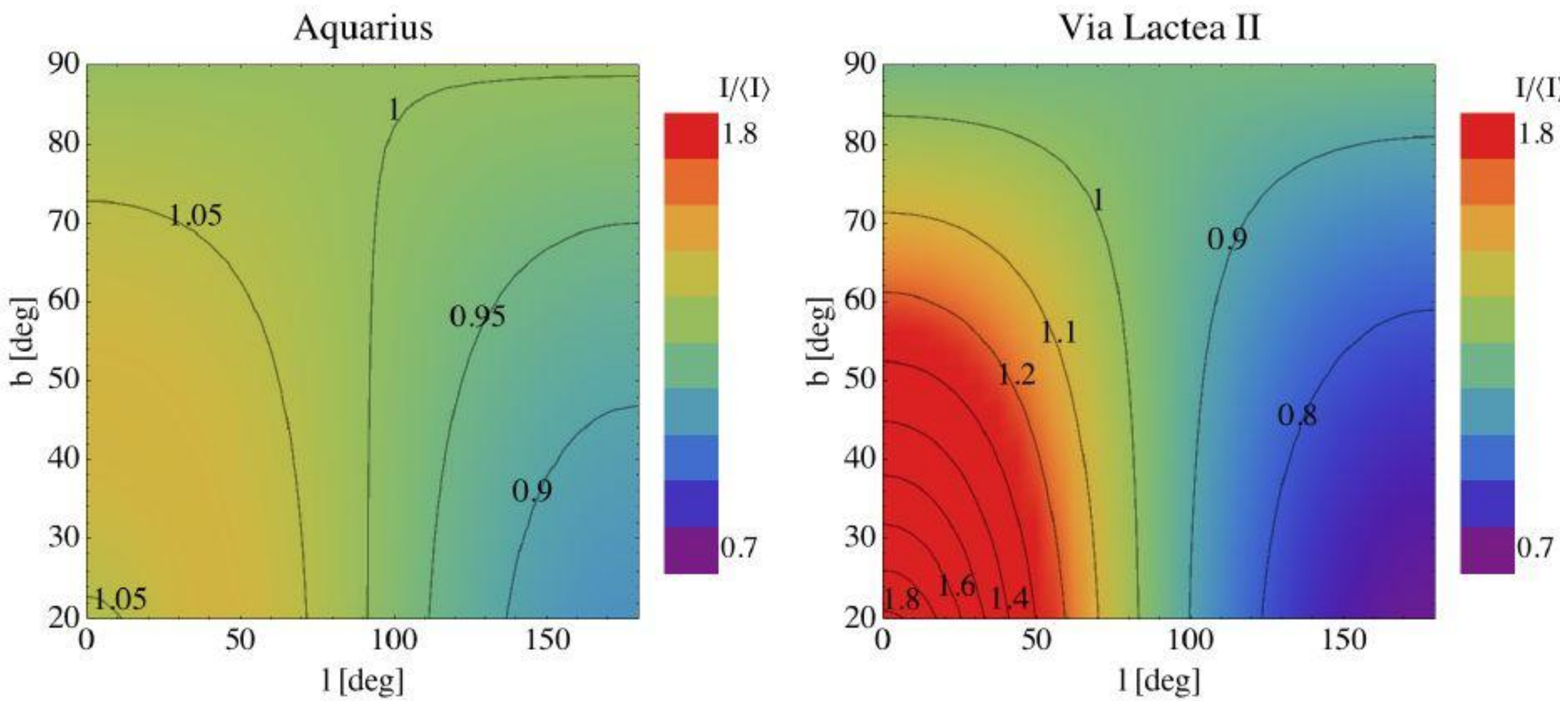

Figure 4. Anisotropy in the gamma-ray annihilation signal from the subhalo distribution found in Aquarius [40] (left) and Via Lactea II [39] (right) simulations, with the former following the prescription in ref. [63]. The plots show the intensities of the substructures relative to their average intensity in the $|b| > 20°$ region.

Isotropic

Variance of DM density

$$\frac{d\phi^{\rm DM}}{dE_0} = \frac{c\,\langle\sigma v\rangle(\Omega_{\rm DM}\rho_c)^2}{8\pi\, m_\chi^2}\int dz \frac{e^{-\tau(E_0,z)}(1+z)^3\zeta(z)}{H(z)}\frac{dN}{dE}\Big|_{E=E_0(1+z)}$$

$$\zeta(z) \equiv \langle\delta^2(z)\rangle = \int^{k_{\rm max}} \frac{d\,k}{k}\frac{k^3 P_{NL}(k,z)}{2\pi^2} \equiv \int^{k_{\rm max}} \frac{d\,k}{k}\Delta_{NL}(k,z),$$

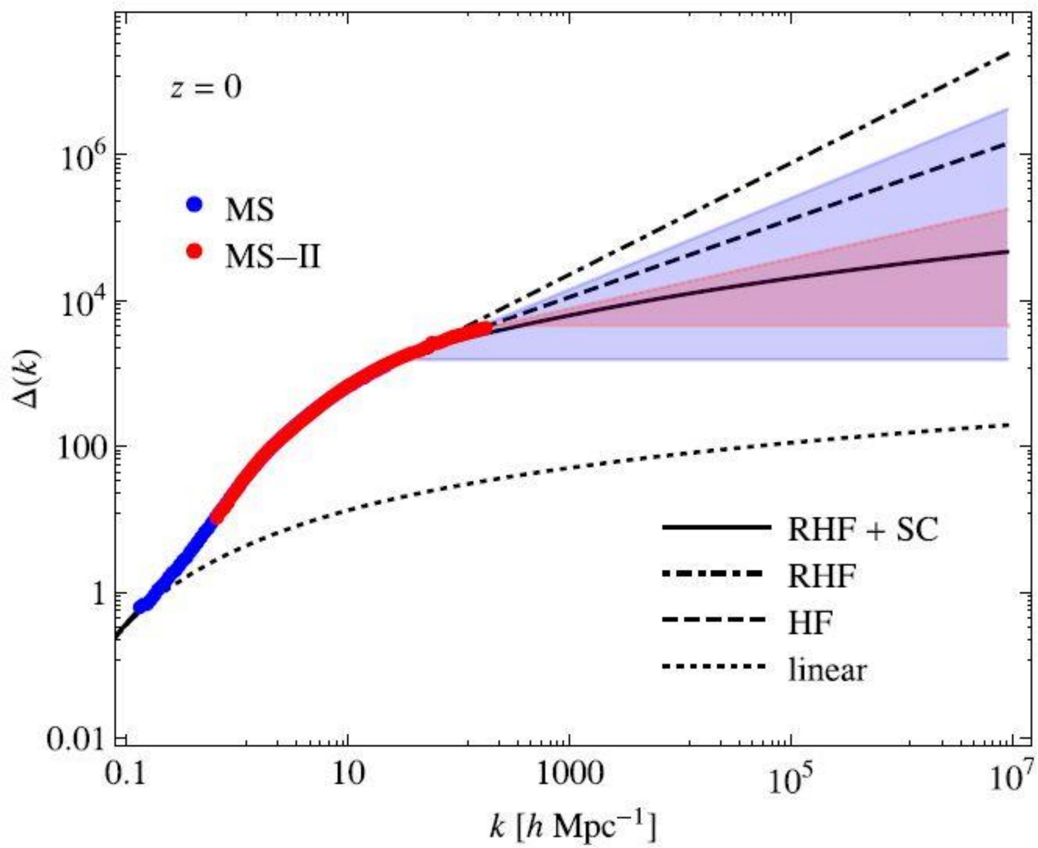

Sefusatti et al., MNRAS **441, 1861–1878 (2014)**

Mmin Dependence

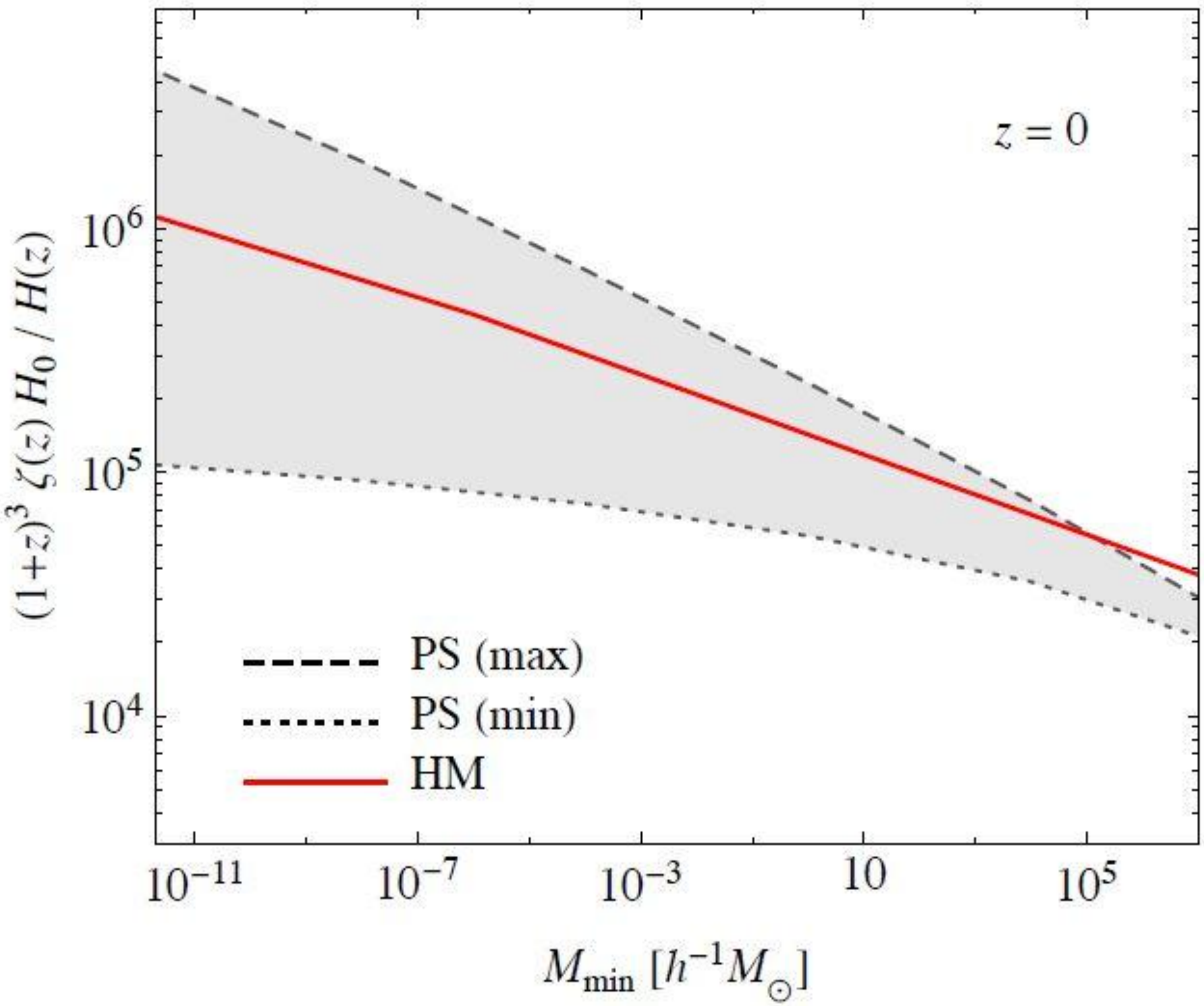

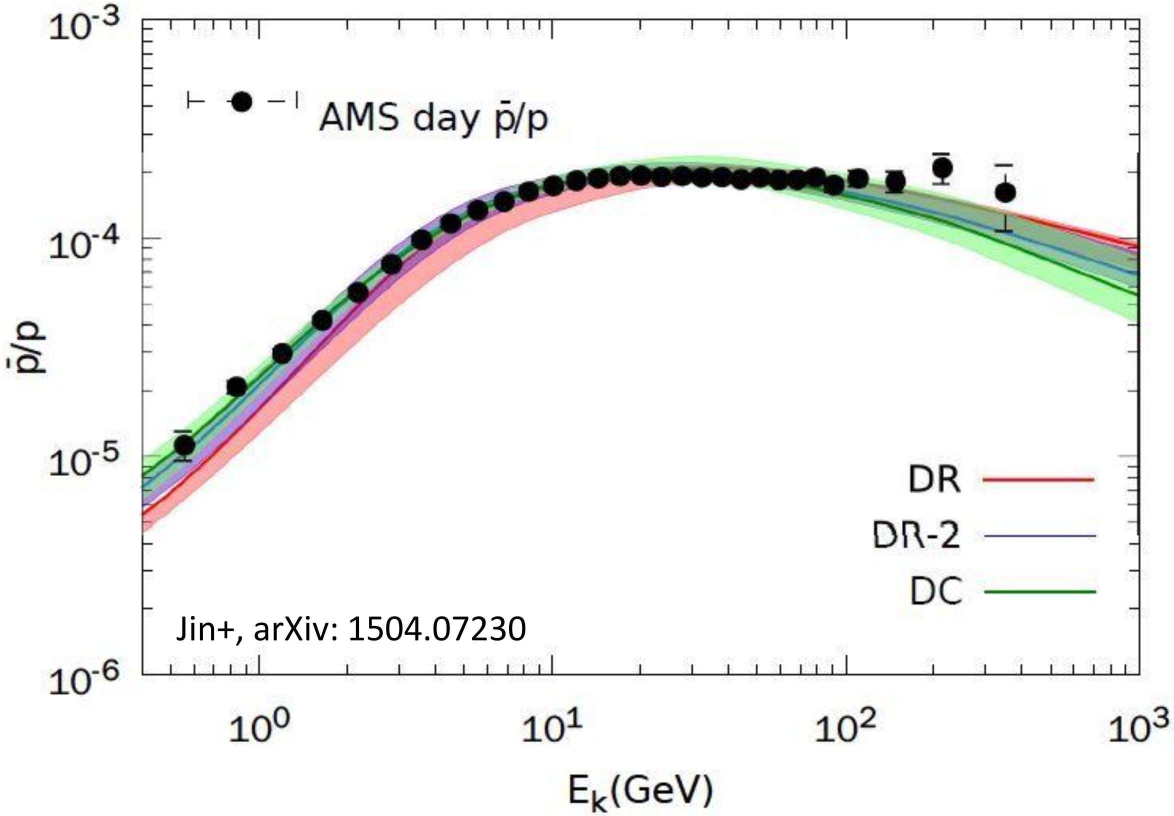

Model	Propagation parameters	Description
DR	D_0, δ, v_A, z_h	Diffusion + reacceleration, $\eta = 1$, $R_0 = 4$ GV
DR-2	D_0, δ, v_A, z_h	Diffusion + reacceleration, $\eta = -0.4$, $R_0 = 4$ GV
DC	D_0, δ, dV_c/dz, R_0, z_h	Diffusion + convection, $\eta = 1$, $\delta = 0$ for $R < R_0$

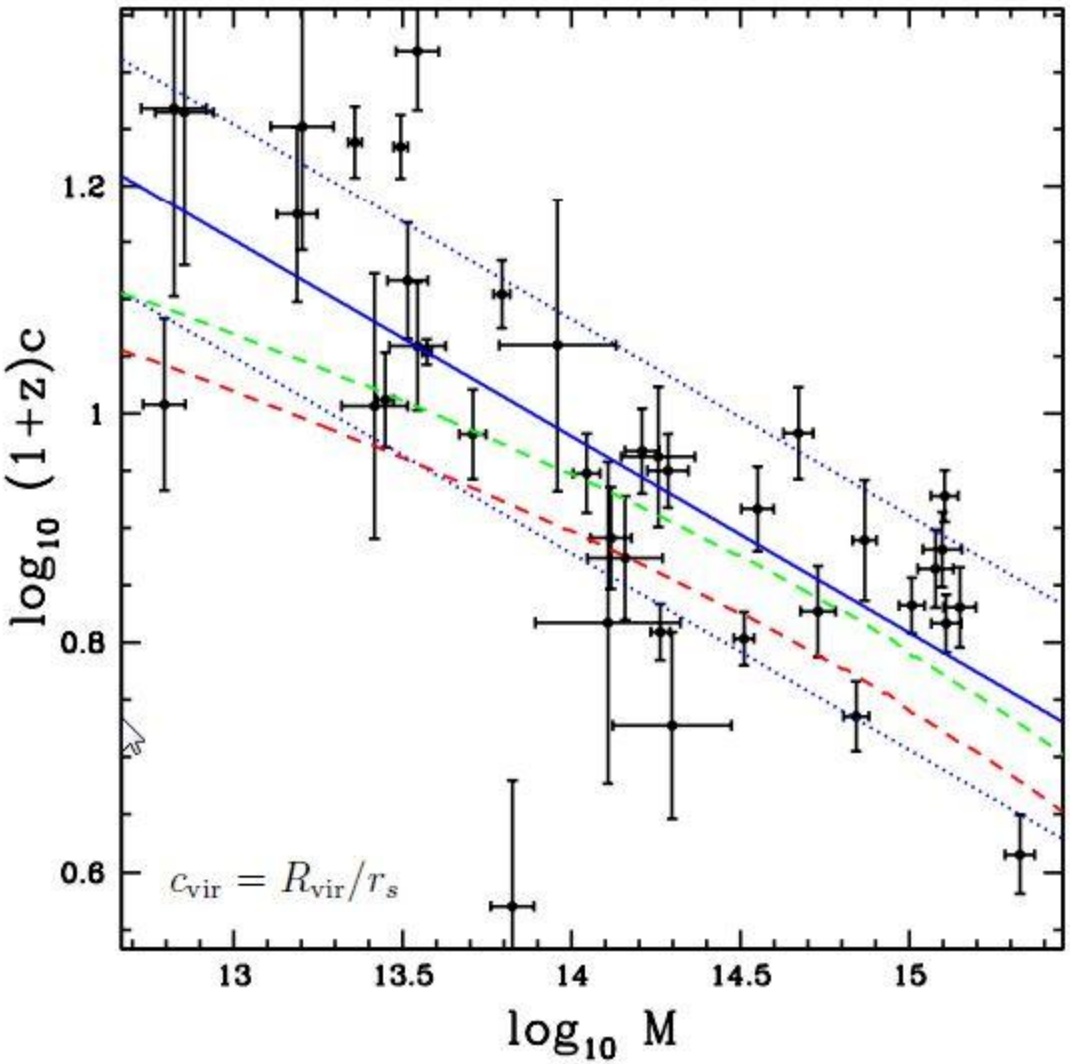

Buote+, arXiv: 0610135

taken to be the radius within which the average density equals $\Delta\rho_c$, where ρ_c is the critical density of the universe, and Δ is a number typically between $100 - 500$. The quantity r_s is the scale radius of the NFW profile (Navarro et al. 1997), but it is replaced by r_{-2}, the radius where the logarithmic density slope equals -2, for more general profiles (Navarro et al. 2004; Graham et al. 2006). The virial mass (M) is the mass enclosed within r_Δ.

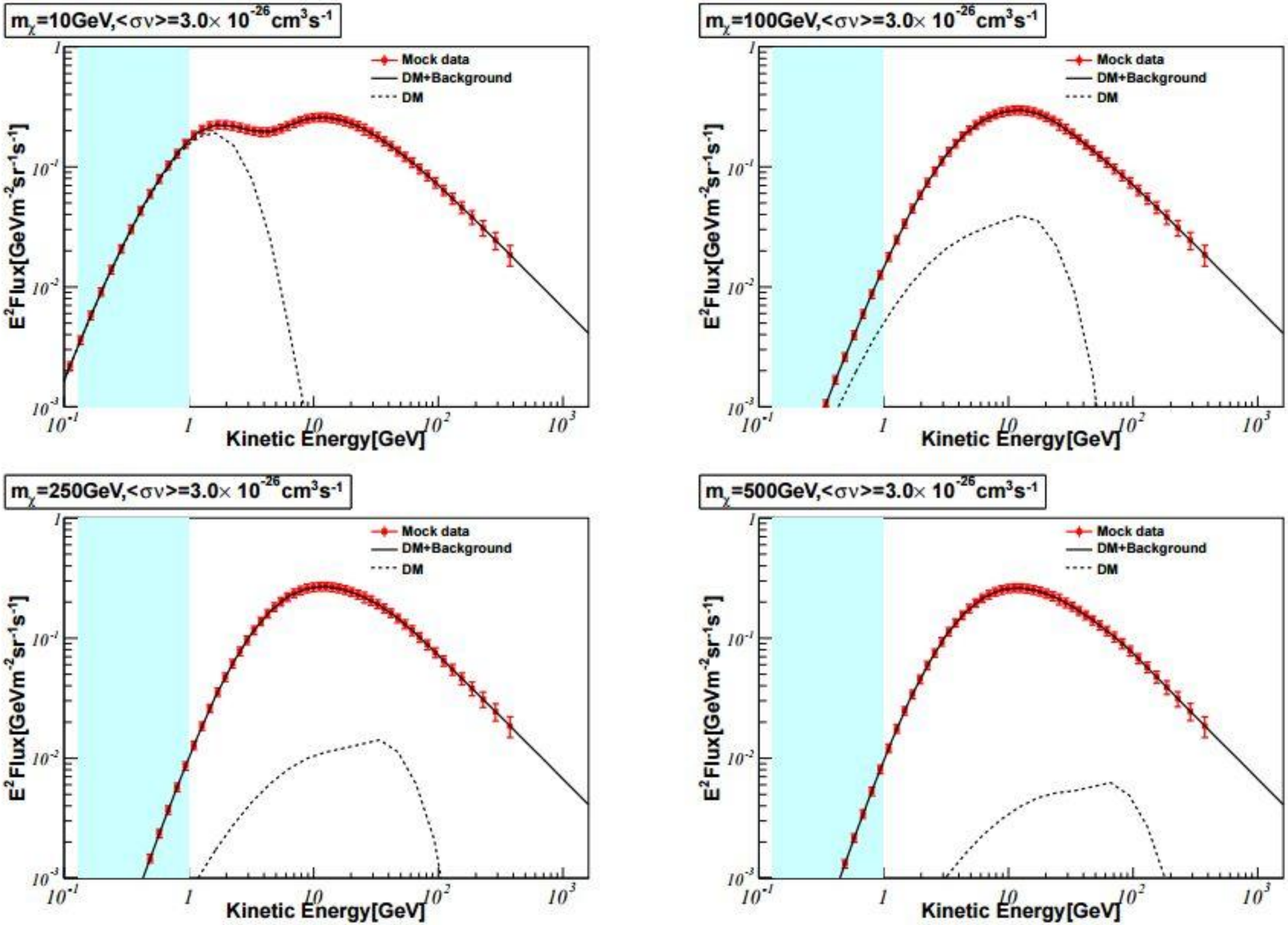

Jin+, arXiv:1410.0171

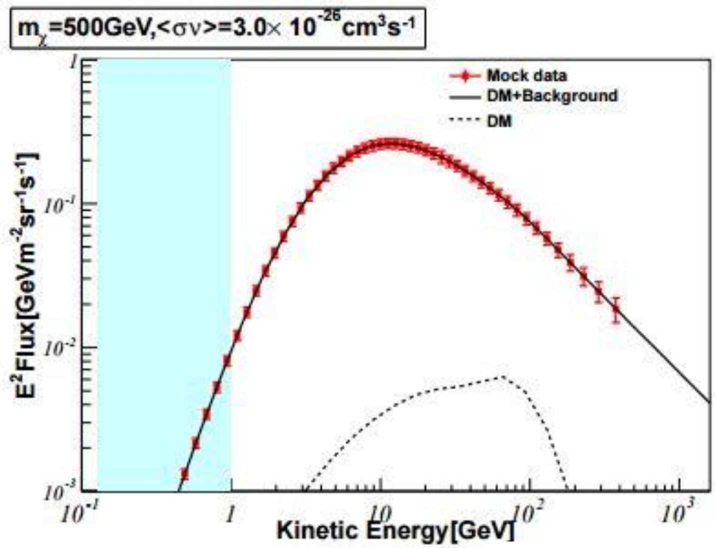

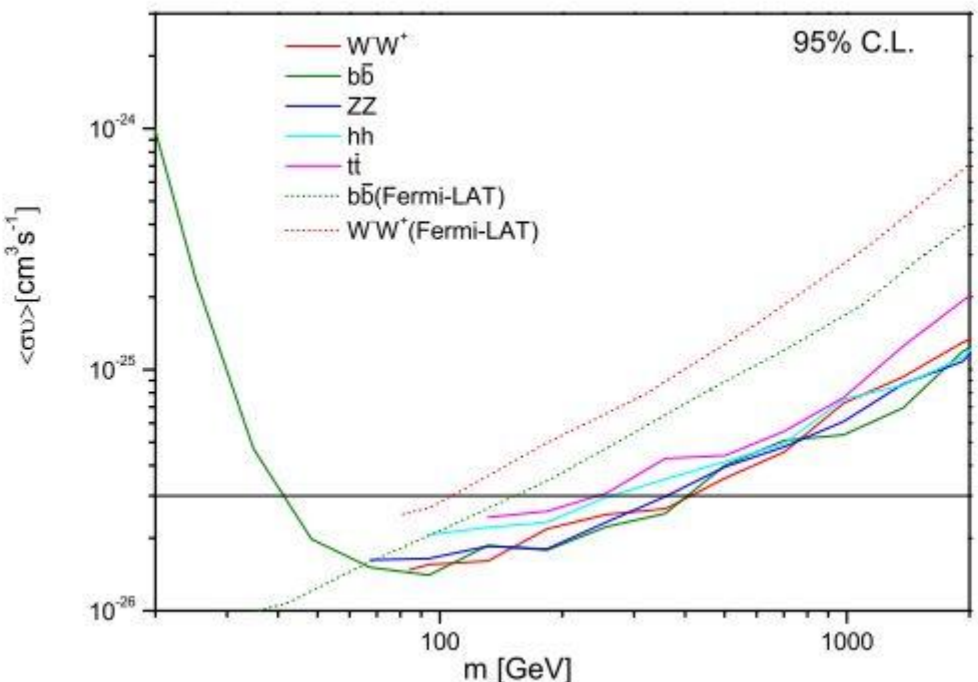

Jin+, arXiv:1410.0171

Proton Flux Comparison with Earlier Measurements

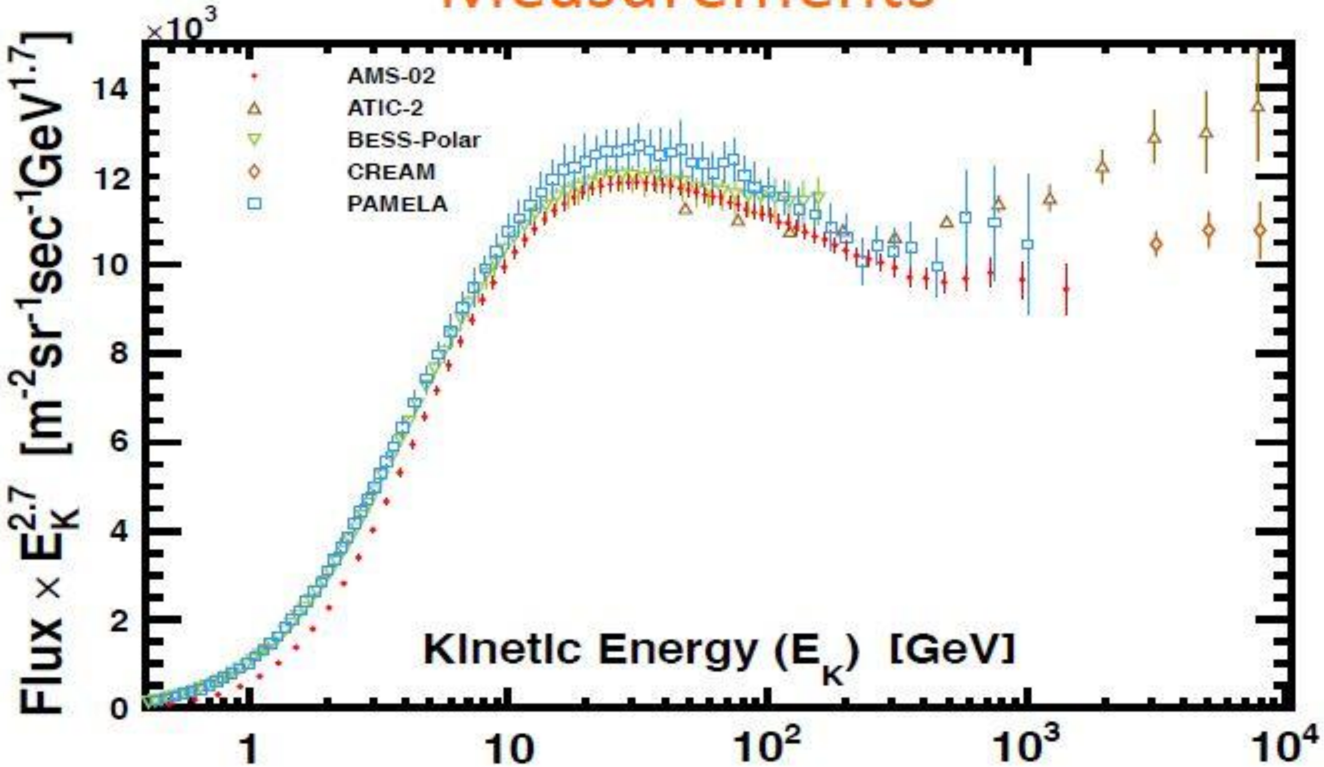

Detector

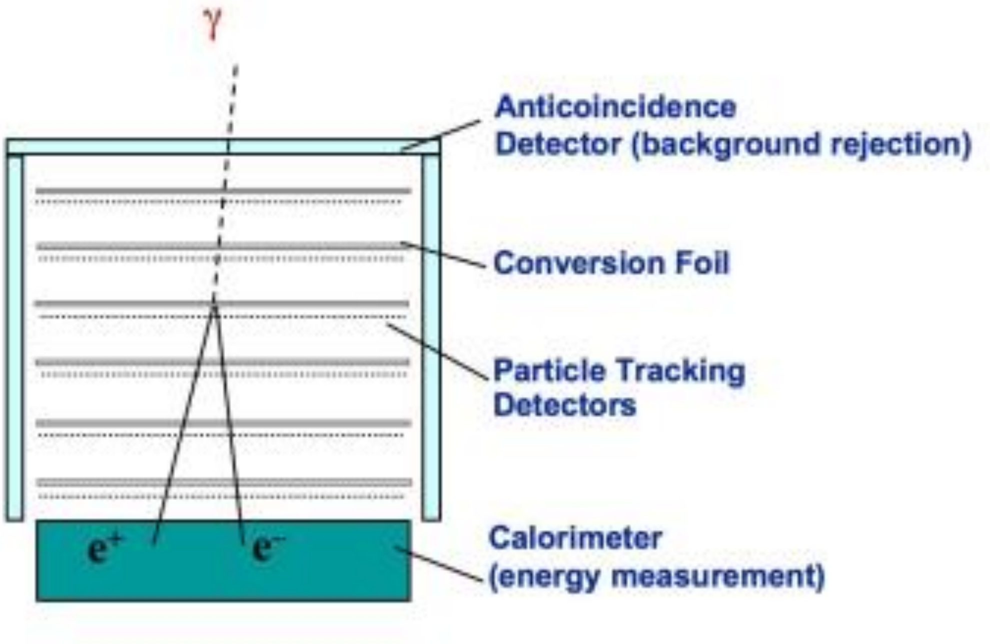

1.8 * 1.8 * 0.72 (m^3)
2789 kg

16 Tower:
37cm * 37cm * 66cm

Calorimeter 96 (8 layer)

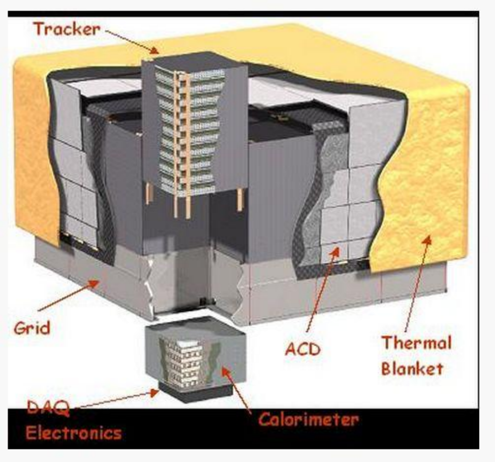

Detector

Tracker

Silicon Strip

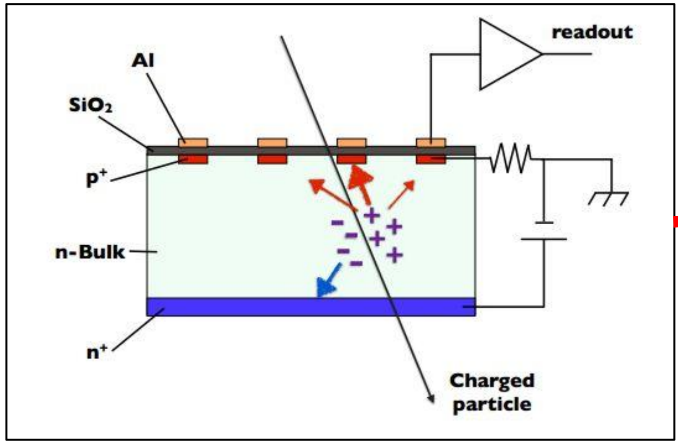

Spark Chamber

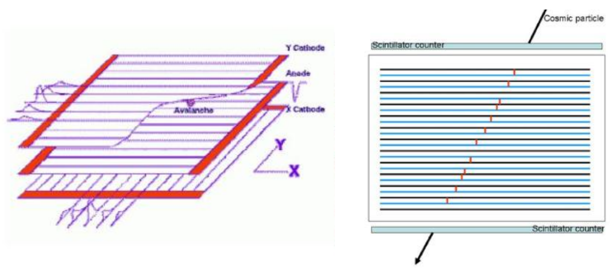

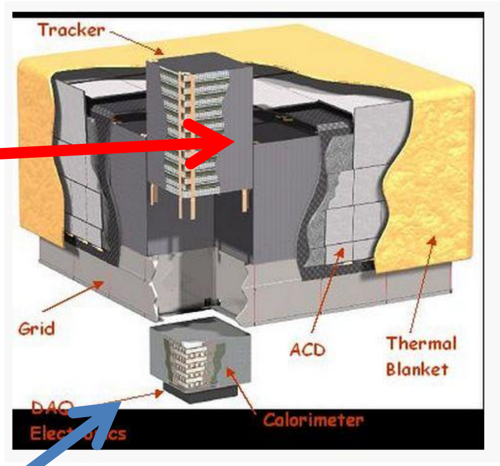

Calorimeter

CsI (Fermi-LAT)

326 × 26.7 × 19.9 mm lode

12 lodes × 8 layer

([arXive: 1206.1896])

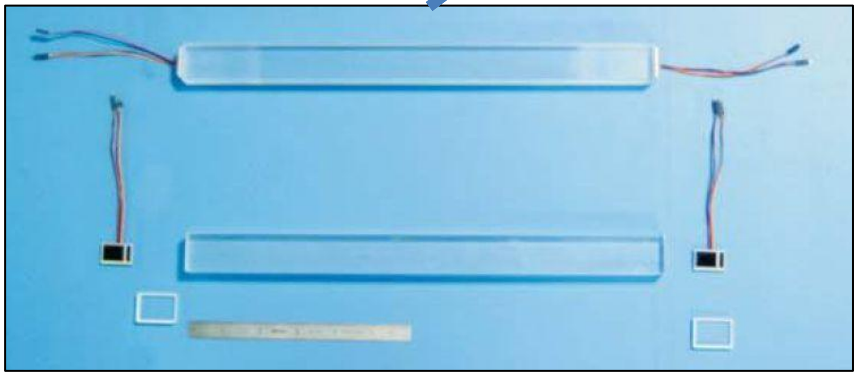

Milky Way

- The nearest DM signal source

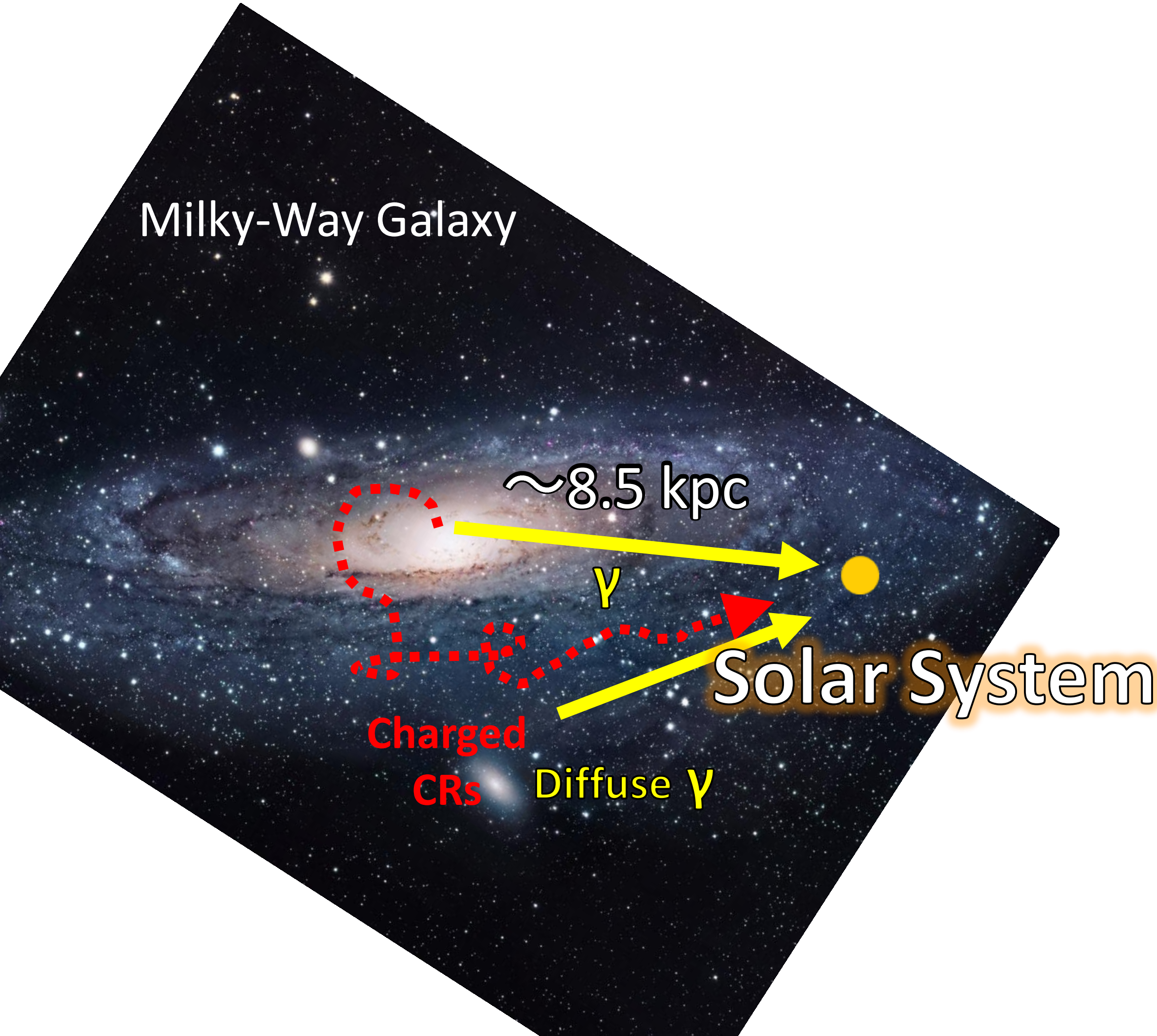

Milky Way

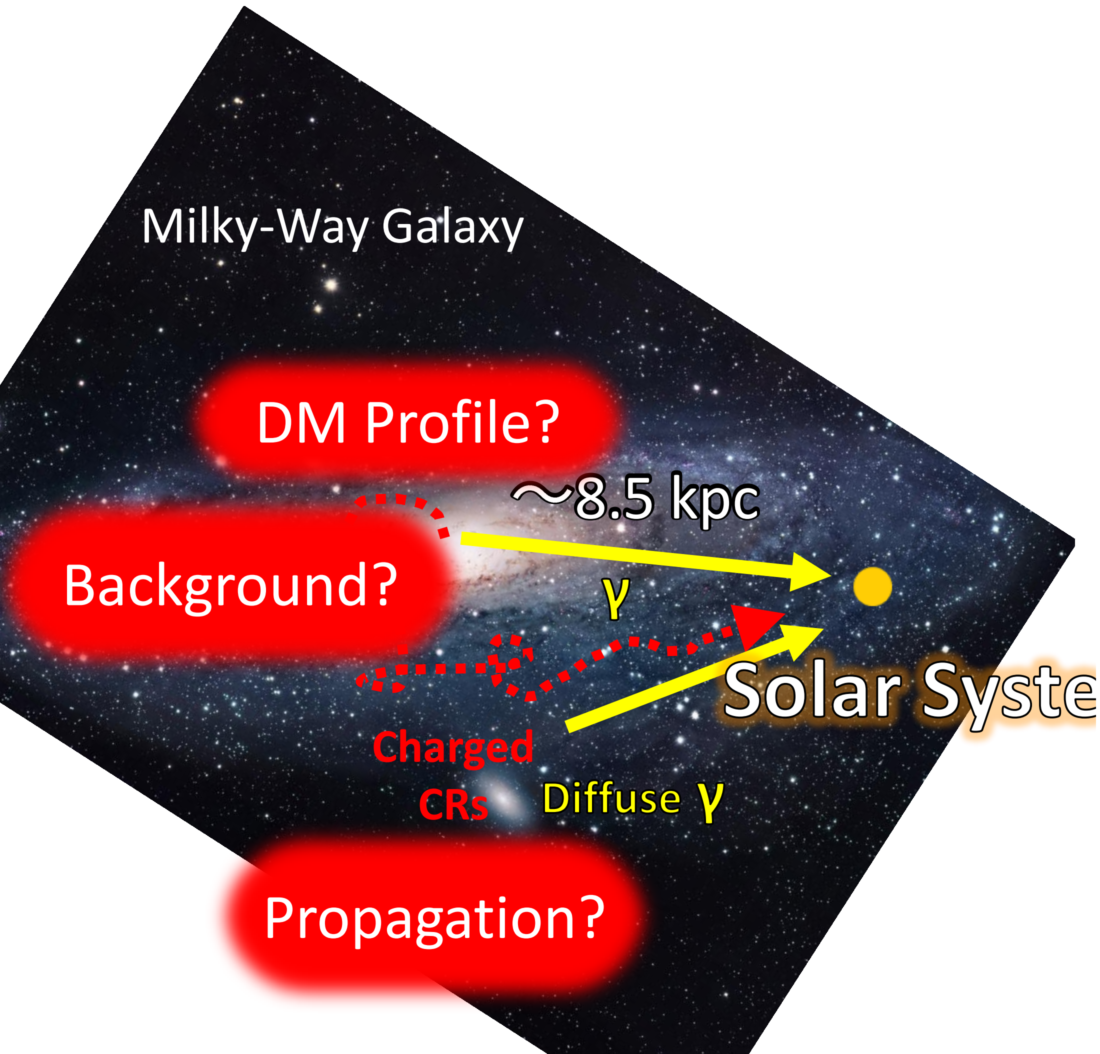

Profile

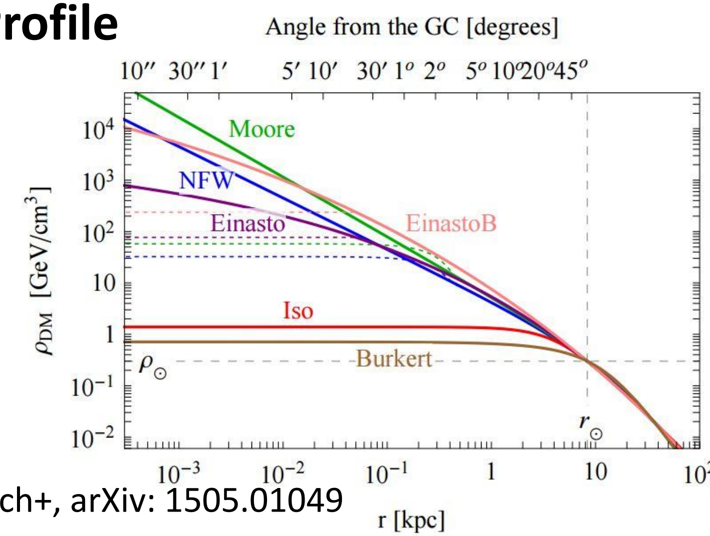

Buch+, arXiv: 1505.01049

Flux(Antiproton)

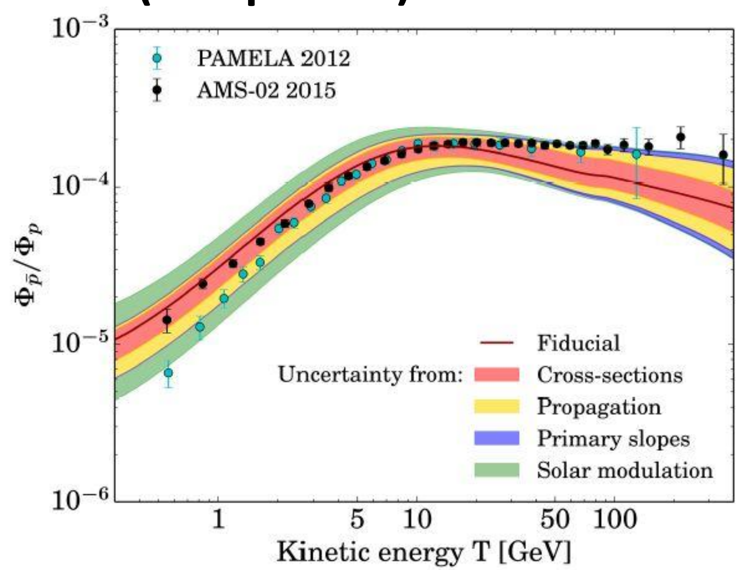

Gaelle+, arXiv: 1504.04276

Milky Way

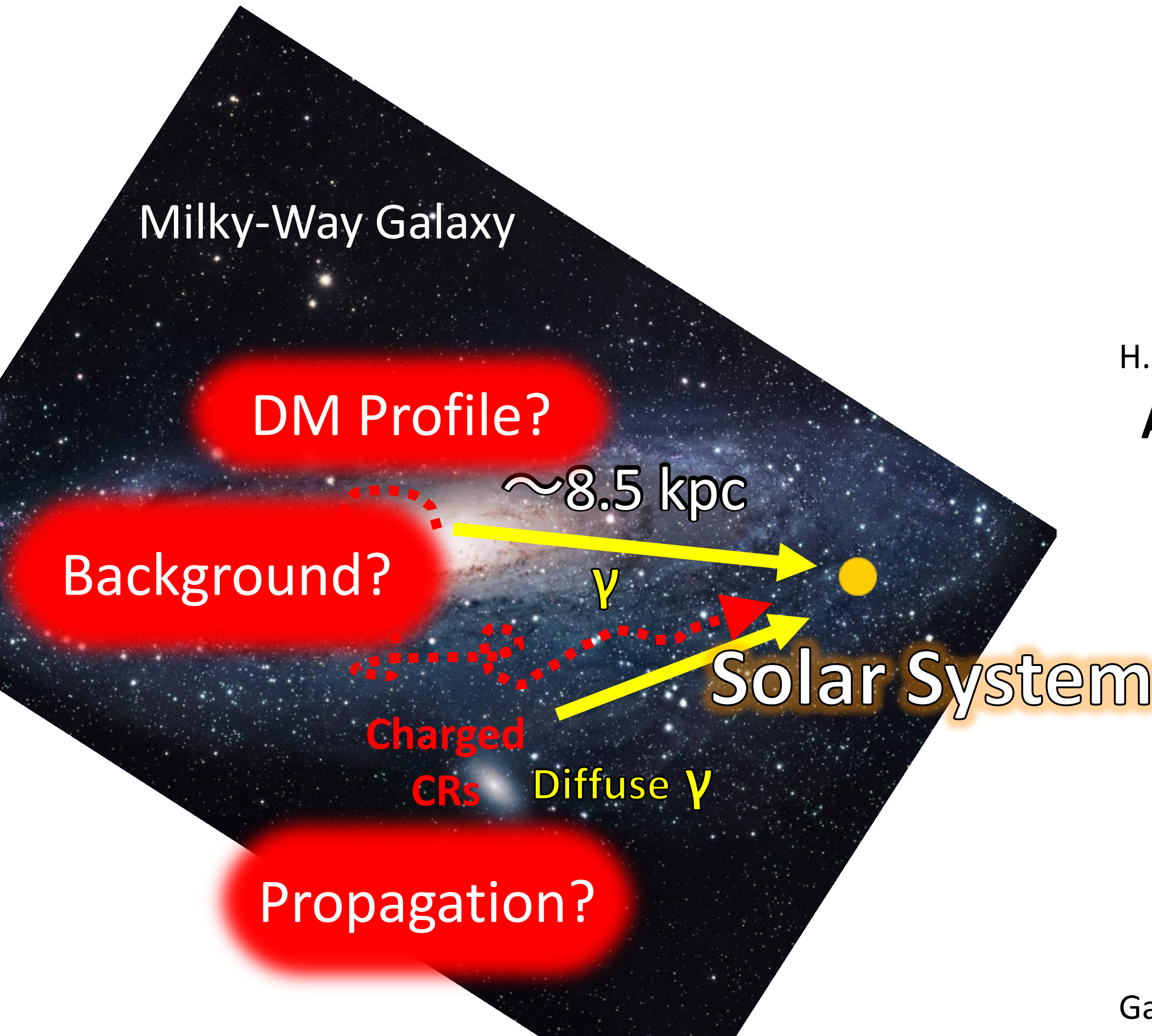

Gamma (Continuum)

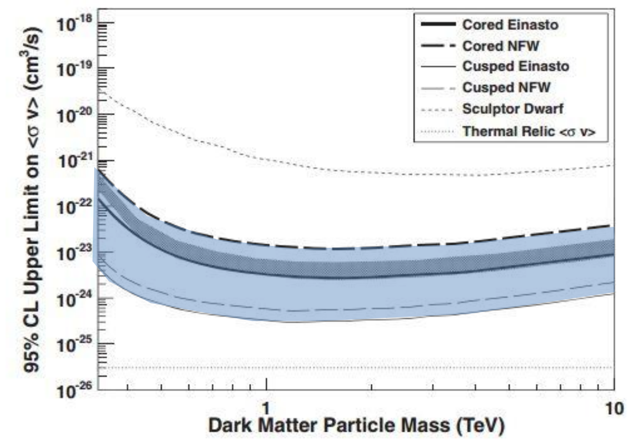

H.E.S.S, arXiv: 1502.03244

Antiproton

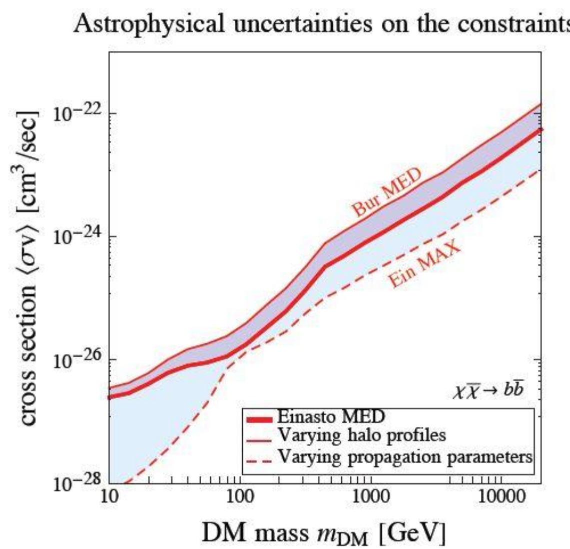

Gaelle+, arXiv: 1504.04276

Extra Galaxy / Cluster

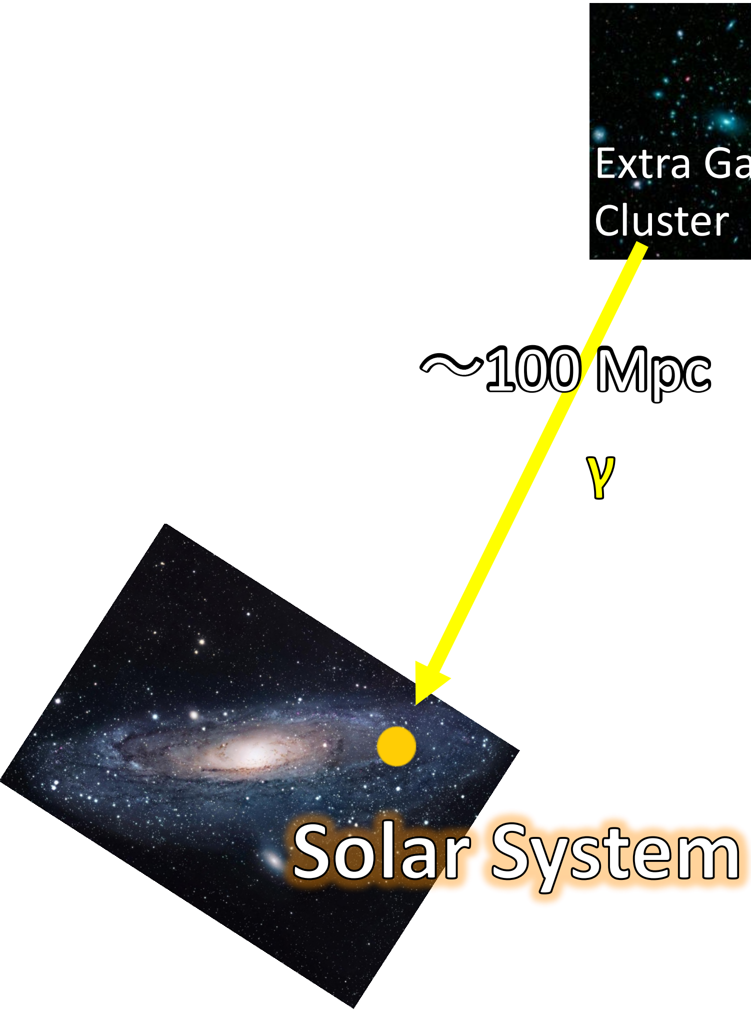

Extra Galaxy / Cluster

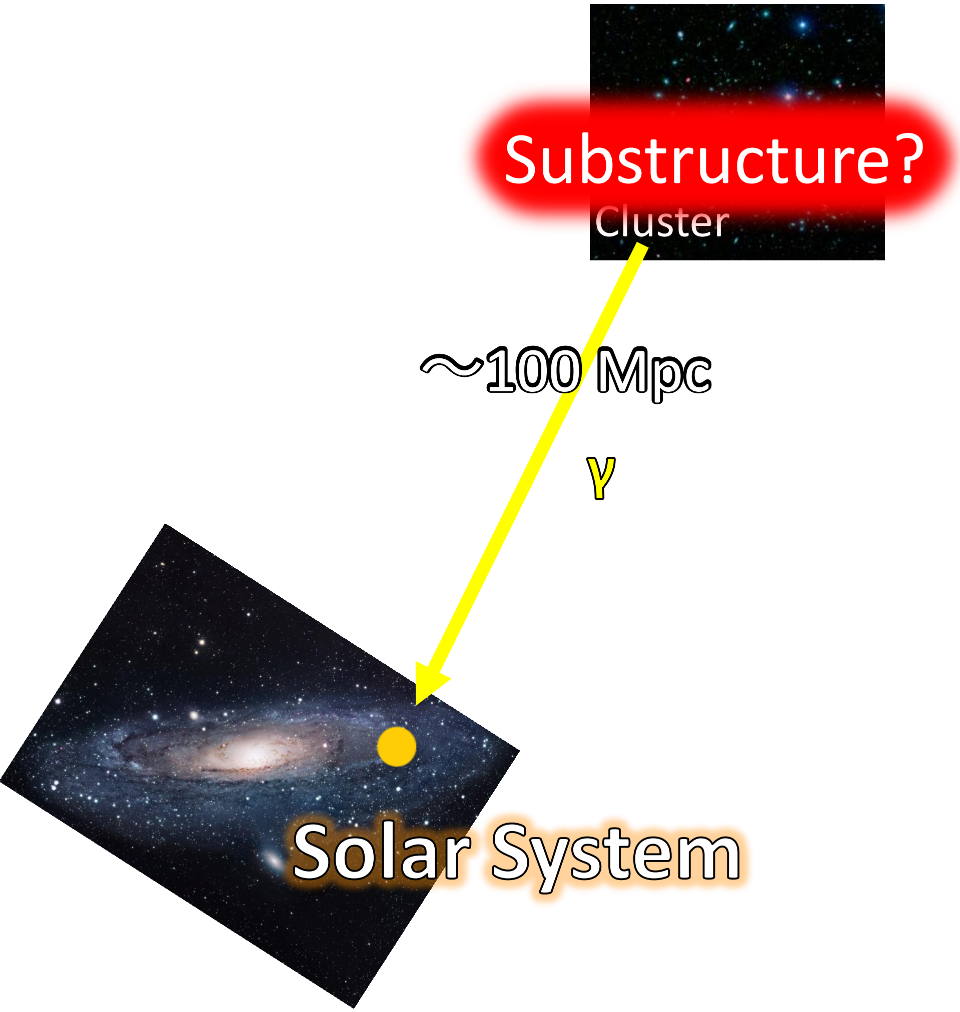

Substructure

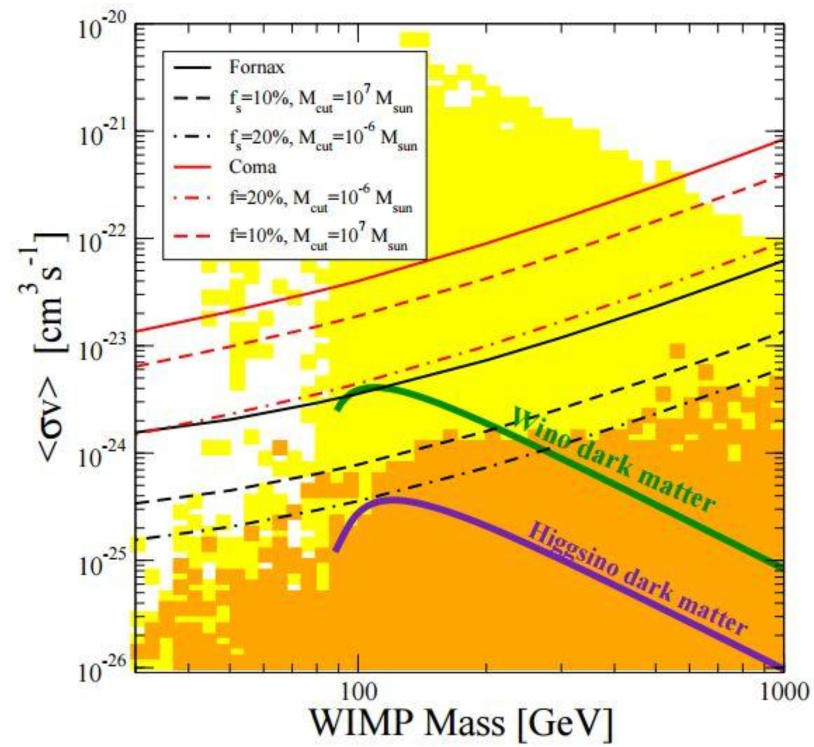

LAT, arXiv: 1002.2239

Extra Galaxy / Cluster

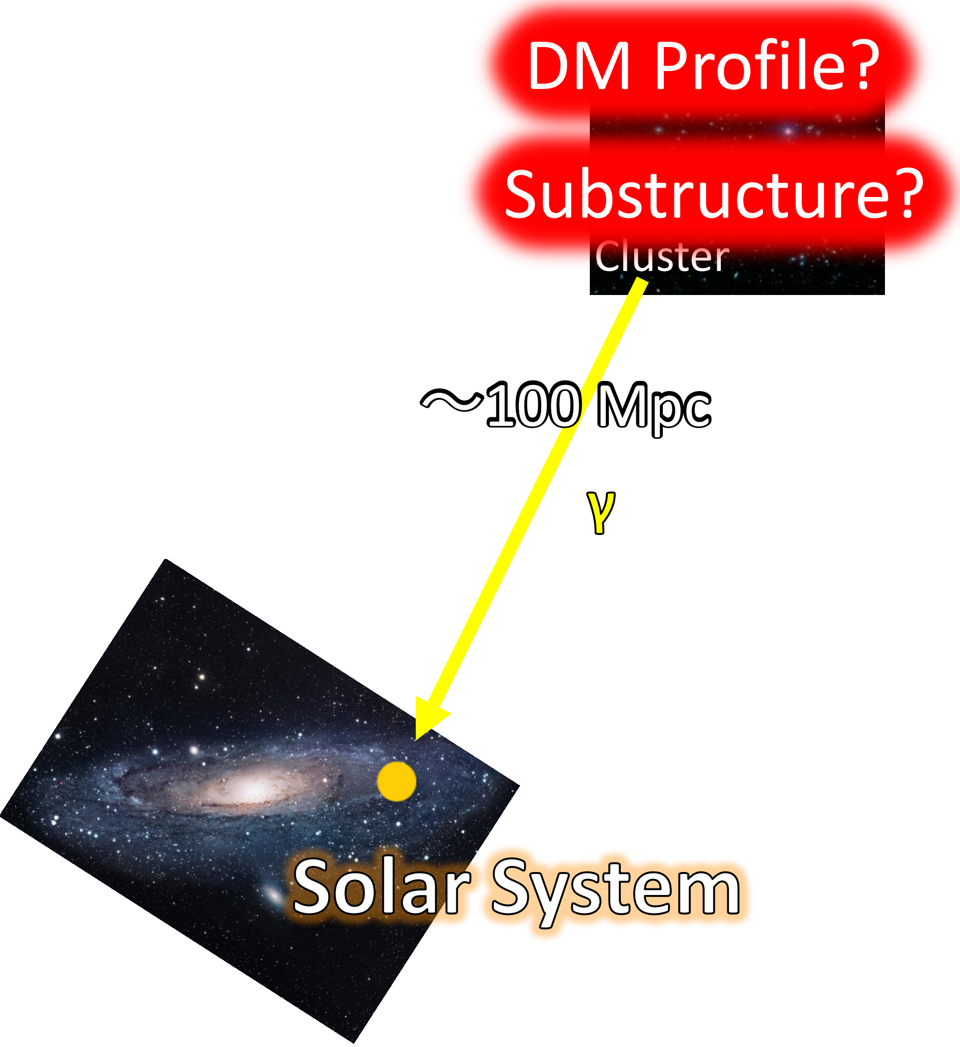

Profile (with super-massive BH)

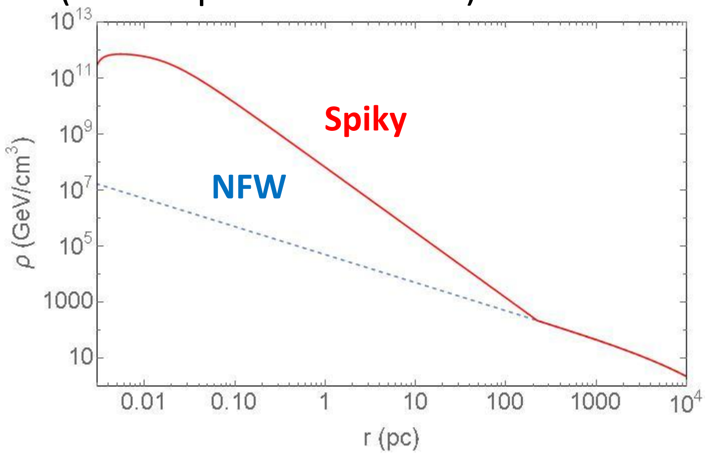

M87 (~16 Mpc)

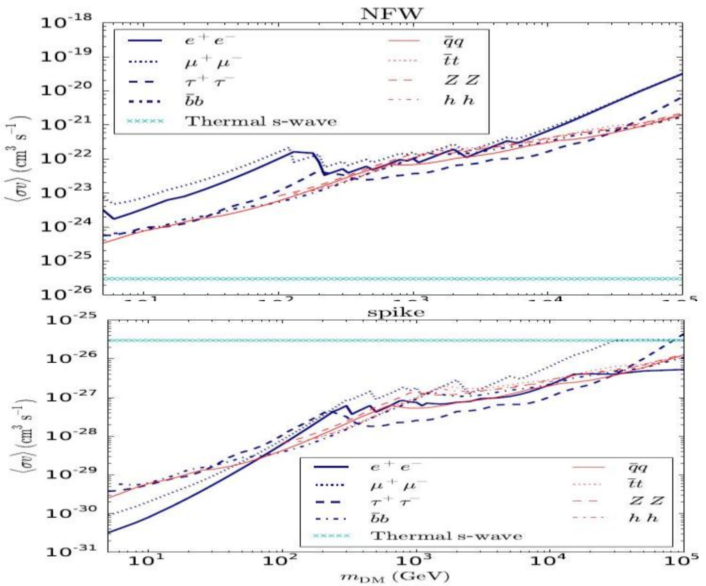

Lacroix+, arXiv: 1505.00785

Isotropic

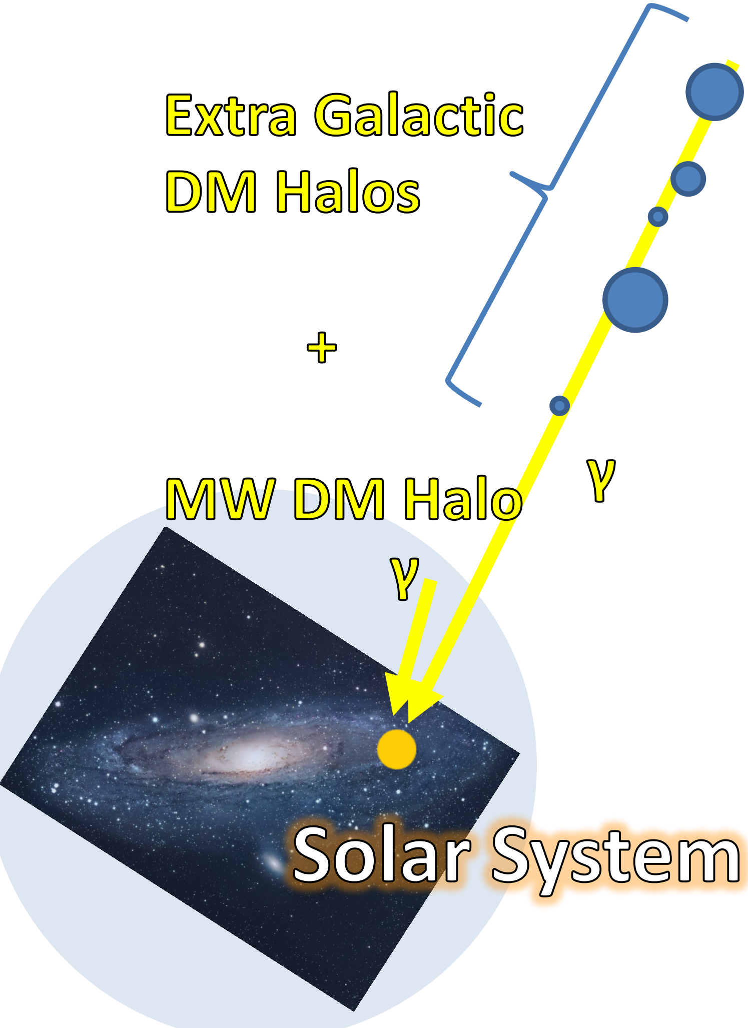

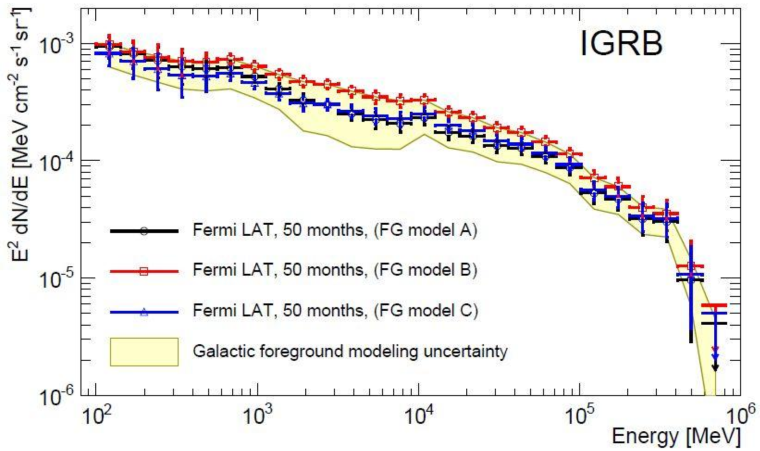

Fermi-LAT, arXiv: 1410.3696

Isotropic

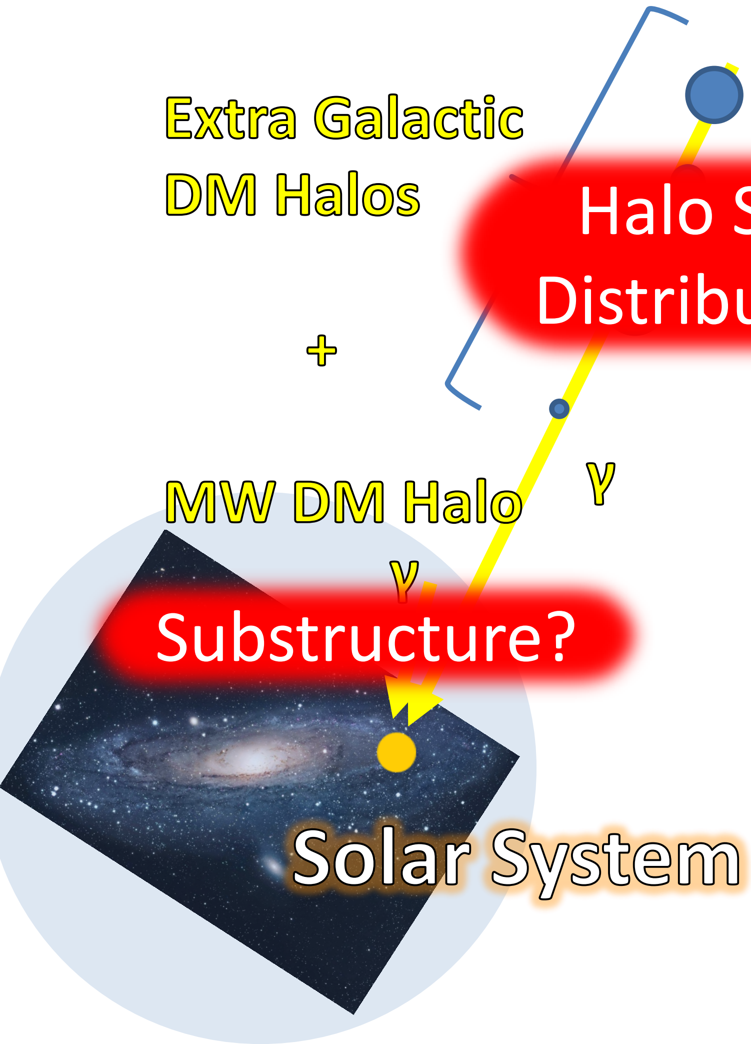

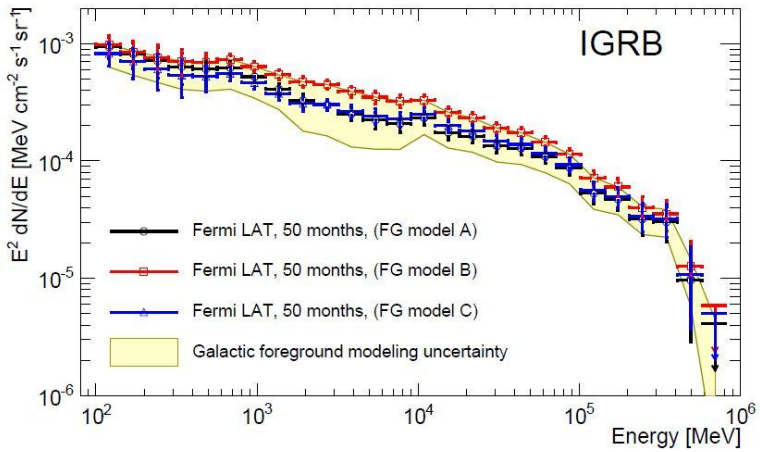

Fermi-LAT, arXiv: 1410.3696

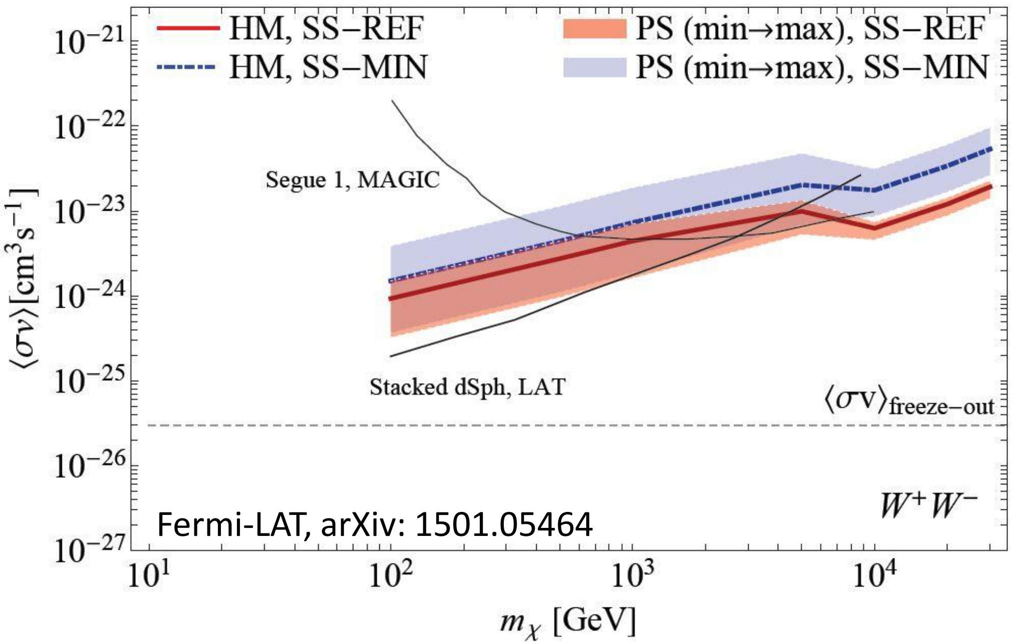

Fermi-LAT, arXiv: 1501.05464

Current observational limit

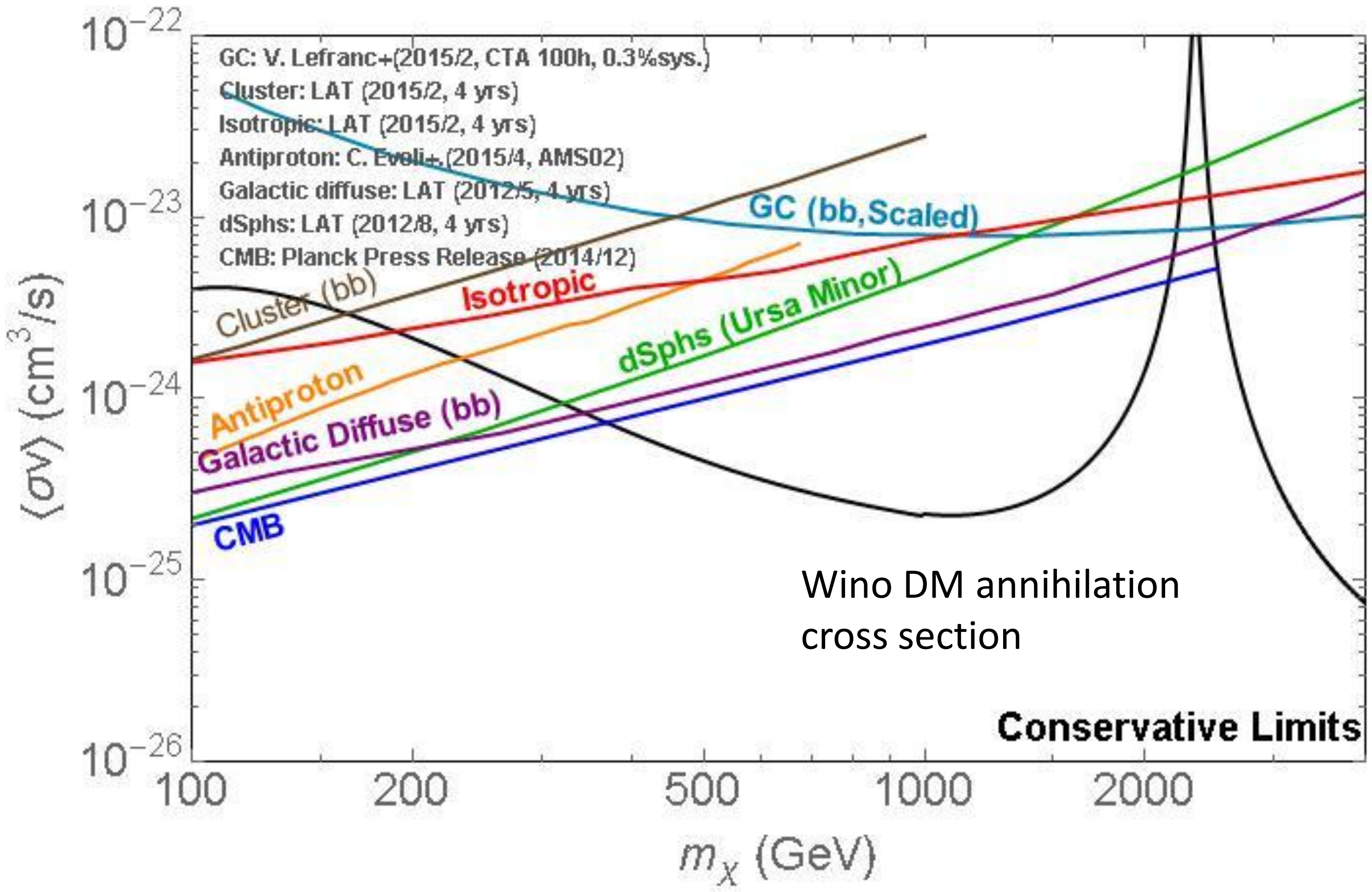

Current observational limit

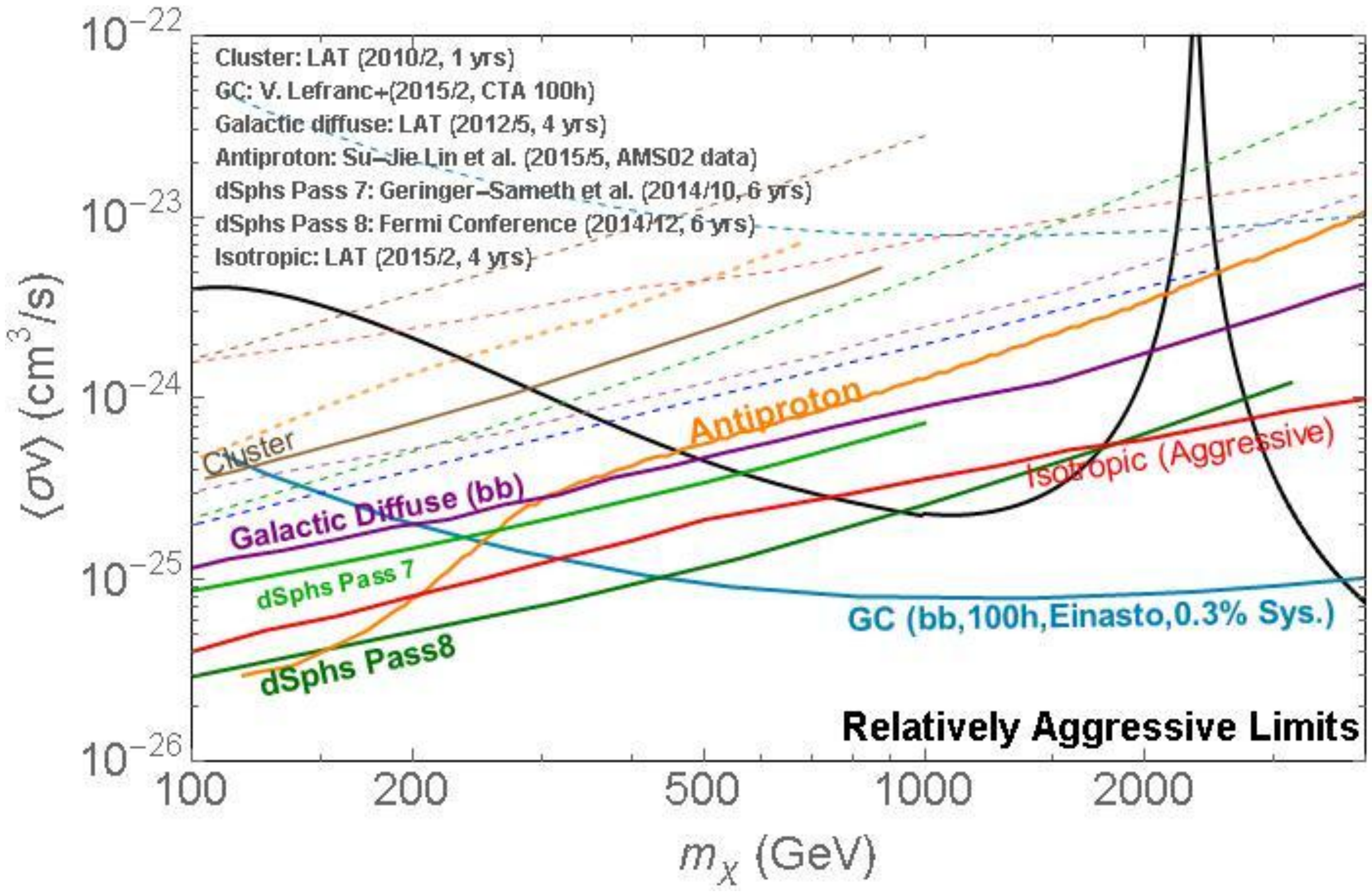

Astrophysical Factor

Name	GLON (deg)	GLAT (deg)	Distance (kpc)	$\log_{10}(J^{\rm NFW})^{a}$ ($\log_{10}$[GeV^2 cm^{-5} sr])	$\log_{10}(\alpha_s^{\rm NFW})$ ($\log_{10}$[deg])	$\log_{10}(J^{\rm Burkert})^{a}$ ($\log_{10}$[GeV^2 cm^{-5} sr])	$\log_{10}(\alpha_s^{\rm Burkert})$ ($\log_{10}$[deg])
Bootes I	358.1	69.6	66	18.8 ± 0.22	-0.6 ± 0.3	18.6 ± 0.17	-1.1 ± 0.2
Bootes II	353.7	68.9	42	–	–	–	–
Bootes III	35.4	75.4	47	–	–	–	–
Canes Venatici I	74.3	79.8	218	17.7 ± 0.26	-1.3 ± 0.2	17.6 ± 0.17	-1.6 ± 0.1
Canes Venatici II	113.6	82.7	160	17.9 ± 0.25	-1.1 ± 0.4	17.8 ± 0.19	-1.6 ± 0.2
Canis Major	240.0	-8.0	7	–	–	–	–
Carina	260.1	-22.2	105	18.1 ± 0.23	-1.0 ± 0.3	18.1 ± 0.16	-1.5 ± 0.1
Coma Berenices	241.9	83.6	44	19.0 ± 0.25	-0.6 ± 0.5	18.9 ± 0.21	-1.1 ± 0.3
Draco	86.4	34.7	76	18.8 ± 0.16	-0.6 ± 0.2	18.7 ± 0.17	-1.0 ± 0.2
Fornax	237.1	-65.7	147	18.2 ± 0.21	-0.8 ± 0.2	18.1 ± 0.22	-1.1 ± 0.1
Hercules	28.7	36.9	132	18.1 ± 0.25	-1.1 ± 0.4	17.9 ± 0.19	-1.6 ± 0.2
Leo I	226.0	49.1	254	17.7 ± 0.18	-1.1 ± 0.3	17.6 ± 0.17	-1.5 ± 0.2
Leo II	220.2	67.2	233	17.6 ± 0.18	-1.1 ± 0.5	17.5 ± 0.15	-1.9 ± 0.5
Leo IV	265.4	56.5	154	17.9 ± 0.28	-1.1 ± 0.4	17.8 ± 0.21	-1.6 ± 0.2
Leo V	261.9	58.5	178	–	–	–	–
Pisces II	79.2	-47.1	182	–	–	–	–
Sagittarius	5.6	-14.2	[illegible]	–	[illegible]	[illegible]	[illegible]
Sculptor	287.5	-83.2	[illegible]	[illegible]	[illegible] ±0.3	[illegible]	[illegible]
Segue 1	220.5	50.4	23	19.5 ± 0.29	-0.4 ± 0.5	19.4 ± 0.24	-0.9 ± 0.2
Segue 2	149.4	-38.1	35	–	–	–	–
Sextans	243.5	42.3	86	18.4 ± 0.27	-0.9 ± 0.2	18.4 ± 0.16	-1.2 ± 0.1
Ursa Major I	159.4	54.4	97	18.3 ± 0.24	-1.0 ± 0.3	18.2 ± 0.18	-1.4 ± 0.2
Ursa Major II	152.5	37.4	32	19.3 ± 0.28	-0.5 ± 0.4	19.2 ± 0.21	-0.9 ± 0.2
Ursa Minor	105.0	44.8	76	18.8 ± 0.19	-0.5 ± 0.2	18.7 ± 0.20	-0.9 ± 0.2
Willman 1	158.6	56.8	38	19.1 ± 0.31	-0.6 ± 0.5	19.0 ± 0.28	-1.1 ± 0.2

[a] J-factors are calculated over a solid angle of $\Delta\Omega \sim 2.4$ ...

Halo shape insensitive!

Prior dependence

Coma B.	241.9	83.6	44	$0.25^{+0.34}_{-0.17}$	*19.0 ± 0.25*

Large ambiguity!

Observed Events

Signal: $$S_{ai} = t_{\rm obs} \times \int_{\Delta E_i} dE\, \mathcal{F}_a^{\rm (S)}(E, \Delta\Omega_i)\, A_{\rm eff}(E)$$

Background: $$B_{ai} = t_{\rm obs} \times \int_{\Delta E_i} dE\, \mathcal{F}_a^{\rm (B)}(E, \Delta\Omega_i)\, A_{\rm eff}(E)$$

a: dSph
i: Energy Bin

Energy Bin

ROI

Effective Area

Signal Flux: $F^{(S)}$

- Particle Factor
- Astrophysical Factor

BG Flux: $F^{(B)}$

- Galactic Diffuse
- Isotropic Diffuse
- Point-like Source

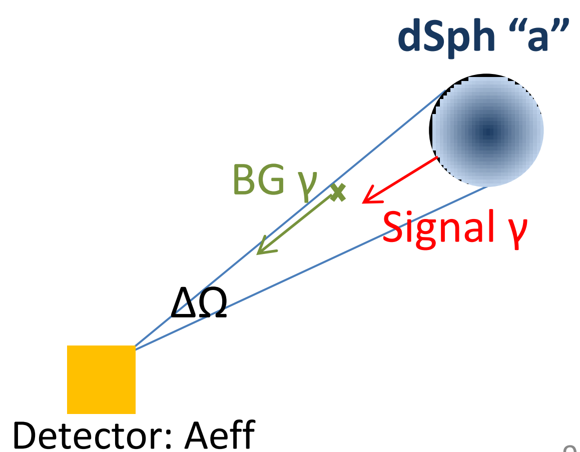

Background Flux

1. Galactic Diffuse

CR + ISM, Brems of CRe, IC (CRe + Interstellar radiation field)

→ Simulation (e.g. GALPROP) with ISM, ISRF, Large Scale Structure.

2. Isotropic Diffuse

AGN, Starburst, γ-Ray burst, unknown sources

→ Evaluated from |b| > 30^{o} sky data

3. Point-like Source

AGN, SNR, Pulsars, Unidentified

→ Mask/Model

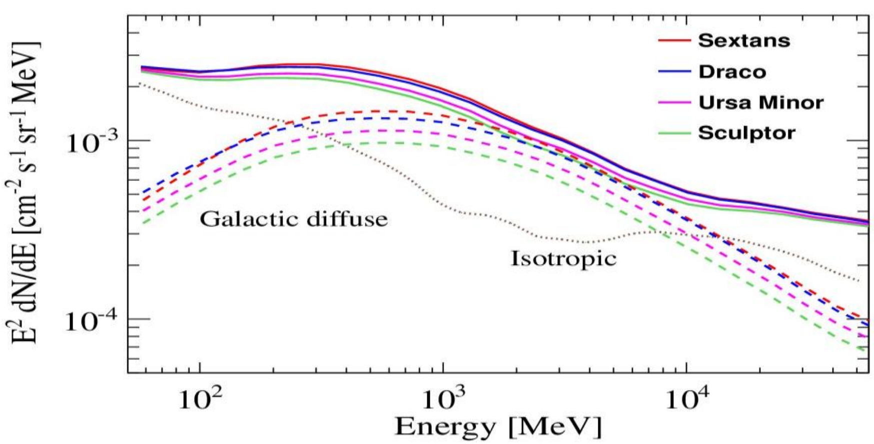

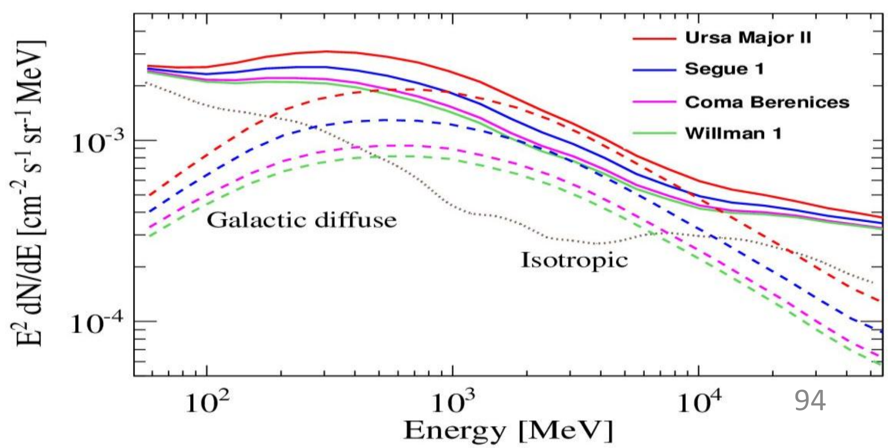

Detector Capabilities

Satellite- type Obs

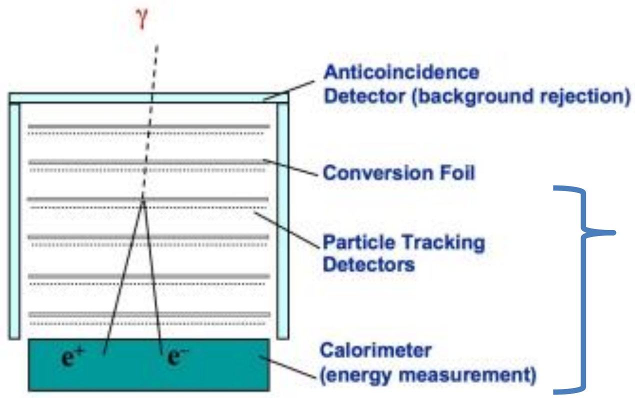

Direction Reconstruction

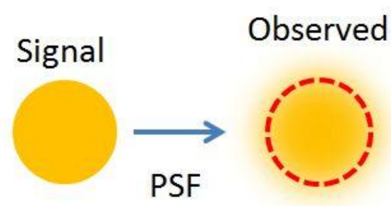

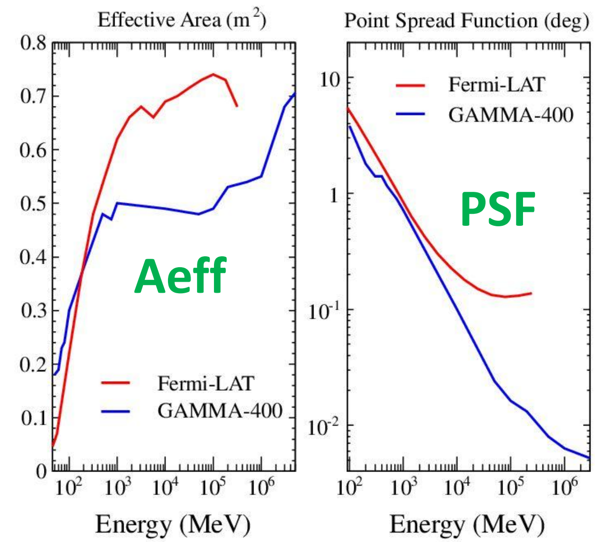

ROI: $\Delta\Omega_i = 2\pi(1 - \cos\alpha_i)$

$$\alpha_i = [(0.5^\circ)^2 + \psi_{68}^2(E_i)]^{1/2}$$

Typical dSphs Size   PSF (68 % containment angle)

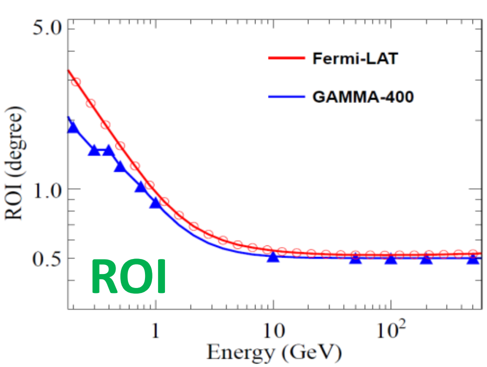

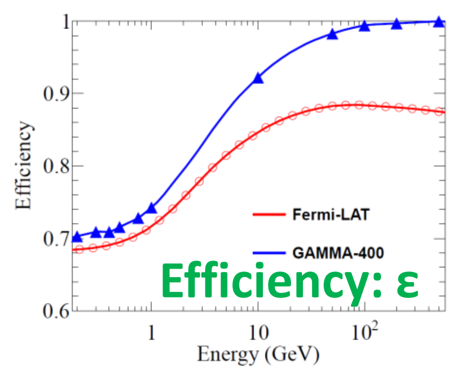

Signal Flux

$$\mathcal{F}_a^{(\mathrm{S})}(E, \Delta\Omega_i) = \epsilon(\Delta\Omega_i)\,\Phi_a(E, \Delta\Omega_i)$$

PSF effect -> efficiency ε

Background Flux

$$\mathcal{F}_a^{(\mathrm{B})}(E, \Delta\Omega_i) = \Delta\Omega_i\,(d\Phi_a^{\mathrm{B}}(E)/d\Omega)$$

Large ΔΩ -> Large Background

Sensitivity Line

Profile Likelihood

J-factor error is included

$$\mathcal{L}[\langle\sigma v\rangle, \{J_a\}] \equiv \prod_{a,i} \frac{P\left(N_{ai}; S_{ai}[\langle\sigma v\rangle, J_a] + B_{ai}\right)}{P\left(N_{ai}; N_{ai}\right)} G\left(J_a; \log_{10} J_a^{(\mathrm{obs})}, \delta(\log_{10} J_a^{(\mathrm{obs})})\right)$$

P(N:λ): Poisson
G(x: μ, σ): Log Gaussian
N_{ai}: Observed Events

Test (95% C.L)

$$-2\ln\mathcal{L}(\langle\sigma v\rangle, \{J_{\min}\}) + 2\ln\mathcal{L}(0, \{J_{\min}\}) = 2.71$$

2000 Pseudo Experiments for N_{ai} ($\{N^{(1)}_{ai}, N^{(2)}_{ai}, N^{(3)}_{ai} \ldots\}$)
(Poisson with the mean of B_{ai})

Each $N^{(i)}_{ai} \rightarrow \langle\sigma v\rangle^{(i)}$

Right Figure:
Mean and 68 (95) % band
for the set $\{ \langle\sigma v\rangle^{(1)}, \langle\sigma v\rangle^{(2)}, \langle\sigma v\rangle^{(3)}, \ldots \}$

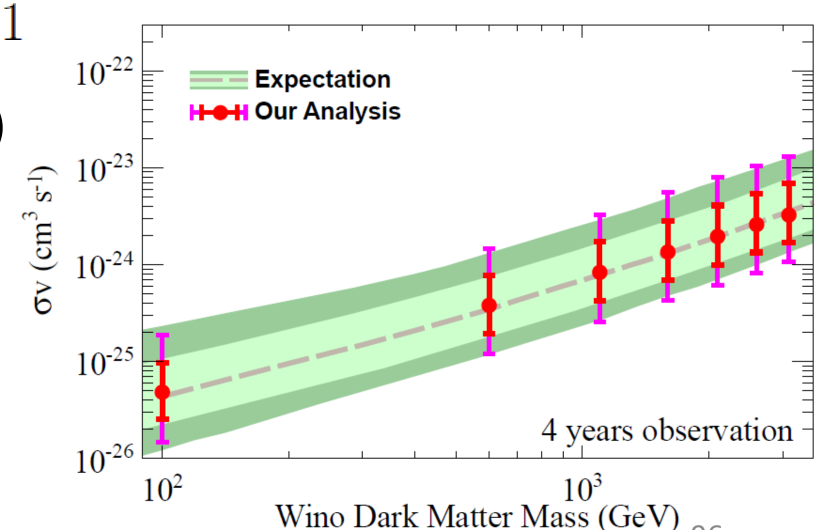

Current Limit

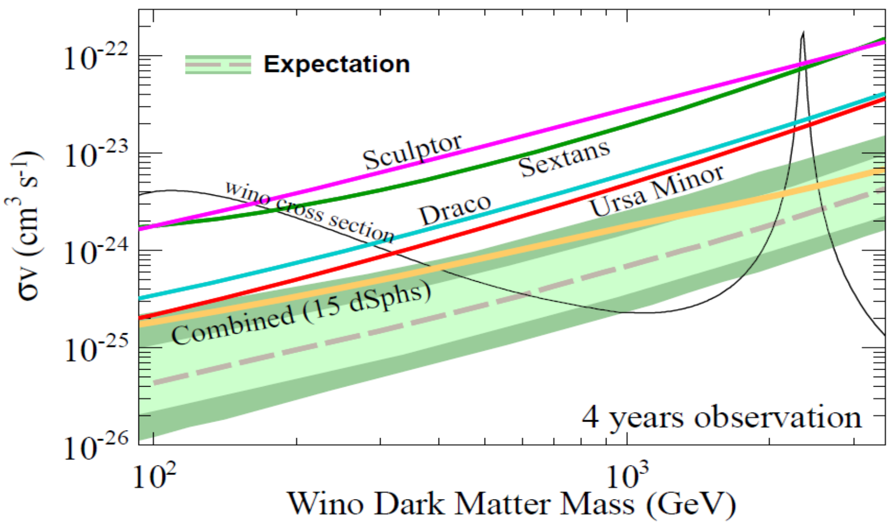

Ursa Minor
320 GeV ≤ m ≤ 2.25TeV and 2.43 TeV ≤ m

Combined (15 dSphs) <- Aggressive
390 GeV ≤ m ≤ 2.14TeV and 2.53 TeV ≤ m

Future Prospects

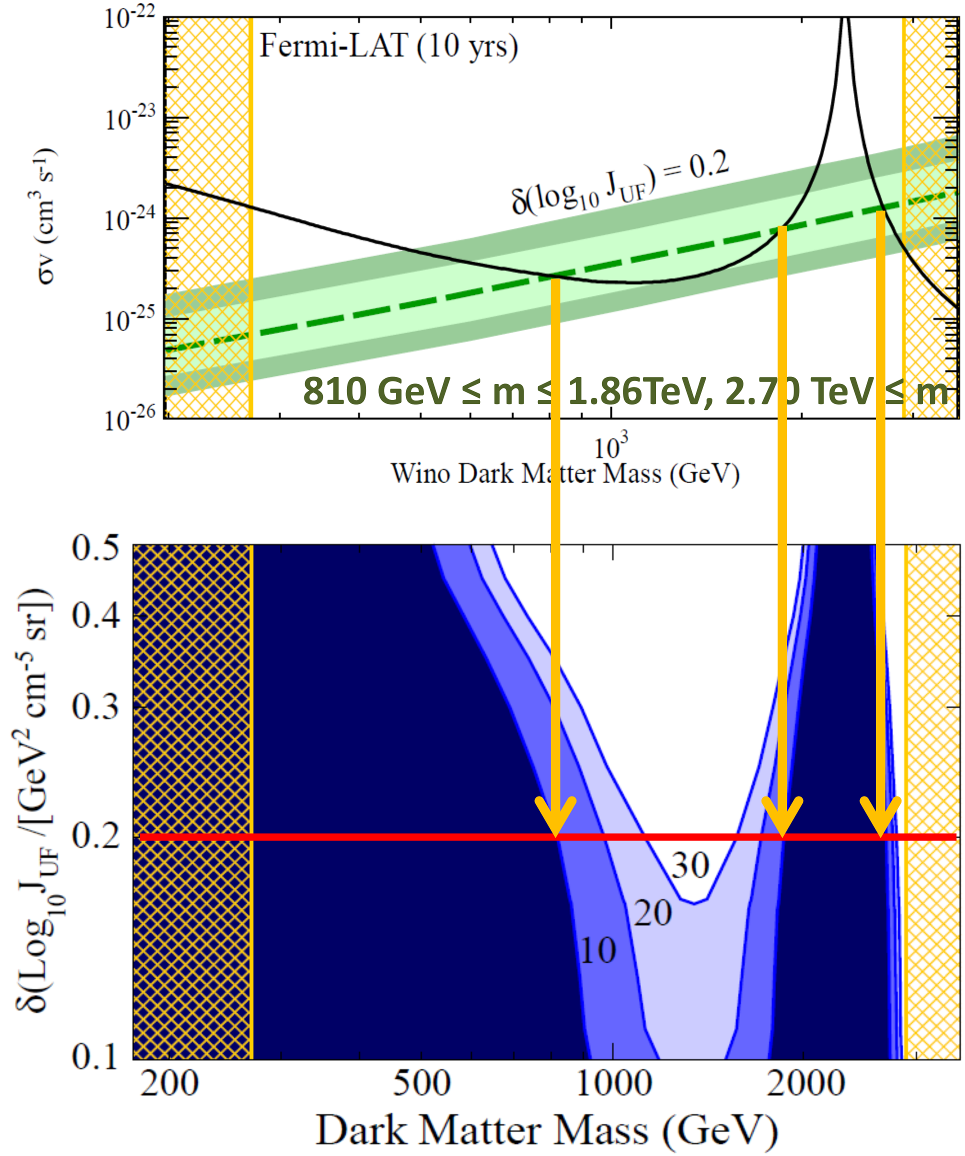

810 GeV ≤ m ≤ 1.86TeV, 2.70 TeV ≤ m